A Mathematical Model for Airfoils with Spoilers or Split Flaps

by

William Wai-Hung Yeung

B.A.Sc. The University of British Columbia, 1983

A THESIS SUBMITTED IN PARTIAL FULFILMENT OF
THE REQUIREMENTS FOR THE DEGREE OF

MASTER OF APPLIED SCIENCE

in

THE FACULTY OF GRADUATE STUDIES

Department of Mechanical Engineering

We accept the thesis as conforming
to the required standard

THE UNIVERSITY OF BRITISH COLUMBIA

August 1985

In presenting this thesis in partial fulfilment of the requirements for an advanced degree at the University of British Columbia, I agree that the Library shall make it freely available for reference and study. I further agree that permission for extensive copying of this thesis for scholarly purposes may be granted by the head of my department or by his or her representatives. It is understood that copying or publication of this thesis for financial gain shall not be allowed without my written permission.

Department of Mechanical Engineering

The University of British Columbia
1956 Main Mall
Vancouver, Canada
V6T 1Y3

Date August 28, 1985

Abstract

A flow model for a Joukowsky airfoil with an inclined spoiler or split flap is constructed based on the early work by Parkinson and Jandali. No restriction is imposed on the airfoil camber, the inclination and length of the spoiler or split flap, and the angle of incidence. The flow is assumed to be steady, two-dimensional, inviscid and incompressible. A sequence of conformal transformations is developed to deform the contour of the airfoil and the spoiler (split flap) onto the circumference of the unit circle over which the flow problem is solved. The partially separated flow region behind these bluff bodies is simulated by superimposing suitable singularities in the transform plane. The trailing edge, the tip of the spoiler (flap) are made critical points in the mappings so that Kutta conditions are satisfied there. The pressures at these critical points are matched to the pressure inside the wake, the only empirical input to the model. Some studies of an additional boundary condition for solving the flow problem were carried out with considerable success. The chordwise pressure distributions and the overall lift force variations are compared with experiments. Good agreement in general is achieved. The model can be extended readily to airfoils of arbitrary profile with the application of the Theodorsen transformation.

Table of Contents

LIST OF FIGURES

LIST OF TABLES

ACKNOWLEDGEMENT

I would like to take this opportunity to thank Professor G. V. Parkinson for his enthusiastic and invaluable guidance during the course of this research. His support and suggestions were much appreciated.

Mr. T. Y. Lu, graduate student, designed and carried out the wind tunnel measurements on split flaps. Mr. E. Abel of the Mechanical Engineering Machine Shop built the parts for the author's experiments on spoilers. Their help is gratefully acknowledged.

The author would also like to thank the Computing Center of the University of British Columbia for the use of their facilities.

1. INTRODUCTION

Theoretical as well as experimental investigations of bluff body aerodynamics, especially partially separated flows associated with airfoils equipped with spoilers, have been conducted in the Department of Mechanical Engineering at the University of British Columbia for some years. The motivation behind this study is that spoilers have been widely used on aircraft wings as a device for landing and maneuvering purposes. They decrease the lift by reducing circulation, and also function as airbrakes to increase strongly the drag, thus reducing considerably the speed and generating a steeper glide angle. They can also serve for roll control if deflected asymmetrically.

The counterpart of a spoiler, a split flap, has been studied recently for one of its features of producing high lift at lower angles of incidence. With the split flap deployed, the maximum lift coefficient would be increased so that the take-off distance of an aircraft may be shortened if the lift-to-drag ratio is kept sufficiently high. Although multi-slotted flaps are used in aircraft wings in recent years for various reasons, a somewhat unexpected result [1] has been observed that when based on the extended chord at a Reynolds number (Re) 6×10^6 or higher, the maximum attainable C_L is nearly the same for split, slotted, and double-slotted flaps.

In other words, for producing the lift force, the split flap may be just as efficient as other types of flap. Both spoilers and split flaps have been employed, for instance, on the B-52 stratofortress and other recent operational airplanes, and they continue to play an important role in the design of airplanes.

In practice, wing flaps and spoilers as used on wings, are three dimensional devices, limited in span and sometimes rake-like in shape, usually interrupted by the fuselage and interfered with by nacelles and propeller slipstreams. However, the two dimensional aerodynamic characteristics are the basis from which more complicated configurations can be understood. The simple two dimensional wake singularity model for bluff body flows developed by Parkinson and Jandali [2,3] provides the basic information for the flow associated with airfoil normal spoilers. In addition, its reliablity, mathematical elegance and flexibility allow the model to be used for accurate prediction of the loading on any airfoil-shaped profile equipped with a spoiler or split flap. Costly and tedious wind tunnel tests for pressure distribution and lift variation may then be reduced to a certain extent.

A split flap is formed by deploying the rear portion of the lower surface of the airfoil about the forward edge of the flap. Therefore, the length of the flap is equal to the distance between its hinge and the trailing edge. Whereas for a spoiler, it is located on the upper surface and usually

positioned somewhere between the mid-chord and the trailing edge, in order to achieve the desired performance. Its height often extends from 5 to 10 % of the chord. In practice, the angle of deflection, δ, for both devices ranges from 0° to 60°, although no such restriction is imposed on δ in the present theory. Fig. 1 from [4] shows experimentally how C_L varies with α, angle of incidence, as δ is increased from 0° to 60° for the NACA 23012 profile fitted with a split flap of 20 % chord. It is clear from Fig.1 that deflecting the split flap is equivalent to altering the effective camber of the airfoil, or more precisely, to decreasing the angle of zero lift, but without considerably distorting the lift curve slope. The opposite effect takes place if a spoiler is erected. Deploying the split flap or spoiler provides the simplest method of accomplishing the desirable lift coefficient through the temporary alteration of the airfoil geometry.

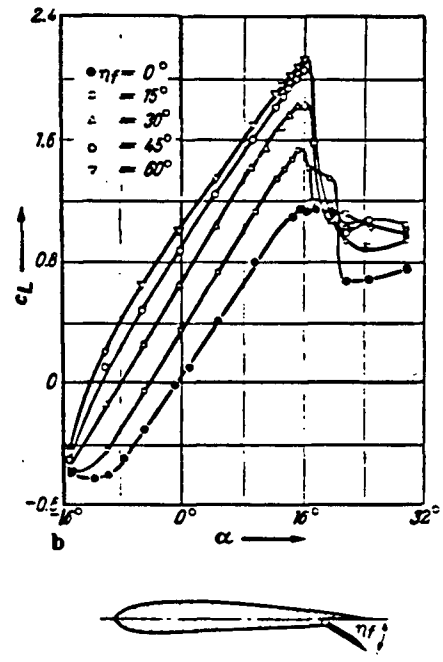

Fig. 1 Experimental C_L Variation of NACA 23012 Profile

2. HISTORICAL SURVEY

An early theoretical study of potential flow around an airfoil with a split flap and circulation control by suction, was conducted by Whitehead, Cheers and Mandl [5] at NAE. The combination of the airfoil and the split flap is idealized by a straight-line configuration with suction produced by a sink located on the upper surface of the flap in order to simulate the effect of the separated wake. The effects from the leading edge separation bubble, the finite thickness of the airfoil and the wind tunnel constraint tend to widen the discrepancy between the experimental and theoretical lift variation over a range of angles of incidence. Besides, no information concerning the loading over the airfoil is available.

Woods [6] dealt with a similar problem in the form of a linear perturbation free streamline potential theory. As pointed out in Parkinson [7], Woods' theory is awkward to apply because it requires two empirical details of the separated flow, and does not account for airfoil thickness, which may be a significant contribution. A comparsion between the theoretical pressure distributions by Woods and Parkinson & Jandali can be found in reference [8].

The present work follows closely Jandali's [3] approach but has been extended to deal with arbitrarily inclined

spoilers or split flaps. The flow is also assumed to be inviscid but the theory is exact in the sense that no linearization technique is applied. That is, the airfoil is of finite thickness and camber. Therefore, the resulting pressure loading over the airfoil does not possess a leading edge singularity. The only empirical input is the pressure inside the wake behind the spoiler or split flap because there is not any theory to predict its values at various geometrical configurations.

3. THEORY

The work described herein concerns only the Joukowsky airfoil family. However, it can be readily extended to other airfoil shapes by applying the Theodorsen transformation to the physical plane where the airfoil is located. In fact, Jandali [3] accomplished this extension to a Clark-Y airfoil with a normal spoiler and achieved satisfactory results.

The present theory deals with the kinematics as well as the dynamics of the fluid flow around an airfoil with an inclined spoiler or split flap. It is assumed that the flow is everywhere steady, two dimensional, inviscid and incompressible except in the region where a broad wake, caused by flow separation, is located (Figs. 2a,b). Therefore, the potential flow theory with the technique of conformal transformation can be used to deal with the kinematics. The dynamical input is through the prescribed boundary conditions with an empirical parameter, which is the constant pressure in the wake behind the spoiler or split flap. Shear layers emanating from the points of separation (i.e. the trailing edge, and the tip of the spoiler or split flap) are modelled as separating streamlines of initially constant pressure.

Before separation takes place, it is reasonable to assume, partly as a matter of observation and partly from

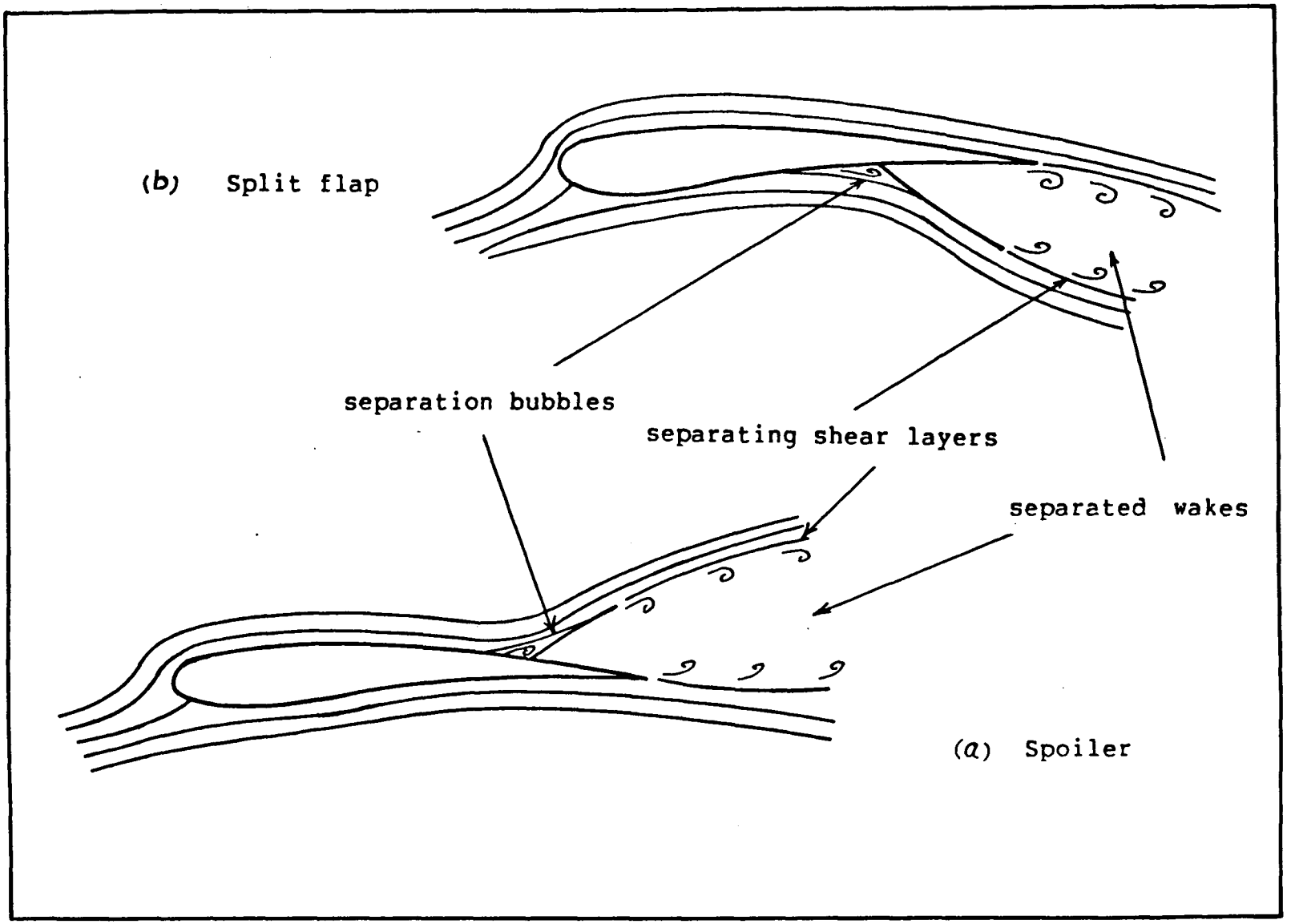

Fig. 2 Streamline Patterns around Airfoil with Spoiler /Split Flap

mathematical analysis, that the viscous boundary layer is thin over an airfoil surface. Therefore, the flow can be treated as irrotational and Bernoulli's principle is applicable to calculate the pressure variation along a streamline of interest, which is the airfoil profile as considered here.

However, inserting a spoiler or split flap will definitely slow down the fluid particles approaching it, and thus alter the thickness of the boundary layer ahead of this obstacle. In fact, in the case of an inclined spoiler, the strong adverse pressure gradient over the upper surface and near the leading edge of the airfoil enhances this deceleration of fluid flow so that an early flow separation, including some backward flow, takes place upstream of the spoiler. This separation of flow followed by reattachment over the spoiler surface, forms a closed bubble of circulatory air at a fairly constant pressure. Fig.3 is a flow visualization of the bubble taken in a smoke tunnel at low Reynolds number. As the Reynolds number is increased, stronger flow outside the boundary layer resists the backward flow from starting further upstream of the spoiler, and thus causes the size of the bubble to diminish. On the other hand, the occurrence of the bubble is less pronounced in front of the split flap because the pressure gradient is in general less prominent over the lower surface. Therefore, the separation bubble is smaller and the theoretical prediction of the pressure near it is reasonably good. Nevertheless, since viscous effects dominate in this region, the potential flow theory presented here is,

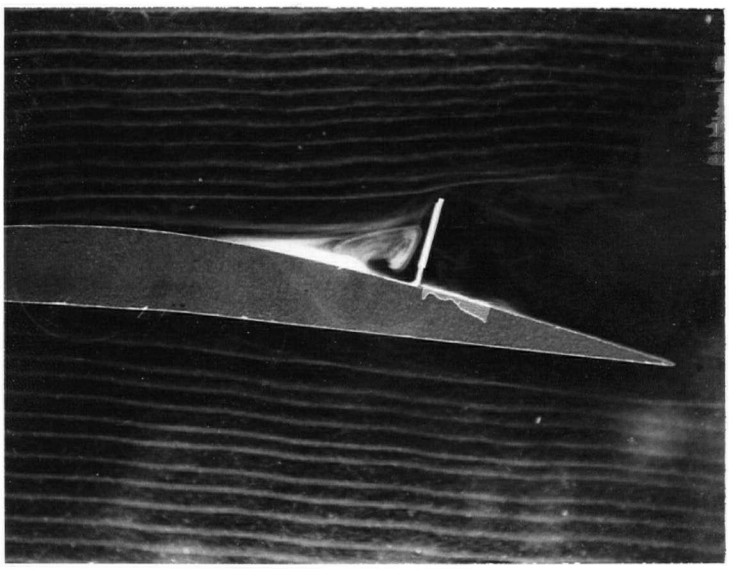

Fig. 3 Separation Bubble in front of Spoiler (Jandali, Unpublished Data)

in general, expected to predict less satisfactory results. Evidence is found in both Jandali [3] and the present work. No attempt has been made in the theory to model the presence of the bubble in either case.

3.1 Kinematics

Solving the flow problem of any bluff body section directly in the physical plane is not always easy. More often, the degree of complexity of the geometry can be substantially reduced if the method of conformal transformation is utilized. Parkinson and Jandali [2] successfully found the mappings for a number of bluff body shapes. In Jandali [3], conformal maps were used to deform the contour of an airfoil with a normal spoiler onto the circumference of a unit circle over which the flow problem was solved.

For an airfoil with an inclined spoiler or split flap, the use of conformal mapping is inevitable because of the non-trivial geometry involved. Jandali's method is used here but the sequence of mappings is more intricate.

3.1.1 Conformal Transformations for an Inclined Spoiler

A circle of radius R centered at t_0 $(-\epsilon,\mu)$ in the t-plane (Fig. 4b) will become a Joukowsky airfoil in the z-plane (Fig. 4a) when given the well-known Joukowsky transformation :

$$z = t + 1/t \qquad \ldots \quad (1)$$

The camber and the thickness of the derived airfoil are

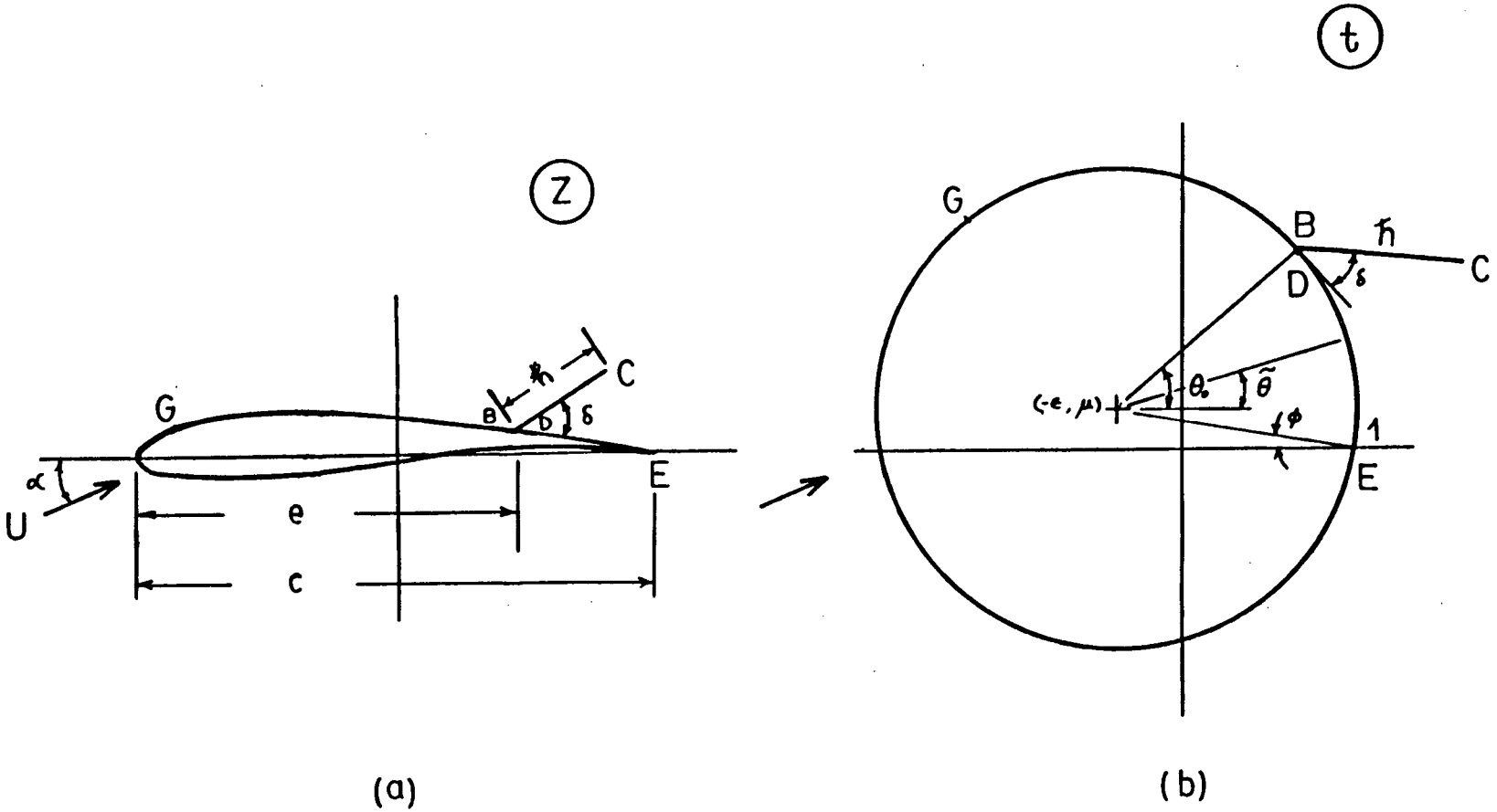

(a) (b)

Fig. 4 Complex Transform Planes (Spoiler)

related to the location of t_0. The magnitude of R can be calculated by the formula

$$R = \sqrt{(1 + \epsilon)^2 + \mu^2} \qquad \ldots \quad (1a)$$

An inclined spoiler which is represented by the fence BCD in the z-plane is mapped from a straight line segment BCD emanating from point B in the t-plane. The inclination δ ($\leq 90°$), which is the measure of the angle of intersection between BC and the tangent line at B, stays constant under the forementioned conformal transformation. In other words, the spoiler in the physical plane z is also making the same angle δ with the surface of the airfoil. However, since (1) is not a linear transformation, the spoiler BCD becomes a slightly curved segment which is not inappropriate for practical spoiler heights. Nevertheless, it should be noted that the spoiler (split flap) tip deflection angles will be from 0.5° to 1.0° less than the root values of δ used throughout the thesis. The chordwise location e and the height $\bar{\bar{h}}$ of the spoiler in the z-plane are related to the angular variable θ_0, height $\bar{h}$ and inclination δ in the t-plane. Table 1 provides some values of e/c, θ_0, δ, $\bar{\bar{h}}$ and $\bar{h}$ used in the calculations.

A counter-clockwise rotation through γ combines with translation of Λ to produce the transformation

$$s = (t - \Lambda)\, e^{i\gamma} \qquad \ldots \quad (2)$$

where

$$\gamma = \pi/2 - \theta_0 - \delta \qquad \ldots \quad (2a)$$

and

$$\Lambda = t_0 + R \cos \delta\, e^{i(\theta_0 + \delta)} \qquad \ldots \quad (2b)$$

Table 1: *Spoiler*

e/c	θ_0
.90	32.25°
.70	61.25°
.50	86.25°

$\bar{h}/c$ = 5 %, δ = 45°, n = 1.5

e/c	$\bar{h}$	$\bar{\xi}$	$\bar{\eta}$
.90	.2013	5.9817	6.9252
.70	.1284	9.4638	10.4268
.50	.1183	10.2855	11.2513

$\bar{h}/c$ = 10 %, δ = 30°, n = $1\frac{2}{3}$

e/c	$\bar{h}$	$\bar{\xi}$	$\bar{\eta}$
.90	.4832	2.3162	2.0201
.70	.2616	4.3887	3.2539
.50	.2366	4.8730	3.5380

$\bar{h}/c$ = 10 %, δ = 60°, n = $1\frac{1}{3}$

e/c	$\bar{h}$	$\bar{\xi}$	$\bar{\eta}$
.90	.4329	2.1979	4.8253
.70	.2668	3.6177	7.3304
.50	.2418	4.0015	8.0026

This mapping results in bringing the line segment BCD in the t-plane onto the horizontal axis in the s-plane. And the circle is centered at $s = -R \cos \delta \, i$, Fig 4c.

With the Kàrmàn-Trefftz transformation

$$s = i \, R \sin \delta \cot (\omega/2) \qquad \ldots \quad (3)$$

the contour in the s-plane becomes a degenerate polygon in the ω-plane as shown in Fig. 4d. The two circular arcs DEAG and GFB become two infinite vertical lines to the left and the right of the origin of the ω-plane, respectively, whereas the straight line segment BCD is a vertical ray starting from the point $\omega = h \, i$. The flow outside the airfoil in the z-plane is mapped onto the interior of the polygon bounded by GBDG. $\omega = 0$ corresponds to $z = \infty$. Table 2 summarizes the co-ordinates of the points of interest in the t, s and ω-planes.

Note that $$n = 2 \, (1 - \delta/\pi) \qquad \ldots \quad (3a)$$

and $$h = \ln \left[\frac{2 \sin \delta + \hbar}{\hbar} \right] \qquad \ldots \quad (3b)$$

where $1 \leq n \leq 2$.

The interior of the polygon is mapped onto the upper half plane of λ (Fig. 4e) by the Schwarz-Christoffel transformation

$$\frac{d\omega}{d\lambda} = k \, \lambda \, (\lambda + n)^{-1} \, (\lambda - 2 + n)^{-1} \qquad \ldots \quad (4)$$

which can be integrated to

$$\omega = - \frac{\pi}{2}(2-n) + ih - \frac{i}{2} \{ n \ln(\frac{\lambda}{n} + 1) + (2-n) \ln(\frac{\lambda}{2-n} - 1 \} \qquad \ldots \quad (5)$$

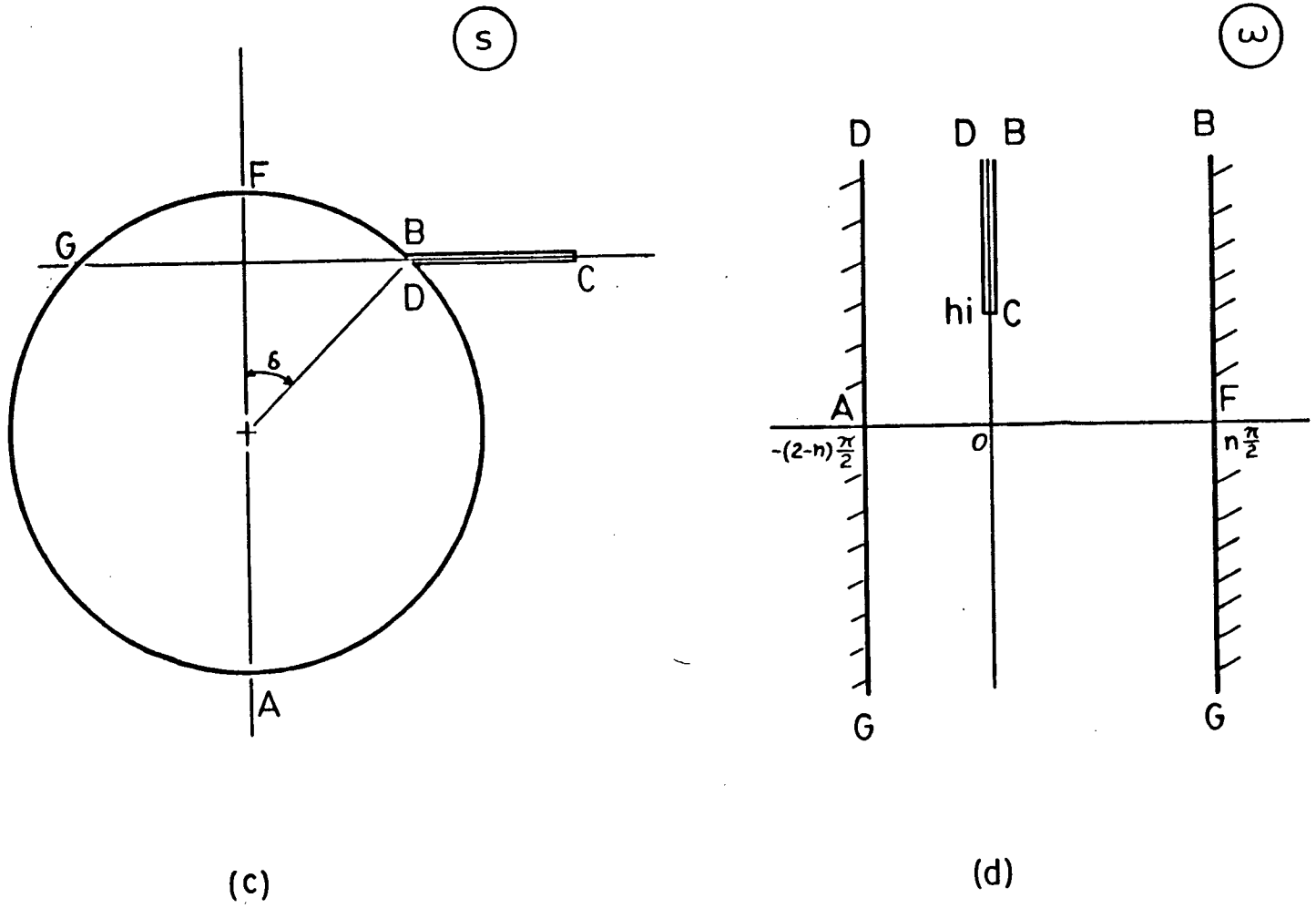

Fig. 4 Complex Transform Planes (Spoiler)

Table 2 : Co-ordinates of points B, C, D, E, A, G, F in different planes for *spoilers.*

Point	t-plane	s-plane	ω-plane
B	$t_o + R\, e^{i\theta_o}$	$R \sin \delta$	$n\pi/2 + i\infty$ or $+ i\infty$
C	$t_o + R\, e^{i\theta_o} + \acute{h}\, e^{-i\gamma}$	$R \sin \delta + \acute{h}$	h i
D	$t_o + R\, e^{i\theta_o}$	$R \sin \delta$	$(2-n)\pi/2 + i\infty$ or $+ i\infty$
E	1	$(1 - \Lambda)e^{i\gamma}$	$2 \cot^{-1} [(\Lambda - 1)e^{i\gamma}/(R \sin \delta)]$
A	$t_o - R\, e^{i(\theta_o+\delta)}$	$-(R + R \cos \delta)i$	$-(2-n)\pi/2$
G	$t_o + R\, e^{i(\theta_o+ 2\delta)}$	$-R \sin \delta$	$n\pi/2 - i\infty$ or $-(2-n)\pi/2 - i\infty$
F	$t_o + R\, e^{i(\theta_o+\delta)}$	$(R - R \cos \delta)i$	$n\pi/2$

The scale factor k and the integration constant are evaluated by setting

$$\omega = h\,i \qquad \text{for} \qquad \lambda = 0$$
$$\omega = n\frac{\pi}{2} + i\infty \qquad \text{for} \qquad \lambda = -n^{-}$$
$$\omega = \infty\, i \qquad \text{for} \qquad \lambda = -n^{+}$$

, as shown in appendix E.

Let $\lambda_\infty = \xi + i\tilde{\eta}$ correspond to $\omega = 0$ or $z = \infty$. Then ξ and $\tilde{\eta}$ are given by

$$e^{2h} = [(\frac{\xi}{n} + 1)^2 + (\frac{\tilde{\eta}}{n})^2]^{n/2}\ [(\frac{\xi}{2-n} - 1)^2 + (\frac{\tilde{\eta}}{2-n})^2]^{(2-n)/2} \qquad \ldots \quad (6)$$

$$\pi(2-n) = n\ \tan^{-1}(\frac{\tilde{\eta}}{\xi+n}) + (2-n)\ \tan^{-1}(\frac{\tilde{\eta}}{\xi-2+n}) \qquad \ldots \quad (7)$$

When n=1 or $\delta = 90°$, (6) & (7) can be simplified to

$$\xi = 0 \quad \text{and} \quad \tilde{\eta} = \sqrt{(e^{2h}-1)}.$$

For $1 < n < 2$, ξ and $\tilde{\eta}$ have to be found numerically. See Table 1 for a summary of values of ξ, $\tilde{\eta}$, n and $\hbar$.

The transformation (8), which is a combination of shifting and scaling,

$$\lambda = \xi + \tilde{\eta}\,\tilde{\lambda} \qquad \ldots \quad (8)$$

ensures that $\tilde{\lambda}_\infty = i$ is equivalent to $z = \infty$, see Fig. 4f. Here, $\tilde{\eta}$ is taken to be non-zero.

Finally, a bilinear transformation and a rotation,

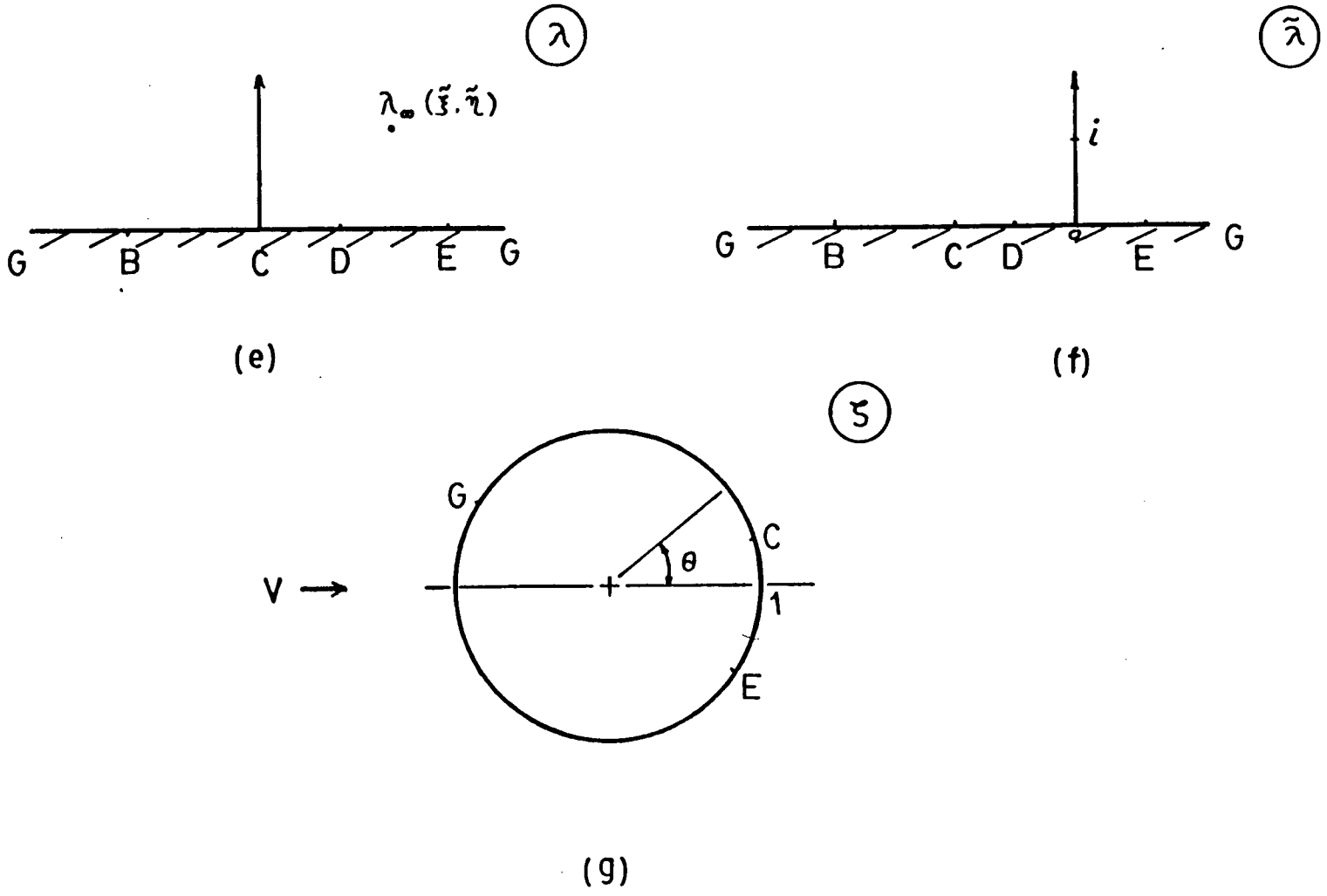

Fig. 4 Complex Transform Planes (Spoiler)

$$\zeta = e^{-ia_0}\left(\frac{i+\tilde{\lambda}}{i-\tilde{\lambda}}\right) \qquad \ldots \quad (9)$$

map the flow on the upper half plane of $\tilde{\lambda}$ to the exterior of the unit circle in the ζ-plane. Angle a_0, which is defined by (13), is chosen so that the uniform flow at infinity is parallel to the real axis in the ζ-plane, Fig. 4g.

After a sequence of 6 mappings, the contour of the airfoil with the spoiler becomes the perimeter of the unit circle, Fig.4g. The distribution of points B, C, D, E, etc., can be obtained once the formula for a_0 is established.

The combined transformation derivative $\frac{dz}{d\zeta}$ can be obtained by the chain rule :

$$\frac{dz}{d\zeta} = \frac{dz}{dt}\frac{dt}{ds}\frac{ds}{d\omega}\frac{d\omega}{d\lambda}\frac{d\lambda}{d\tilde{\lambda}}\frac{d\tilde{\lambda}}{d\zeta}$$

and reduces to

$$\frac{dz}{d\zeta} = \frac{t^2-1}{t^2}\, e^{-i\gamma}\left[-iR\,\frac{\sin\delta}{2}\,\csc^2\left(\frac{\omega}{2}\right)\right]\left[\frac{\lambda i}{(\lambda+n)(\lambda-2+n)}\right]\frac{\tilde{\eta}(i-\tilde{\lambda})^2}{2i}\, e^{ia_0} \qquad \ldots \quad (10)$$

(10) has essentially two simple zeros and two simple poles in the region corresponding to the flow field and the airfoil boundary :

a) simple zero at the trailing edge E, $t = 1$,

b) simple zero at the tip of the spoiler C, $\lambda = 0$,

c) simple pole at the spoiler base B, $\lambda = -n$, and

d) simple pole at the spoiler base D, $\lambda = 2-n$.

The points at which $\frac{dz}{d\zeta}$ has simple zeros are called the critical points. Because of the doubling of the angles at critical points, the stagnation streamlines leaving E and C in the ζ-plane become the tangential separation streamlines at the corresponding points in the z-plane. The points at which $\frac{d\zeta}{dz}$ has simple zeros will be stagnation points in the z-plane. Only point B is of interest because point D is within the wake in which the flow is ignored.

However, the point G on the airfoil surface, $\omega = -(2-n)\frac{\pi}{2} - i\infty$ or $n\frac{\pi}{2} - i\infty$, and the point at infinity, $\bar{\lambda} = i$, are not simple zeros of (10) but removable singularities. The proofs are given in appendices A and B, respectively.

Let Ue^{-ia} and V be the velocities of the flow at infinity in the z and ζ-planes. They are related through

$$Ue^{-ia} \longrightarrow V\left(\frac{d\zeta}{dz}\right)\Big|_{z=\infty} \quad \ldots \quad (11)$$

From equations (11) and (B4,appendix B), one can deduce that

$$\frac{V}{U} = \left|\frac{dz}{d\zeta}\right|_{z=\infty}$$

$$= \frac{R \sin \delta}{\tilde{\eta}} \sqrt{\frac{[(\xi+n)^2 + \tilde{\eta}^2][(\xi-2+n)^2 + \tilde{\eta}^2]}{(\xi^2 + \tilde{\eta}^2)}} \quad \ldots \quad (12)$$

And $$a_o = \frac{\pi}{2} + a + \gamma + \theta_1 - \theta_2 - \theta_3 \quad \ldots \quad (13)$$

where $$\theta_1 = \tan^{-1}\left(\frac{\tilde{\eta}}{\xi}\right) \quad \ldots \quad (13a)$$

$$\theta_2 = \tan^{-1}\left(\frac{\tilde{\eta}}{\xi+n}\right) \quad \ldots \quad (13b)$$

and $$\theta_3 = \tan^{-1}\left(\frac{\tilde{\eta}}{\tilde{\xi}-2+n}\right) \quad \ldots \quad (13c)$$

The angular positions of the simple zeros in the ζ-plane are given by

$$\theta_C = \pi - 2\tan^{-1}\left(\frac{\tilde{\eta}}{\tilde{\xi}}\right) - a_0 \quad \ldots \quad (14)$$

$$\theta_E = -\cos^{-1}\left[(1-\tilde{\lambda}_E^2)/(1+\tilde{\lambda}_E^2)\right] - a_0 \quad \ldots \quad (15)$$

The equations used to determine the point E in the $\tilde{\lambda}$ plane, $\tilde{\lambda}_E$, are given in appendix C.

Equations (14) and (15) should reduce to the corresponding ones given in Jandali [3] when $\delta = 90°$ and $n = 1$ since both Jandali's and the current mapping sequences deform the airfoil contour onto the circumference of the unit circle. The details of the derivation are given in appendix D.

3.1.2 Conformal Transformation for Inclined Split Flaps

The mappings for an inclined split flap are similar to those for an inclined spoiler. Figs. 5 a-g depict the sequence involved. The equations of Transformations are :

$$z = t + 1/t \quad \ldots \quad (16)$$

$$s = (t - \Lambda)\, e^{-i\gamma} \quad \ldots \quad (17)$$

$$s = iR \sin\delta \cot\left(\frac{\omega}{2}\right) \quad \ldots \quad (18)$$

$$\omega = -\frac{n\pi}{2} + ih - \frac{i}{2}\left\{n \ln\left(\frac{\lambda}{n} - 1\right) + (2-n)\ln\left(\frac{\lambda}{2-n} + 1\right)\right\} \quad \ldots \quad (19)$$

$$\lambda = -\xi + \tilde{\eta}\,\tilde{\lambda} \qquad \ldots \quad (20)$$

$$\zeta = e^{-ia_0}\left(\frac{i+\tilde{\lambda}}{i-\tilde{\lambda}}\right) \qquad \ldots \quad (21)$$

where $\Lambda = t_0 + R\cos\delta\, e^{-i(\theta_0+\delta)}$

$$\gamma = \frac{\pi}{2} - \theta_0 - \delta$$

and equations (3a), (3b), (6), (7) apply with $\lambda_\infty = -\xi + i\tilde{\eta}$. Also

$$\frac{dz}{d\zeta} = \frac{t^2-1}{t^2}\, e^{i\gamma}\left[-iR\,\frac{\sin\delta}{2}\,\csc^2\left(\frac{\omega}{2}\right)\right]\left[\frac{-\lambda i}{(\lambda-n)(\lambda+2-n)}\right]\frac{\tilde{\eta}(i-\tilde{\lambda})^2}{2i}\, e^{ia_0} \qquad \ldots \quad (22)$$

$$a_0 = \frac{\pi}{2} + \alpha - \gamma + \theta_1 - \theta_2 - \theta_3 \qquad \ldots \quad (23)$$

where $\theta_1 = \pi - \tan^{-1}\left(\frac{\tilde{\eta}}{\xi}\right)$ ... (23a)

$$\theta_2 = \pi - \tan^{-1}\left(\frac{\tilde{\eta}}{\xi+n}\right) \qquad \ldots \quad (23b)$$

and $\theta_3 = \tan^{-1}\left(\frac{\tilde{\eta}}{\xi-2+n}\right)$ ... (23c)

The angular positions of the simple zeros in the ζ-plane are given by

$$\theta_C = -\pi + 2\tan^{-1}\left(\frac{\tilde{\eta}}{\xi}\right) - a_0 \qquad \ldots \quad (24)$$

$$\theta_E = \cos^{-1}\left[(1-\tilde{\lambda}_E^2)/(1+\tilde{\lambda}_E^2)\right] - a_0 \qquad \ldots \quad (25)$$

where $\tilde{\lambda}_E$ is defined in appendix C. Values of e/c, θ_0, δ, $\hbar$, ξ and $\tilde{\eta}$ are given in Table 3. Table 4 gives the locations of points B, C, D, E, A, G and F.

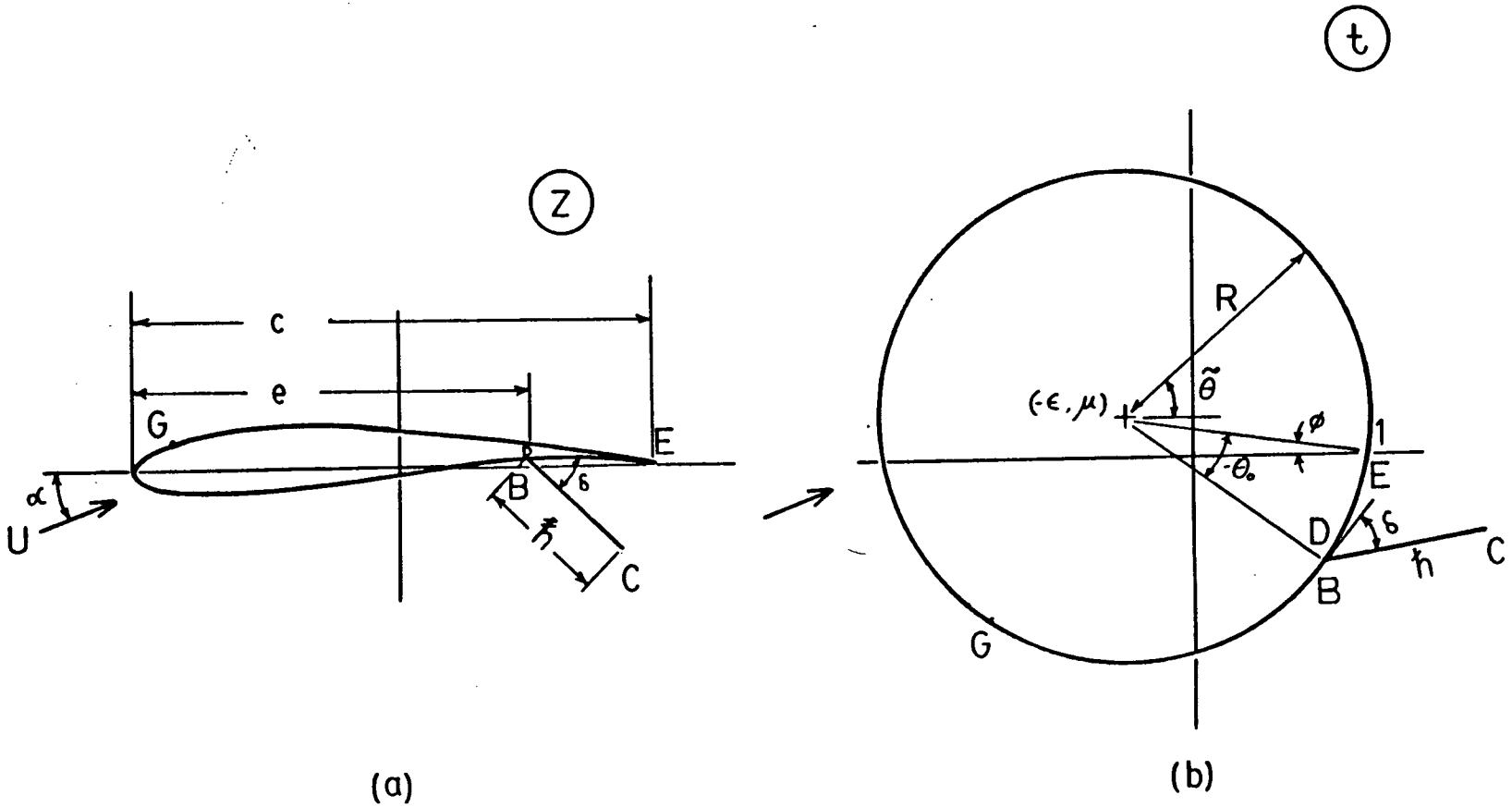

Fig. 5 Complex Transform Planes (Split Flap)

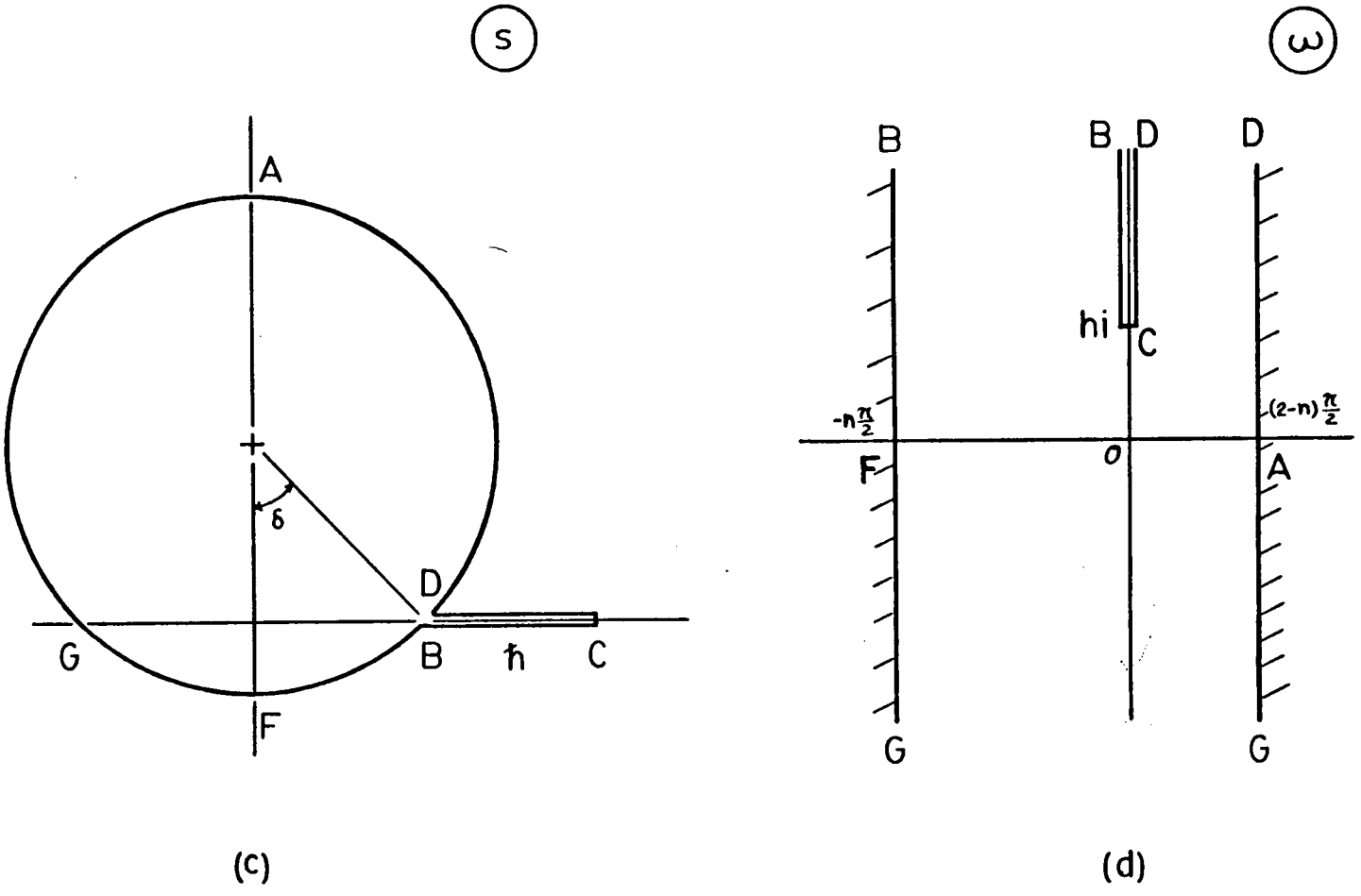

Fig. 5 Complex Transform Planes (Split Flap)

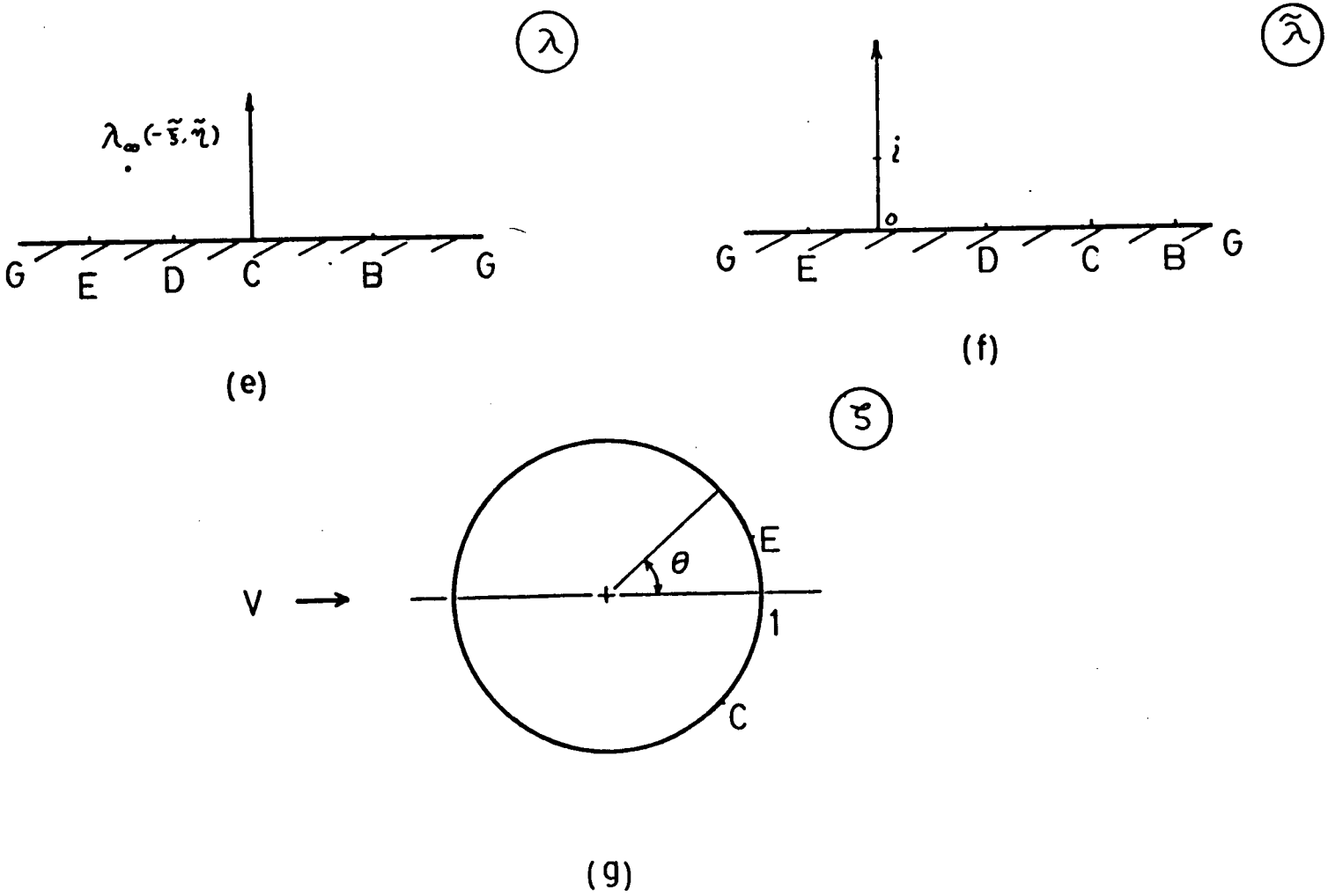

Fig. 5 Complex Transform Planes (Split Flap)

Table 3: *Split Flap*

$e/c = .80$, $\theta_0 = 51.25°$

δ	$\hbar$	$\tilde{\xi}$	$\tilde{\eta}$
10°	.7647	0.6769	0.3865
30°	.7146	1.5339	1.5341
45°	.6842	1.6851	2.5233
60°	.6591	1.4212	4.3691

$e/c = .70$, $\theta_0 = 63.75°$

δ	$\hbar$	$\tilde{\xi}$	$\tilde{\eta}$
10°	.9861	0.5139	0.3461
30°	.9459	1.1403	1.2768
45°	.9257	1.2278	2.0250
60°	.9056	1.0208	2.6849

Table 4 : Co-ordinates of points B, C, D, E, A, G, F in different planes for *split flaps.*

Point	t-plane	s-plane	ω-plane
B	$t_0 + R\,e^{-i\theta_0}$	$R \sin \delta$	$-n\pi/2 + i\infty$ or $+ i\infty$
C	$t_0 + R\,e^{-i\theta_0} + \acute{h}\,e^{i\gamma}$	$R \sin \delta + \acute{h}$	h i
D	$t_0 + R\,e^{-i\theta_0}$	$R \sin \delta$	$(2-n)\pi/2 + i\infty$ or $+ i\infty$
E	1	$(1 - \Lambda)e^{-i\gamma}$	$2 \cot^{-1} [(\Lambda - 1)e^{i\gamma}/(R \sin \delta)]$
A	$t_0 - R\,e^{-i(\theta_0+\delta)}$	$(R + R \cos \delta)i$	$(2-n)\pi/2$
G	$t_0 + R\,e^{-i(\theta_0+ 2\delta)}$	$-R \sin \delta$	$-n\pi/2 - i\infty$ or $(2-n)\pi/2 - i\infty$
F	$t_0 + R\,e^{-i(\theta_0+\delta)}$	$-(R - R \cos \delta)i$	$-n\pi/2$

3.2 Dynamics

In the physical plane z the uniform flow, when approaching the airfoil, separates from the trailing edge and the tip of the spoiler or split flap. A highly turbulent broad wake, situated behind the spoiler or split flap and bounded by the separating shear layers emanating from the points of separation, is formed and found, experimentally, to be nearly at constant pressure. Owing to the complexity of the wake dynamics, including the formation of Kàrmàn vortex streets, and to the insufficient understanding of the interaction between the wake and the shear layers, no theories are available to correctly predict the pressure inside the wake. A good review of the work done in this field can be found in Chang [9]. As a result, this base pressure is treated as a constant value and provided empirically, as done in [2,3]. It is expressed in a dimensionless form,

$$C_{p_b} = (p_b - p_\infty)/(\tfrac{1}{2}\rho U^2)$$

where p_b is the pressure inside the wake,
and p_∞ is the upstream undisturbed pressure.

The flow exterior to the airfoil is transformed to that outside of the unit circle in the ζ-plane. It is modelled by superimposing on the basic flow past the transform circle, suitable singularities inside the appropriate region to simulate the wake and its effects on the outer flow. The semi-infinite wake thus created is enclosed by two

non-intersecting streamlines, see Fig. 28 of [3], which, when viewed from the physical plane, is assumed to represent the approximate shapes of the separated shear layers or the time-averaged boundaries of the wake bubble. These source singularities, however, have to be located on the circumference, in the wake region, to satisfy the separation pressure boundary conditions.

3.2.1 Mathematical Flow Model

Figs. 6a,b depict the representation of the required singularities in the ζ-plane. They must lie within arc EC. If the case of a spoiler is considered, then Fig. 6a shows that point C will represent the spoiler tip and point E, the trailing edge. For the case of a split flap, point E becomes the trailing edge and point C is the tip of the flap, as shown in Fig. 6b.

The basic flow past a circle is the usual combination of the uniform flow at zero incidence with respect to the real axis, and a doublet of suitable strength at the origin. Since an airfoil is a lifting body of non-zero circulation around it, a vortex located at the origin is needed. In order to simulate flow separation at points E and C, either one or two sources are added on the arc EC. Both possibilities have been explored and will be referred to as 1-source and 2-source models respectively.

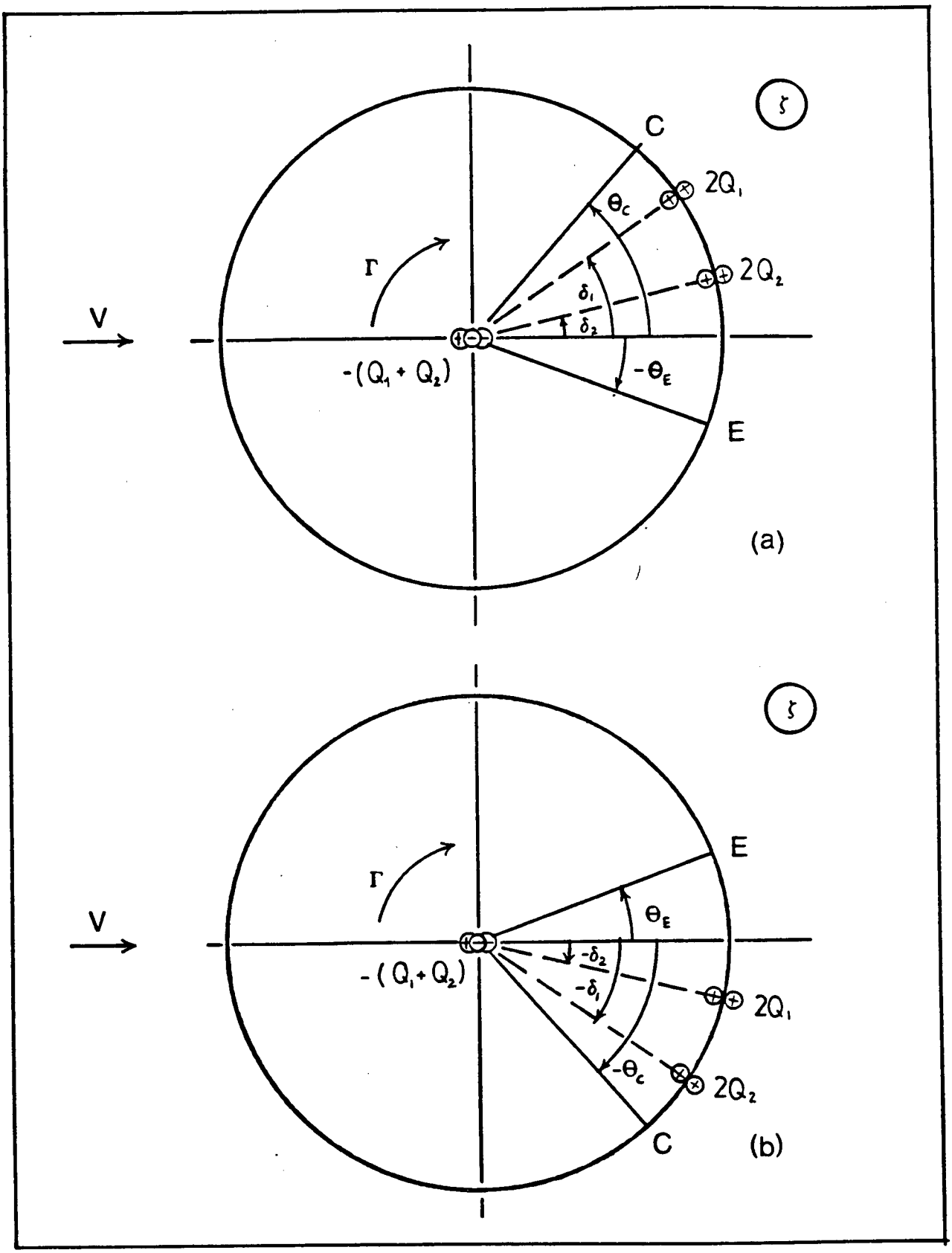

Fig. 6 Locations of Singularities

From Milne-Thomson's Circle Theorem, with a source placed outside a solid circular boundary, an image source and a sink are required inside the boundary so that the circular shape of the streamline is preserved. In the limiting case when the added source is on the perimeter, the image source will move to the same location as the added source, and the sink will still be at the origin. It is the reason why two double sources on arc EC and a double sink at the origin are shown in Figs. 6a,b for the 2-source model.

The complex potential for the 2-source model in the ζ-plane is

$$F(\zeta) = V\left(\zeta + \frac{1}{\zeta}\right) + \frac{i\Gamma}{2\pi} \ln \zeta + \frac{Q_1}{\pi} \ln (\zeta - \zeta_1) + \frac{Q_2}{\pi} \ln (\zeta - \zeta_2) - \frac{(Q_1 + Q_2)}{2\pi} \ln \zeta \qquad \ldots \quad (26)$$

The complex velocity, $W(\zeta) = \frac{dF}{d\zeta}$, becomes

$$W(\zeta) = V\left(1 - \frac{1}{\zeta^2}\right) + \frac{i\Gamma}{2\pi} \frac{1}{\zeta} + \frac{Q_1}{\pi} \frac{1}{\zeta - \zeta_1} + \frac{Q_2}{\pi} \frac{1}{\zeta - \zeta_2} - \frac{(Q_1 + Q_2)}{2\pi} \frac{1}{\zeta} \qquad \ldots \quad (27)$$

V is defined in equation (12). Q_1, Q_2, Γ, ζ_1 and ζ_2 are strengths of the sources and circulation, and the angular positions of the sources, respectively. Since the sources are on the surface, one can write

$$\zeta = e^{i\theta}, \qquad \zeta_1 = e^{i\theta_1}, \qquad \zeta_2 = e^{i\theta_2}$$

Equation (27) can then be simplified to

$$\frac{W(\zeta)}{V} = \frac{e^{-i\theta}}{2i}[-4 \sin\theta - 2\gamma + q_1 \cot(\frac{\theta-\delta_1}{2}) + q_2 \cot(\frac{\theta-\delta_2}{2})] \quad \ldots \quad (28)$$

where $q_1 = \frac{Q_1}{\pi V}$, $q_2 = \frac{Q_2}{\pi V}$, $\gamma = \frac{\Gamma}{2\pi V}$

The complex velocity in the z-plane is

$$W(z) = W(\zeta)/(\frac{dz}{d\zeta}) \quad \ldots \quad (29)$$

The quantities q_1, q_2, γ, δ_1 and δ_2 will be determined through suitable boundary conditions. For the 1-source model, only q_1, γ and δ_1 will be of non-zero values. The number of unknowns then reduces from 5 to 3.

3.2.2 Boundary Conditions

There are totally 5 unknowns for the 2-source model so that we have to seek the same number of independent boundary conditions.

In the sequence of transformations, sharp edges such as points E and C are made critical points at which $\frac{dz}{d\zeta} = 0$. According to the equation (29), W(z) at these points will be infinite if $W(\zeta)$ is non-zero, a case considered to be unrealistic, since the pressure will also be infinite. As a result, the first two boundary conditions will correspond to setting $W(\zeta) = 0$ at these points in the ζ-plane. These conditions are usually referred to as Kutta conditions, and are equivalent to having the flow leave the trailing edge and

the tip of the spoiler or split flap tangentially. Therefore, we arrive at

$$q_1 \cot\left(\frac{\theta-\delta_1}{2}\right) + q_2 \cot\left(\frac{\theta-\delta_2}{2}\right) - 4 \sin\theta - 2\gamma = 0$$

$$\text{at } \theta = \theta_E \qquad \ldots \quad (30)$$

$$\text{at } \theta = \theta_C \qquad \ldots \quad (31)$$

The pressure at the points of separation will be matched to that of the wake through Bernoulli's equation :

$$\frac{p}{\rho} + \frac{|W(z)|^2}{2} = \frac{p_\infty}{\rho} + \frac{U^2}{2} \qquad \ldots \quad (32)$$

Therefore, two additional boundary conditions are evolved :

$$C_{p_E} = \frac{p_E - p_\infty}{\frac{1}{2}\rho U^2} = 1 - \left|\frac{W(z)}{U}\right|^2_E = C_{p_b} \qquad \ldots \quad (33)$$

and

$$C_{p_C} = \frac{p_C - p_\infty}{\frac{1}{2}\rho U^2} = 1 - \left|\frac{W(z)}{U}\right|^2_C = C_{p_b} \qquad \ldots \quad (34)$$

However, the limiting values of $\left|\frac{W(z)}{U}\right|$ at E and C must be obtained by using l'Hôpital's rule since W(z) is in an indeterminate form, see appendices F & G for details.

3.2.3 1-source Models

There are two distinct 1-source models, depending on the choice of the boundary conditions. These models are obtained by setting either q_1 or q_2 to zero. To be consistent, q_2 is eliminated for the following discussion. The unknowns are then q_1, δ_1 and γ.

The first model corresponds to satisfying the Kutta condition both at the critical points E and C, and to matching the pressure at point E to that of the wake. The other model is obtained in exactly the same way but with the pressure at C, instead of E, equal to that of the wake. Mathematically, they can be written as

first 1-source model:

$$W(\zeta) = 0 \quad \text{at } \zeta = \zeta_E \text{ and } \zeta_C$$

and

$$C_{p_b} = C_{p_E};$$

second 1-source model:

$$W(\zeta) = 0 \quad \text{at } \zeta = \zeta_E \text{ and } \zeta_C$$

and

$$C_{p_b} = C_{p_C}.$$

These models are, however, considered to be unrealistic because, in general, the pressure at E is not the same as that at C in each model. This discontinuity of pressure is undesirable since experimental results do not support this phenomenon. Nevertheless, these models are simple in the sense that only a single empirical input, the base pressure, is required. It will be seen later on that these models play a significant role in constructing a 5^{th} boundary condition for the 2-source model.

3.2.4 Additional Boundary Conditions

Contriving a 5^{th} boundary condition, which is admissible both physically and mathematically, is not a trivial task. More often, more empirical information may be involved, as seen in Jandali's discussion [3]. However, as shown in [10], the criterion of streamlines possessing finite curvature at separation proves to successfully model the flow around a circular cylinder at Re = $2(10)^6$. Consequently, the empirical specification of the angle of separation is eliminated.

This criterion sounds promising for surfaces of continuous curvature, such as the portion near the trailing edge of an airfoil. As indicated by Woods[6], it also leads to the consequence of finite pressure gradient at separation. Although the experimental support of this criterion is not obvious for spoilers, there is a fair amount of data which substantiates this idea even though they are concerned with airfoils other than the Joukowsky family.

The mathematical equation, which describes the criterion of finite pressure gradient, is

$$f_2' f_1'' - f_1' f_2'' = 0 \qquad \ldots \quad (35)$$

where $f_1 = |W(\zeta)|_E$, $f_2 = |\frac{dz}{d\zeta}|_E$ ... (36a,b)

and $( )' = \frac{d}{d\theta}$.

The derivation of (35) and the further simplification of (36a,b) can be found in appendices F and G. Note that the non-dimensional circulation unknown, γ, does not appear in

(35) since only the derivatives of f_1 are involved.

Another plausible boundary condition can be set up to approximate the circulation across the wake. Let Γ be the total circulation around the contour C enclosing the airfoil with a spoiler or a split flap, see Fig. 7. This contour is then shrunk on to the boundary of the airfoil and split into two parts : one running from the tip of the spoiler (the trailing edge) to the trailing edge (the tip of the flap) including the portion exposed to the wake, and the other one going around the left-over portion, Fig. 8. Since the total head is substantially reduced there, experiments show that the time-averaged velocity in the wake is near zero. If the circulation in the wake is defined as (in the z-plane)

$$\Gamma_{wake} = \int_{wake} \bar{v} \cdot d\bar{s} \qquad \ldots \quad (37)$$

then, since $|\bar{v}|$ is small, to the 1^{st} approximation,

$$\Gamma_{wake} = 0$$

Since circulation is invariant under transformations, equation (37) in the ζ-plane can be rewritten as

$$\Gamma_{wake} = \int_{wake} |W(\zeta)| \, d\theta = 0 \qquad \ldots \quad (38)$$

where $W(\zeta)$ is given by (28). After carrying out the integration, the general expression is

$$[4\cos\theta - 2\gamma\theta + 2q_1 \ln|\sin\Delta_1| + 2q_2 \ln|\sin\Delta_2|]_{\theta_2}^{\theta_1} = 0$$

where $\Delta_1 = \left(\frac{\theta-\delta_1}{2}\right)$

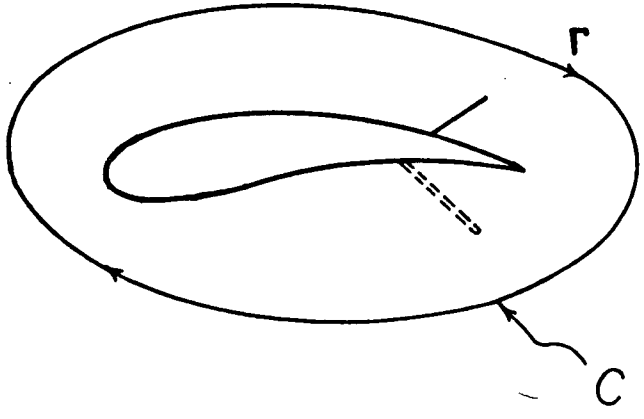

Fig. 7 Circulation around Airfoil

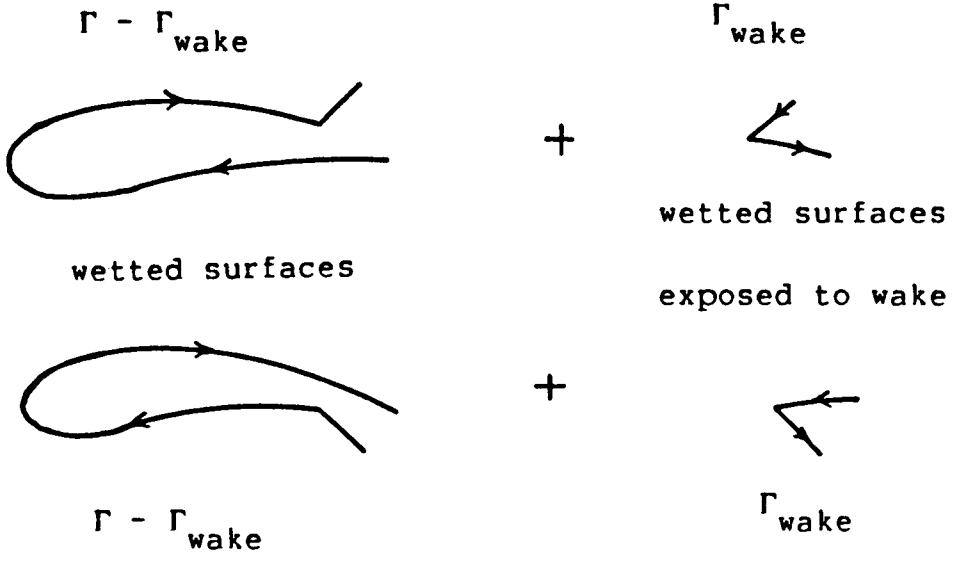

Fig. 8 Contour Deformation

$$\Delta_2 = \left(\frac{\theta-\delta_2}{2}\right)$$

$\theta_1 = \theta_C \qquad \theta_2 = \theta_E \qquad$ for spoilers,

$\theta_1 = \theta_E \qquad \theta_2 = \theta_C \qquad$ for split flaps.

Finally, another boundary condition based on the last one is developed because it gives the best result when compared with experiments. Instead of equating Γ_{wake} to zero, it is changed to a number, which depends upon the solution of the two 1-source models. Let Γ_{w_1} and Γ_{w_2} be the values of the circulation across the wake obtained by the two 1-source models by (37). Then

$$\Gamma_{wake} = (\Gamma_{w_1} + \Gamma_{w_2})/2 \qquad \ldots \quad (39)$$

is the modified 5^{th} boundary condition, where Γ_{wake} is defined in (38).

Equation (39) seems artificial and not physically obvious because it involves the two unrealistic 1-source models. However, its validity surfaces in the light of an example, the flow around a circular cylinder. Because of the geometric symmetry, the sources' strengths must be identical and their locations are at $\theta = \pm\delta_1$, when the wake source model is used to deal with this problem [2]. Therefore, the corresponding "1-source" models will be no different from the 2-source model since the pressures at the points of separation are automatically matched in all cases. Consequently, the solutions of the unknowns are the same and so are the values of Γ_{w_1}, Γ_{w_2} and Γ_{wake}. Equation (39) then reduces to an

identity. In other words, no ambiguous and additional restriction is imposed on the model. In fact, the similar deduction holds for flows around any symmetrical bodies at zero incidence. Of course, the above argument shows that equation (39) is only a necessary condition for bodies around which $\Gamma = \Gamma_{wetted} = \Gamma_{wake} = 0$. Similar deductions, however, cannot be reached for bodies of arbitrary shapes at non-zero incidence. For asymmetric bodies such as the one considered in this work, the non-zero right-hand side of (39) is used to account for the circulation across the wake, which is not necessarily zero in general.

3.2.5 Method of Solution and Calculation

The 3 unknowns associated with each of the 1-source models, q_1, δ_1 and γ, are determined by solving equations (30), (31) and one of (33) and (34), depending upon which model is considered. These equations can be simplified to one involving δ_1 alone because γ can be eliminated between (30) and (31), and q_1 appears only linearly in all equations. However, the reduced single equation must be solved numerically because of its complex form. Several computer subroutines are available in the computer system at UBC. The most robust one, NDINVT, which is written to locate a root of N non-linear simultaneous equations by using the generalized secant method, is invoked to solve for δ_1. An initial estimate of the unknown, which must be provided by the user, can be of any number chosen between the values of θ_E and θ_C, where the source is assumed to lie. If the iterative process does not lead to convergence after 30 iterations, a different choice of the initial estimate should be considered.

Multiple roots within the specified domain are not likely and have been checked either by using another subroutine to search for multiple roots or by sketching the curve representing this single equation. Although a solution is not guaranteed, experience shows that it does exist and can be found without much difficulty. After δ_1 is obtained, q_1 can be computed by substituting δ_1 into equation (33) or (34), again depending upon which model is used. γ is then calculated by

substituting q_1 and δ_1 into (30) or (31).

The solutions from 1-source models are essential because they serve as good estimates of the unknowns and provide the right hand side of equation (39) for the 2-source model which is considered to be more interesting and realistic.

For the case of the 2-source model, equations (30), (31), (33), (34) and one of (35), (38) and (39) are used to determine the 5 unknowns q_1, δ_1, q_2, δ_2 and γ. Again, since γ, q_1, q_2 appear linearly in this set of equations, it is possible to eliminate them and arrive at 2 equations involving δ_1 and δ_2. Further simplification, however, is impossible because these two equations are rather complicated. Therefore, NDINVT is used to solve for δ_1 and δ_2 numerically.

Nevertheless, both δ_1 and δ_2 appear in the arguments of the transcendental functions like cosecant (csc), cotangent (cot), and their products whose periodicities and singularities often prevent the iterative process from converging. Also, solutions do not always exist if (35) or (38) is used as the 5^{th} equation unless the experimental base pressure is altered. The above procedure also does not help in giving any clue to the existence of the solutions.

Consequently, a different strategy towards locating the solutions is devised and described herein. Even though they do not constitute a complete set of equations uniquely determining the 5 unknowns, (30), (31), (33) and (34) are the

fundamental equations in the model in the sense that any set of acceptable solutions must satisfy them. n sets of "solutions" of q_1, δ_1, q_2 and γ, however, can be obtained by solving these equations numerically by NDINVT if the position of q_2 is set to

$$\delta_2 = \theta_E + \frac{(\theta_C - \theta_E)\,i}{n+1} \quad , \quad i = 1,2,\ldots,n$$

where $\theta_E < \theta_C$ is assumed here.

These n sets of "solutions" are then substituted into whichever is chosen as the 5^{th} equation in order to evaluate the residue, which is exactly zero if the corresponding set of solutions satisfies all 5 equations. If the i^{th} and the $i+1^{th}$ sets of solutions cause a change of sign of the residue, then the existence of a set of solutions is guaranteed. More accurate values of this set of solutions can be found numerically by solving all 5 equations using NDINVT with the i^{th} or $i+1^{th}$ set of solutions as the initial guesses. Very often, only a few iterations are required before convergence is arrived at because the initial estimates are reasonably close to the roots. The possibility of the existence of multiple roots within arc EC has to be investigated by using different initial estimates of q_1, δ_1, γ and q_2 at each prescribed value of δ_2 mainly because no computer routines are available for detecting multiple roots of n (n>1) non-linear simultaneous equations. If the residue does not change sign for different values of δ_2 and no multiple roots exist, then it can be concluded that no solutions can satisfy these 5

equations. This is what is often encountered when (35) or (38) is used as the 5^{th} boundary condition.

δ_1 and δ_2 are interchangeable in the above scheme of searching for roots since no particular conditions are imposed to distinguish one from the other. However, because there is no obvious method of determining the upper and lower bounds of q_1, q_2 or γ, using any one of them to function as δ_1 or δ_2 is out of the question. Also, if $\delta_1(\delta_2)$ is specified, the equations are much more easy to solve since only $\delta_1(\delta_2)$ appears non-linearly.

Once the solutions for the above unknowns are obtained, the pressure on the airfoil surface can be calculated by

$$C_p = 1 - |W(\zeta)/(dz/d\zeta)|^2$$

where $W(\zeta)$ is defined by (28) and $\frac{dz}{d\zeta}$ is given by either (10) or (22).

If C_{pl} and C_{pu} are designated as the lower and upper surface pressure coefficients respectively, then integrating $(C_{pl} - C_{pu})$ with respect to the non-dimensional quantity (x'/c), where x' is in the direction of the flow at infinity and c is the chord length of the airfoil, the overall lift coefficient is given by

$$C_L = \int_0^{\cos\alpha} (C_{pl} - C_{pu})\, d(x'/c)$$

According to Fig. 9, only part of the pressure inside the wake contributes to the lift since the pressure is assumed to

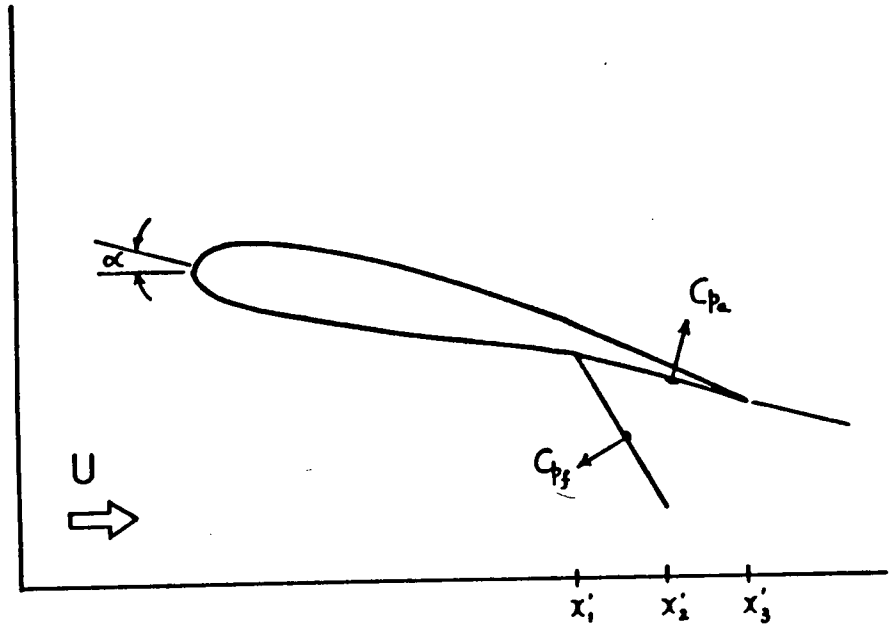

Fig. 9 C_L Contribution from the Wake (Split Flap)

be the same on the portion of the airfoil and the flap both exposed to the wake. In other words,

$$C_L' = \frac{1}{c} \int_{x_1'}^{x_2'} (C_{pa} - C_{pf}) \, dx' = 0$$

since $C_{pa} = C_{pf}$. The same result holds for spoilers.

In the calculations, t_o is (-0.085,0.05). The pressure coefficient is evaluated at 98 points on the airfoil surface and 10 points on the spoiler or split flap facing the upstream flow. The pressure in the wake is assumed constant and equal to that from experiments. A computer subroutine, QINT4P, is used to integrate the C_p values because this is the only available program for integration of a set of unequally spaced data points. The method is that for each interval, x_i to x_{i+1} , a cubic interpolation polynomial based on the four distinct points x_{i-1}, x_i, x_{i+1} and x_{i+2} is integrated. However, over the portion where C_p is constant, this program is not used because meaningless results are obtained in trying to fit a straight line with a cubic spline. This part of C_L is set to $C_p \Delta x'$, where $\Delta x'$ is the length of the portion.

4. EXPERIMENTS

There are two purposes in performing experiments in this work. The first is to measure the base pressure value inside the wake behind the spoiler or split flap because it is the required empirical input to the theory described in the previous sections. The second is to make comparisons between the theoretical and experimental pressure loading and the overall lift force on the airfoil at different angles of attack and for the various configurations involved.

Two series of experiments were carried out : one involving the airfoil and spoilers, and the other with the airfoil and split flaps. They were conducted in the small low speed aeronautical wind tunnel in the Department of Mechanical Engineering at the University of British Columbia. It has a test section of 27 inch height and 36 inch width. The tunnel possesses good flow uniformity and a turbulence level of less than 0.1 percent over its speed range. The Joukowsky airfoil of 27 inch span, 12.08 inch chord, 11 % thickness and 2.4% camber, is the same one used by Jandali. It was mounted vertically and spanned the test section, with small clearances at the ceiling and the floor. The airfoil was attached to a six component pyramidal balance situated beneath the test section of the tunnel, at the quarter chord position. 2 force and 1 moment components were measured over a wide range of

angles of attack.

The airfoil was originally designed for Jandali's experiments on normal upper surface spoilers. The detailed description of it can be found in his thesis [3]. Nevertheless, there is a point worth noting. Since the Joukowsky profile was structurally weak near the cusped trailing edge, the upper surface in this portion was thickened to give an approximately constant thickness of 1/8 inch. The whole profile is shown in Fig. 9 in [3]. This modified portion does not influence the pressure measurements for the upper surface spoiler experiments because it is completely embedded in the wake and has no effect on the outer flow. However, uncertainty in pressure measurements may result from clean airfoil experiments and those with the lower surface split flap deflected. In fact, Fig. 10 in Jandali's thesis provides some evidence. It would be preferable for the split flap experiments to have this modified portion located on the lower surface of the airfoil so that it is exposed to the wake. The information of the pressure variation along this portion of the upper surface is crucial to the criterion of the finite pressure gradient at separation discussed in 3.2.4.

During the course of experiments, end plates were used for supporting the spoiler or split flap but they do not touch either the roof or the floor. These plates were designed to allow the spoiler or split flap to be located at various positions and angles of inclination. The spoilers of height 5%

and 10% chord could be mounted at distances of 50%, 70%, and 90% chord positions from the leading edge of the airfoil. The 5% chord spoiler can only make an inclination of 45° whereas the 10% one is allowed to deflect at 30° and 60° with respect to the local upper surface of the airfoil. The two split flaps used have lengths of 20% and 30% chord. Their locations, measured from the trailing edge, are exactly equal to their lengths. The angles of inclination are 10°, 30°, 45°, and 60°. The small gap between the spoiler or flap and the airfoil surface is unvented by sealing it with masking tapes in the wake.

Owing to the small sizes of spoilers used, pressure measurements were made only on the wetted surface of each flap. They were measured by taping pressure taps over the surface so that the tubes were exposed to the outer flow. The pressures on the surface of the airfoil, including the portion within the wake, however, were measured by using the built-in pressure taps inside the Joukowsky airfoil. All pressure taps were connected to a 48 port scanivalve, a manually scanning pressure transducer. A Setra 237 differential pressure transducer, a HP 6204B D.C. power supply, a Solartron JM 1860 time domain analyser and a Fluke 8000A digital multimeter were used for data recording. Because of the limitation in time, no data acquisition system controlled by a microprocessor was set up .

Besides supporting the airfoil, the balance was used to measure not only the lift, but the drag and pitching moment, which were needed for the wind tunnel wall corrections. The wake blockage term $\epsilon_w = \frac{1}{4}(\frac{c}{H})C_D$, as suggested by Jandali, was employed for giving a better collapse for the data. c is the airfoil chord length and H is the effective test section width, defined as the ratio of the tunnel cross-sectional area to its height. C_D is defined as the difference between the drag coefficients with and without the spoiler or flap deflected. The corrected C_L is given by

$$C_L = C_{L_T} [\ 1 - 2\epsilon - \sigma\ ] - \frac{\sigma}{2\pi}[\ C_{L_T} + 4\ C_{M_{c/4_T}}\ ] \frac{\partial C_{L_T}}{\partial a} \qquad \ldots \quad (40)$$

where blockage factor $\epsilon = \epsilon_s + \epsilon_w$,
and soild blockage factor ϵ_s is as defined in [13],

$$\sigma = \frac{\pi^2}{48}(\frac{c}{H})^2,$$

$C_{M_{c/4}}$ = quarter chord moment.

The formula for correcting the pressure coefficient C_p is

$$\frac{1 - C_p}{1 - C_{p_T}} = \frac{C_L}{C_{L_T}}$$

where $(\ )_T$ denotes a value measured in the tunnel. The corrected C_p values are then integrated to give C_L by using the computer subroutine QINT4P described in the previous section. This reduced C_L instead of the one calculated from the balance data will be compared to the theoretical prediction. The test Reynolds number is $3(10)^5$.

It is just a matter of interest to mention that when the spoiler was located at 50% or 70% chord position when running the experiments, the airfoil was buffeting appreciably. This phenomenon is a result of having a large portion of the airfoil surface exposed to the wake. The corresponding pressure measurements should not be influenced to a great extent.

5. RESULTS AND COMPARISONS

To ensure that all pressure taps on the airfoil were functioning properly, an experiment on the clean airfoil without end plates was performed. The results closely agree with those obtained by Jandali, which can be found in [3] and will not be repeated here. By examining Fig. 10 in [3], it is clear that there is a little discrepancy between the theoretical and experimental pressure distributions at the leading edge at the same angle of attack. Similarly, deviations of the theoretical and experimental results are observed in the variation of lift with the angle of incidence in Fig. 11 in [3]. All these are explained by Jandali in terms of the presence of the boundary layer vorticity.

The measurements of base pressure in the wake exhibit some interesting trends when plotted against δ, at different values of α for split flap cases in Figs. 10a,b. Although there is no existing theory for predicting C_{pb}, it is plausible to consider an empirical formula of the following form

$$C_{pb} = A + B\,\delta + C\,\delta^2 + D\,\delta^3 \qquad \ldots \quad (41)$$

where A, B, C, and D are functions of α, flap length, and other parameters. Of course, more measurements in various geometric configurations must be performed in order to find

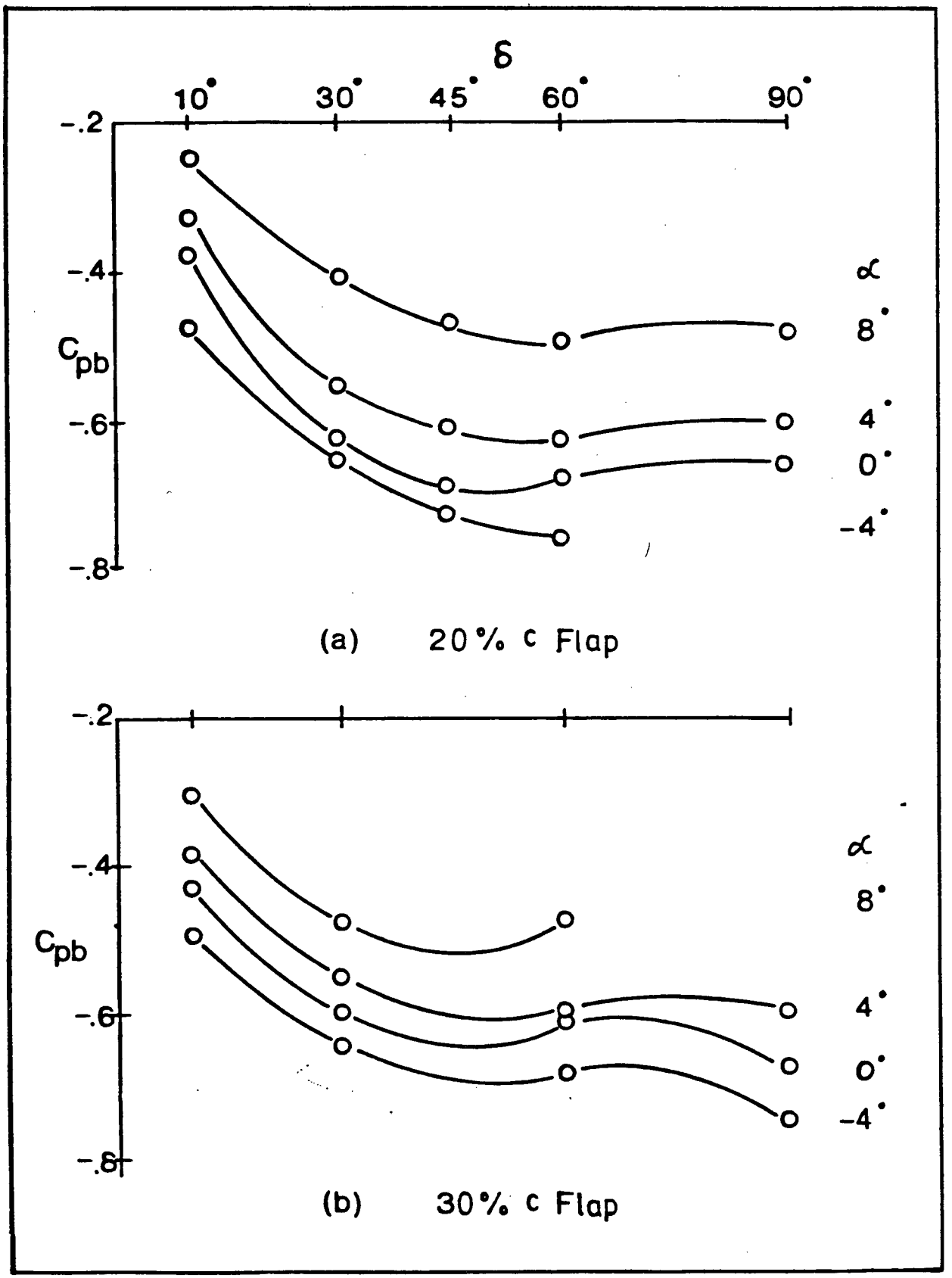

Fig. 10 C_{pb} Variations of 20% & 30% c Split Flaps

out the coefficients of (41). However, a formula for C_{pb} would be valuable to the theory described above. Tam Doo [11] conducted some thorough experimental investigations on C_{pb} for both vented and unvented normal spoilers on 2D and 3D wings. Interesting results can be found in his thesis. The purpose of this work, however, is not on the study of the variation of the base pressure. Consequently, no further work was carried out.

For the sake of simplicity, the theoretical C_p distributions corresponding to the 1-source models were calculated once the experimental C_{pb} values were available. For split flaps, it is found in general that the experimental C_p distribution over the upper surface of the airfoil lies within the two theoretical curves. More precisely, the 1-source model with $C_{pb} = C_p$ at the trailing edge (T.E.) overestimates the C_p distribution, and the model with $C_{pb} = C_p$ at the tip of the flap (T.F.) underestimates it. Over the lower surface, however, the prediction corresponding to $C_{pb} = C_{p\ T.F.}$ fits well to experiments, whereas the other theoretical curve shows a backward shift of the frontal stagnation point so that a discrepancy results. Fig. 11 is a typical result as described above. The theoretical C_p ($C_{pb} = C_{p\ T.E.}$) near the leading edge is finite, about -8.0, too large to be shown in the diagram. Although each of these models fails to match the pressure at the trailing edge to that of the tip of the flap, they provide the aerodynamicist with a fair estimate of the overall pressure distribution.

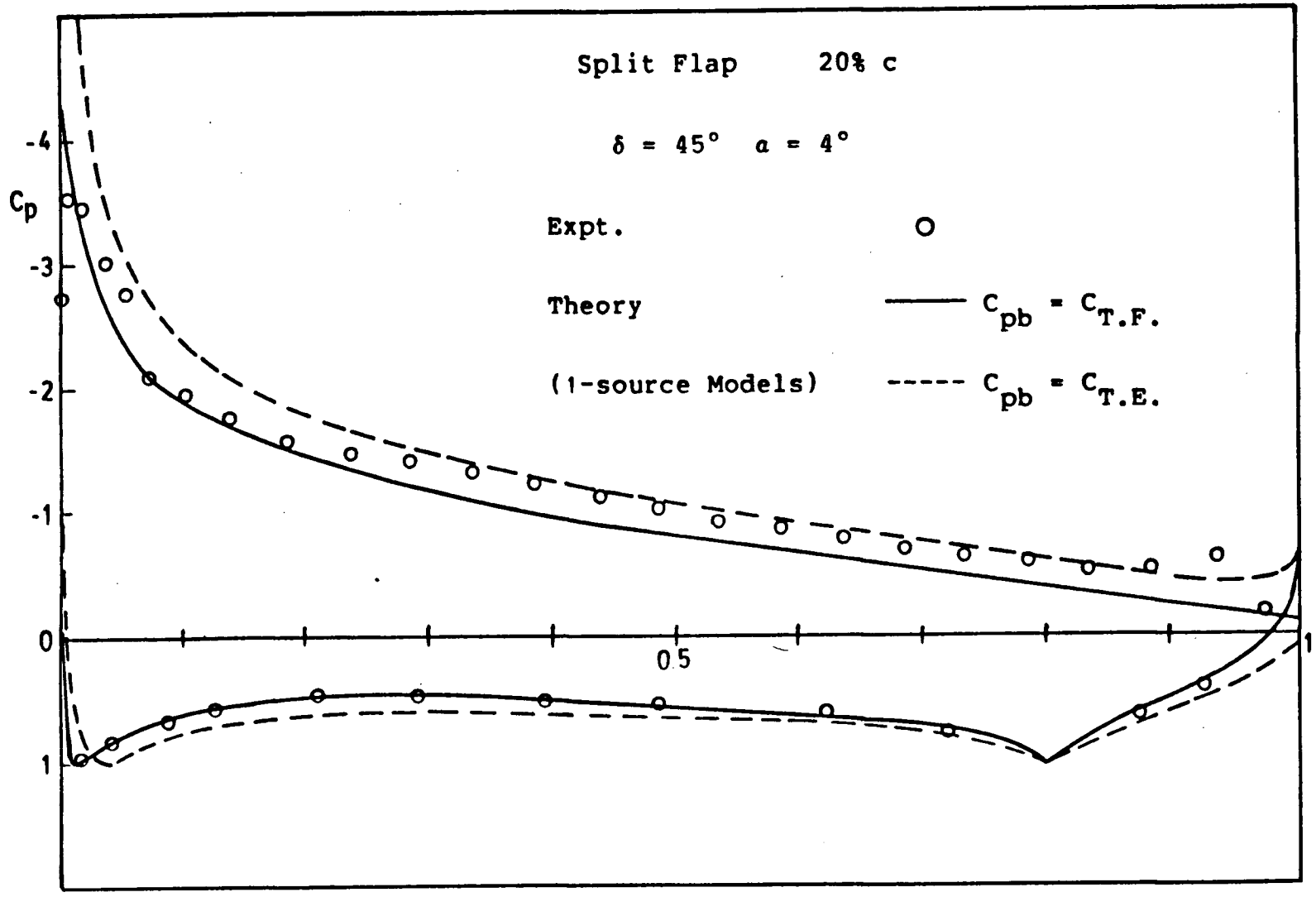

Fig. 11 Comparison on C_p Distributions from 1-source Models and Experiments

Very similar results were obtained for spoilers so that the above description is applicable except that the flap is replaced by the spoiler.

In order to improve the agreement between the theory and experiments, the criterion of finite curvature of the separating streamlines or that of the finite pressure gradient at separation for split flaps was investigated. It is found in general that to have it satisfied, one of the sources in the 2-source model must lie outside the simulated wake if the experimental C_{pb} is applied. This is not desirable because when evaluating the pressure along the airfoil surface, a singular behavior of C_p would be obtained at the location where the source is situated. In order to force the source to locate in the wake region, the input base pressure needs to be altered. Very often, it is more positive than the empirical value. For instance, for the case of the 20% chord split flap deflected at 30° at an angle of attack of 4°, the required C_{pb} is -.10 compared to -.54 from the experiment. Since there is no method of predicting this modified value except by trial and error, the study of this criterion was not pursued further even though the corresponding pressure distribution along the rest of the airfoil surface is not far from the experimental result as depicted in Fig. 12. Similar results have been found for spoilers, which seems understandable since not sufficient experimental data support the behavior of finite pressure gradient at separation.

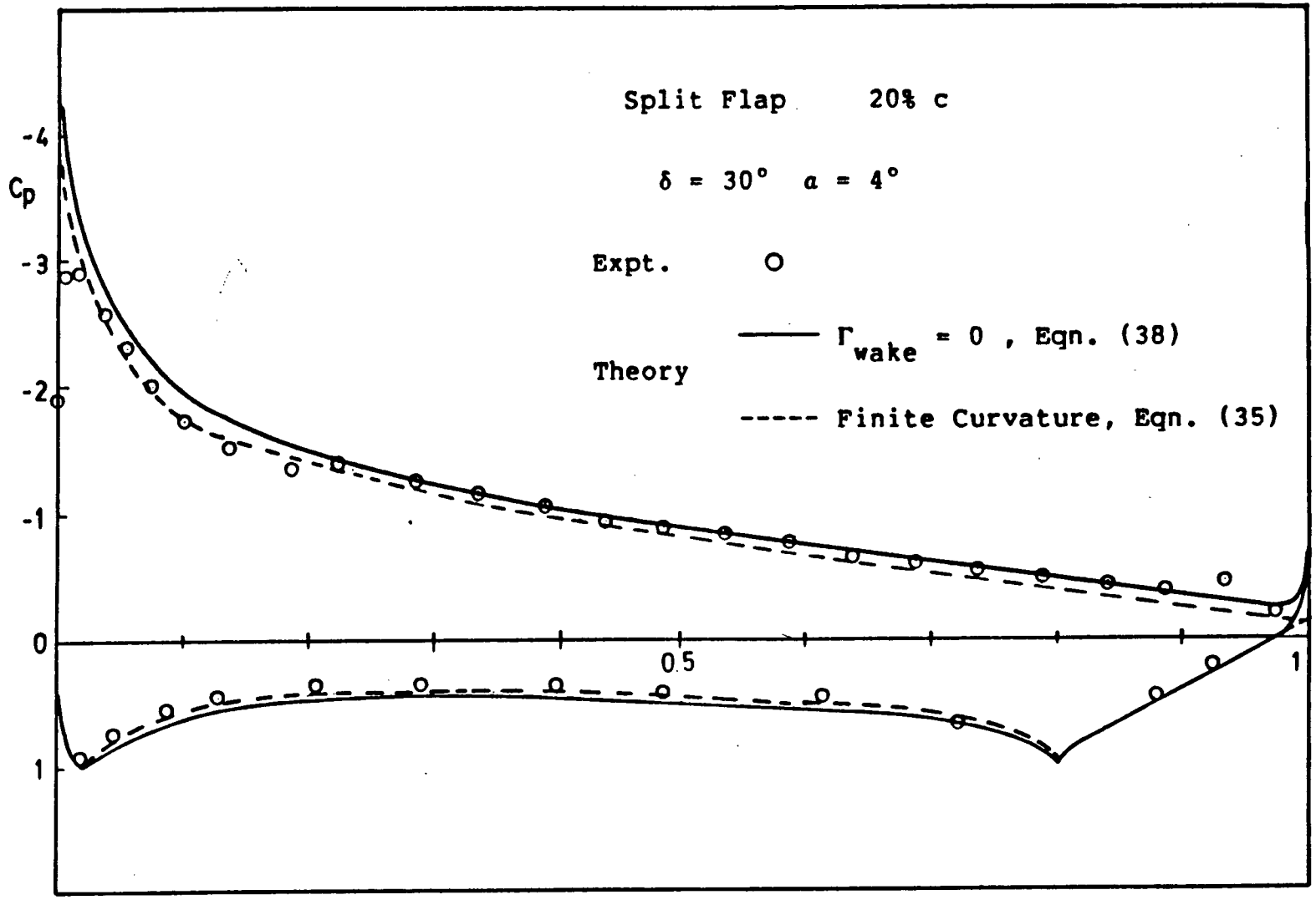

Fig. 12 Comparison on C_p Distributions from Eqns. (35) & (38) and Experiments

The boundary condition of zero circulation across the wake was then explored. Overall agreement on the chordwise pressure distribution is improved as can be seen in Fig. 12. Besides, for a good number of cases, the experimental C_{pb} is accepted by this 5^{th} boundary condition in the sense that both sources are lying within the wake. Near the trailing edge, the pressure gradient is rather steep when compared with that obtained by applying the finite pressure gradient condition. The pressure near the leading edge is overestimated by the theory, a similar result resembling that of the clean airfoil.

The problem of accepting the experimental C_{pb} values comes up again as the angle of deflection increases. For example, Fig. 13 shows the case of the 20 % chord flap at $\delta = 60°$, $\alpha = 0°$. To have $\Gamma_{wake} = 0$ satisfied, the experimental C_{pb} must be changed from -.67 to -.78. The resulting C_p is not accurate on both upper and lower surfaces. Besides, the pressure at the tip of the flap is matched abruptly to that at the trailing edge. It suggests that equation (38) should be used with reservation.

Considerable improvement is achieved if the boundary condition (39) is utilized. The experimental C_{pb} can be used without alteration and the abrupt jump of the C_p no longer prevails. Although the leading edge C_p value is slightly overestimated by the theory, as shown in Fig. 13, the overall agreement between the theory and experiments is remarkable. As a consequence, equation (39) is chosen over the others as the

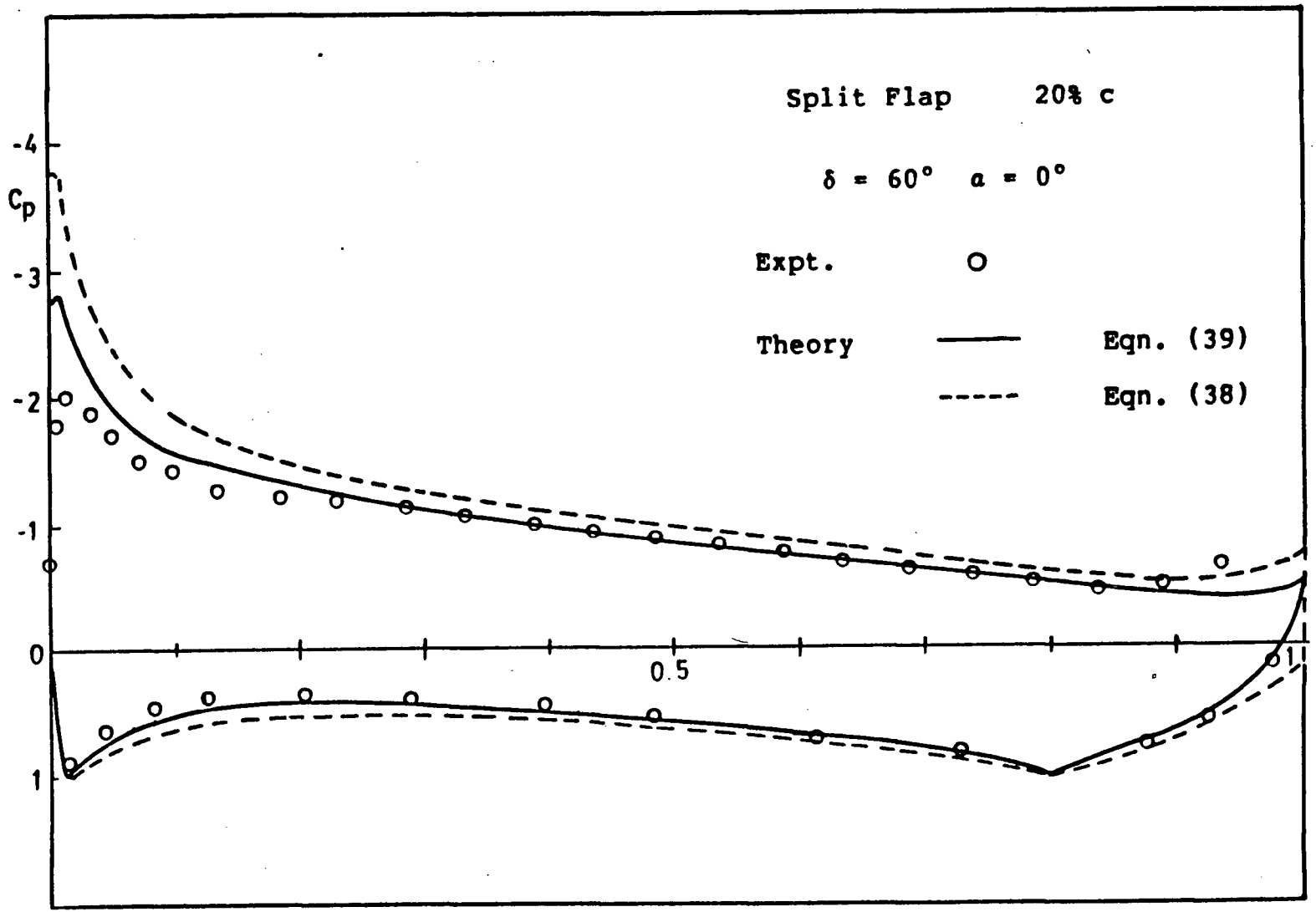

Fig. 13 Comparison on C_p Distributions from Eqns. (38) & (39) and Experiments

boundary condition to determine the C_p and C_L values for both split flaps and spoilers.

Fig. 14 shows the variation of C_p at δ = 10°, 30° and 60° at α = 4° for the 20 % chord flap. The integrated C_L is compared with experiments and shown in Fig. 15. Figs. 16 and 17 are the C_p and C_L variations for the 30 % chord flap, respectively.

Figs. 18-20 show the C_p distributions for the spoiler cases. The spoiler is located at e/c = 50 %, 70 % and 90 % chord distances from the leading edge. The spoiler height is 5 % chord, the angle of deflection is 45° and the angles of attack are 6° and 12°. The corresponding C_L curves are shown in Figs. 21-23.

The C_p distributions on the airfoil with 10 % chord spoiler are depicted in Figs. 24-26 at δ = 30° and 60° and at α = 6°. Figs. 27-29 show the C_p distributions at α = 12°. Figs. 30-32 are the lift coefficients of the airfoil when the spoiler is located at 50 %, 70 % and 90 % chord positions.

The theory predicts the base of the spoiler as a stagnation point. Therefore, the corresponding C_p value is 1.0. However, experiments show that flow separation takes place to form a separation bubble before the fluid particles reach this location. The presence of the bubble is not so clear in front of the split flap but rather obvious upstream of the spoiler. As a result, difference between theoretical

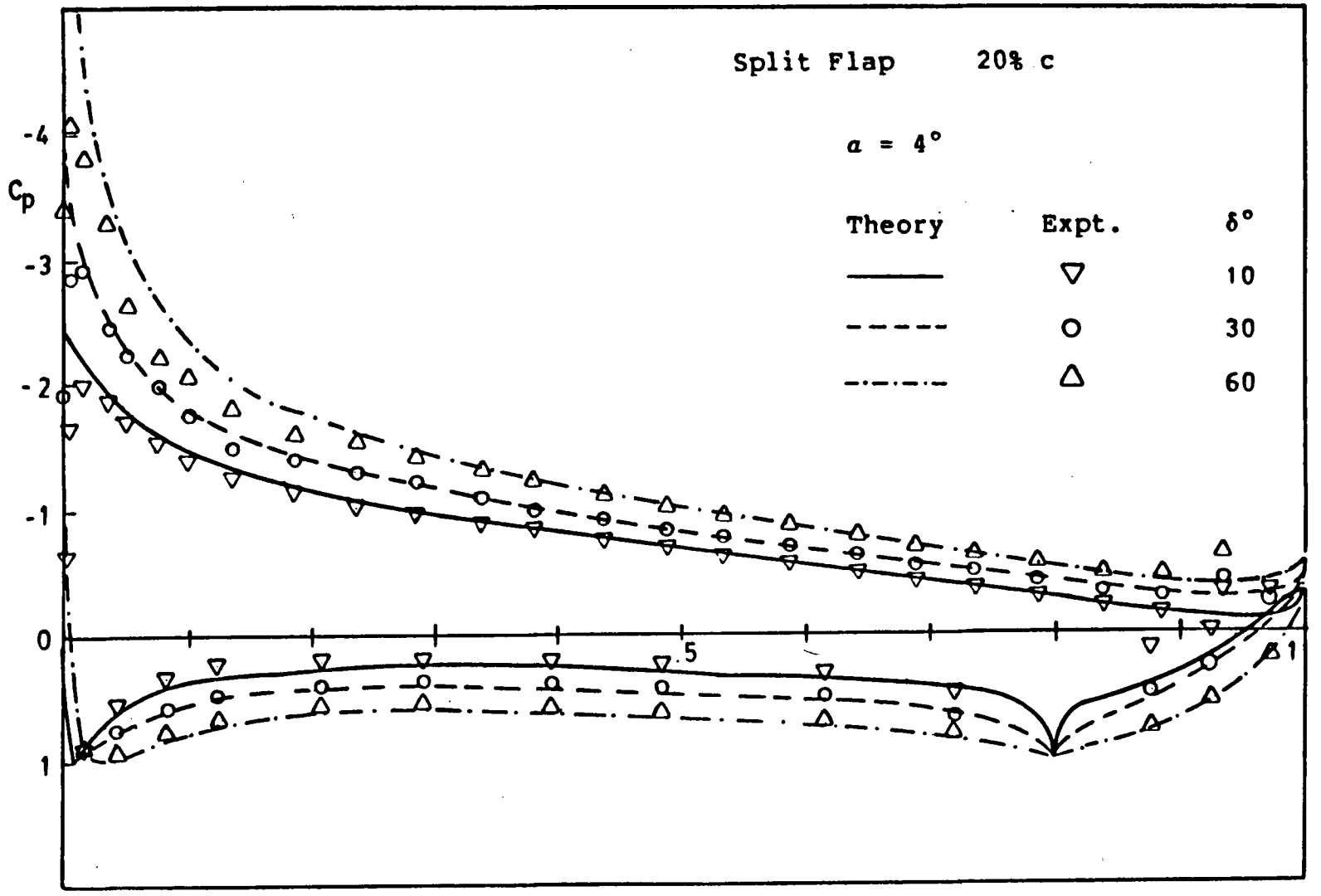

Fig. 14 C_p Distributions at Different δ (20% c Split Flap)

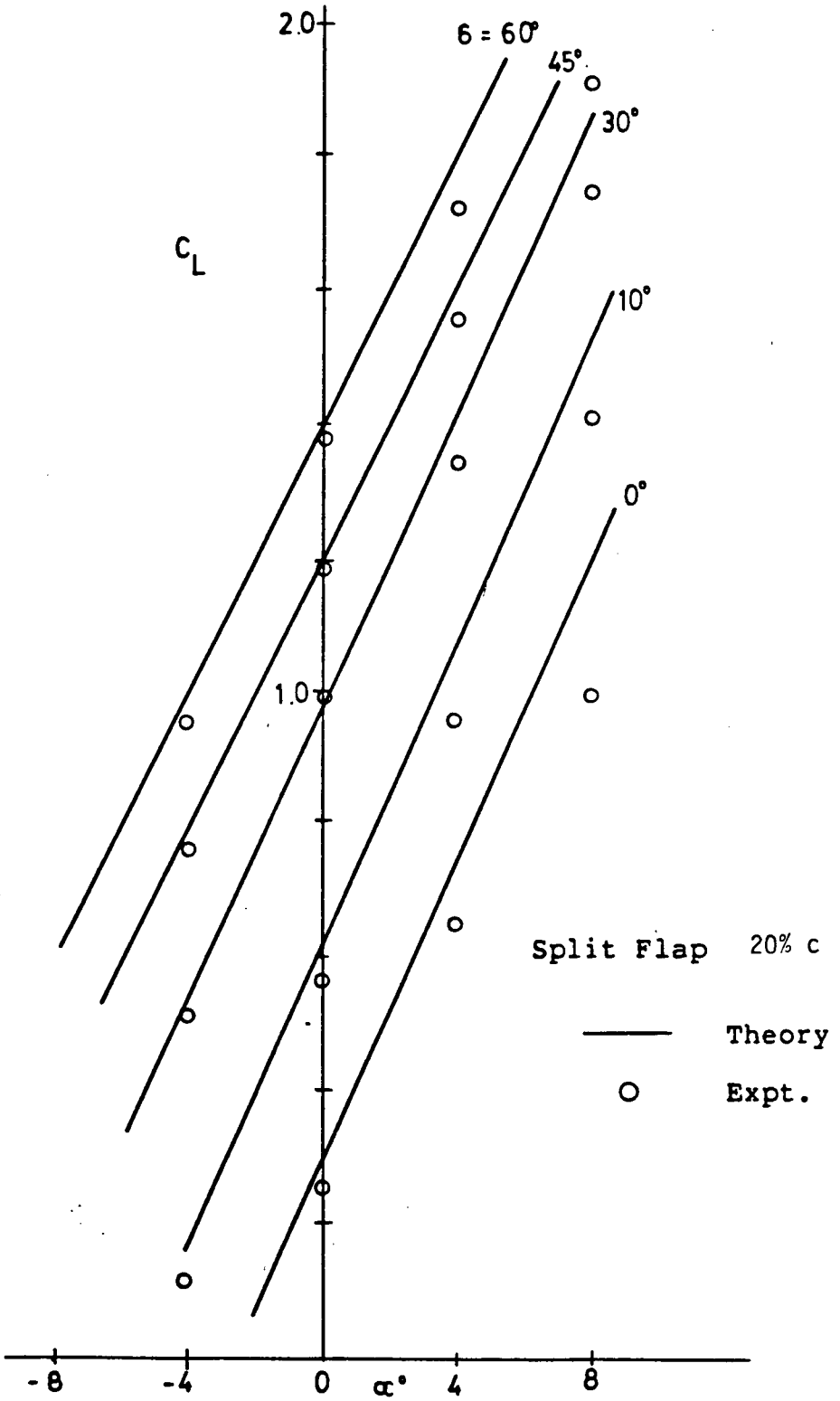

Fig. 15 C_L Variations over α at Different δ

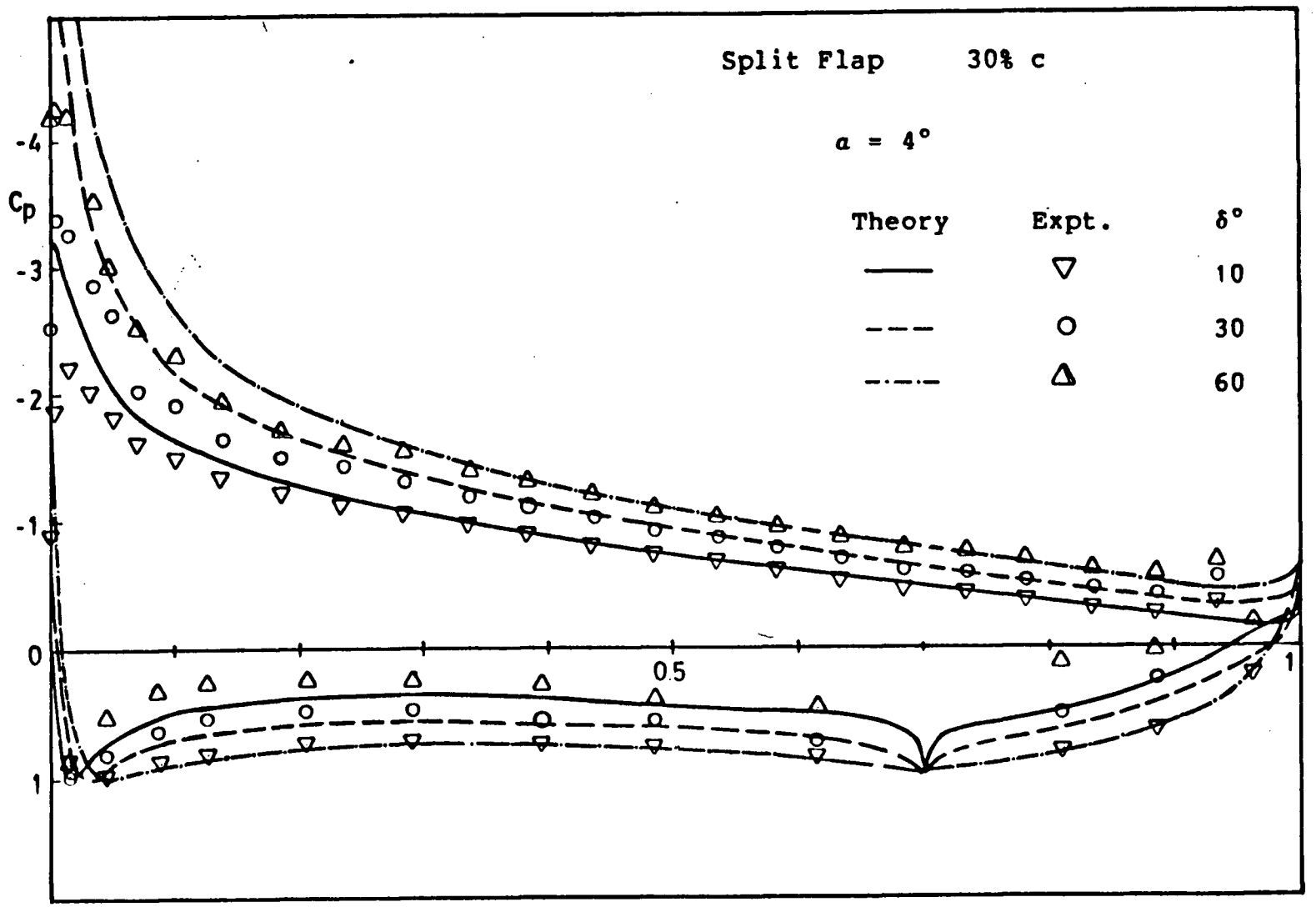

Fig. 16 C_p Distributions at Different δ (30% c Split Flap)

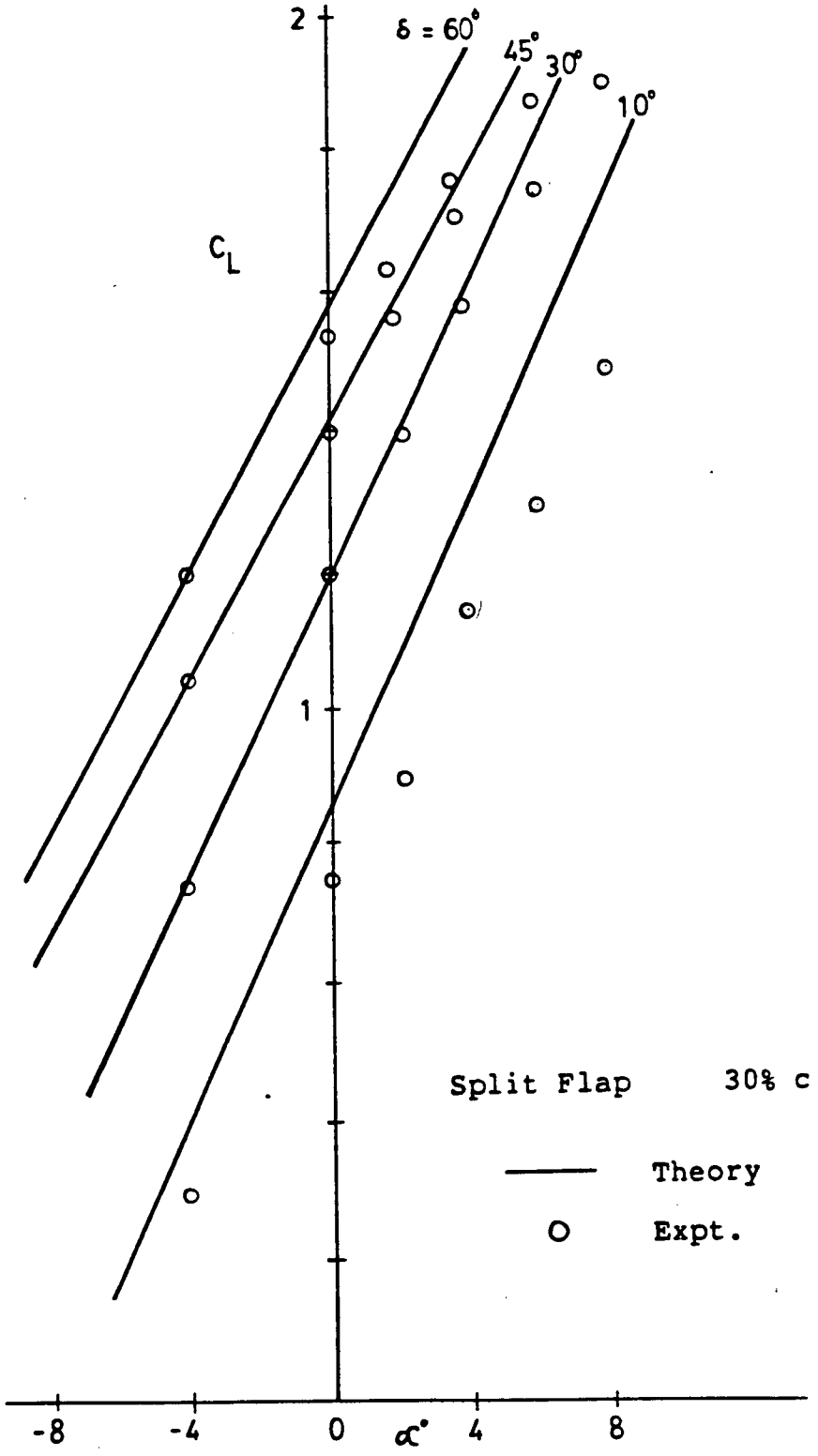

Fig. 17 C_L Variations over α at Different δ

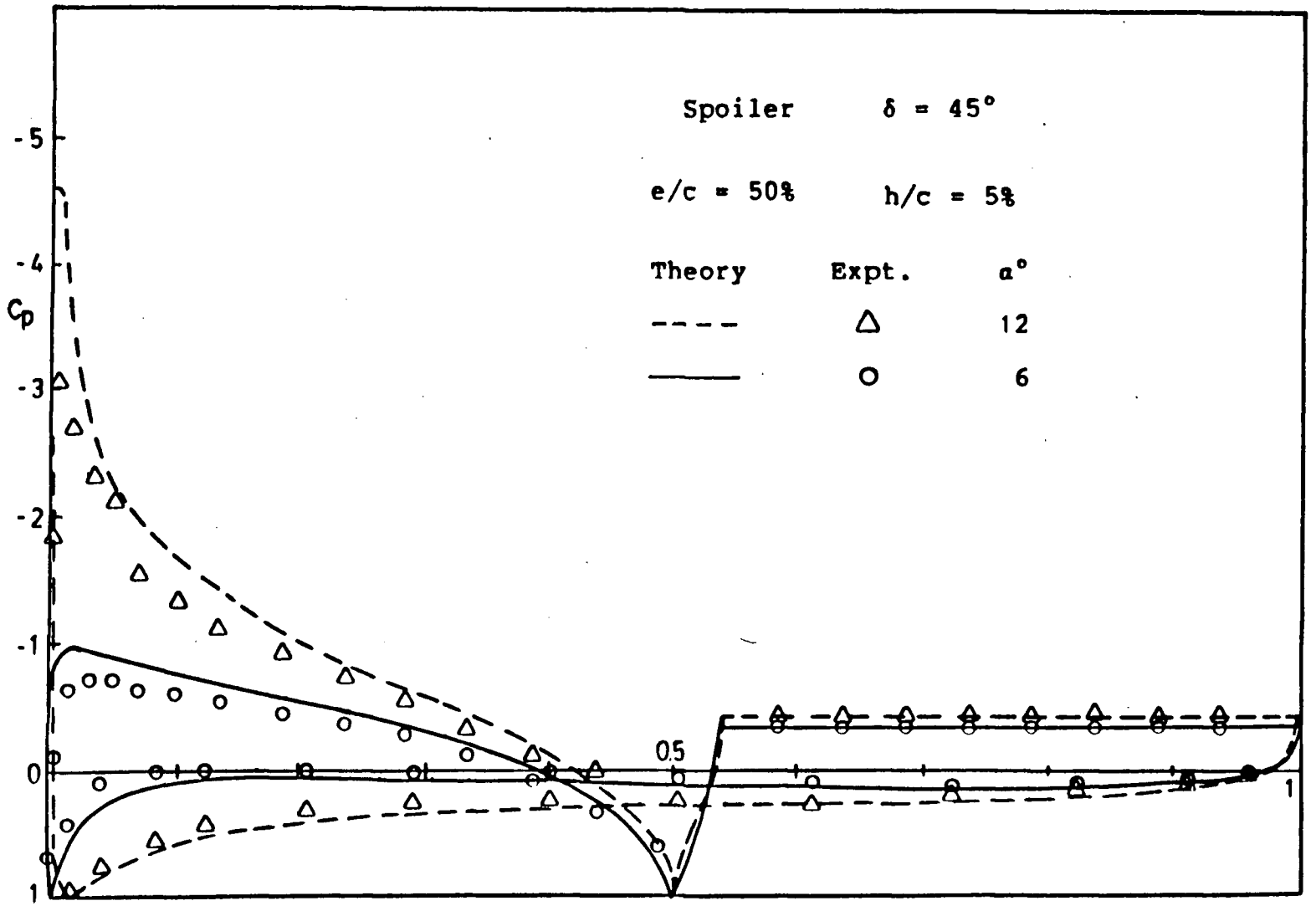

Fig. 18 C_p Distributions (spoiler, e/c = 50%, h/c = 5 %, δ = 45°)

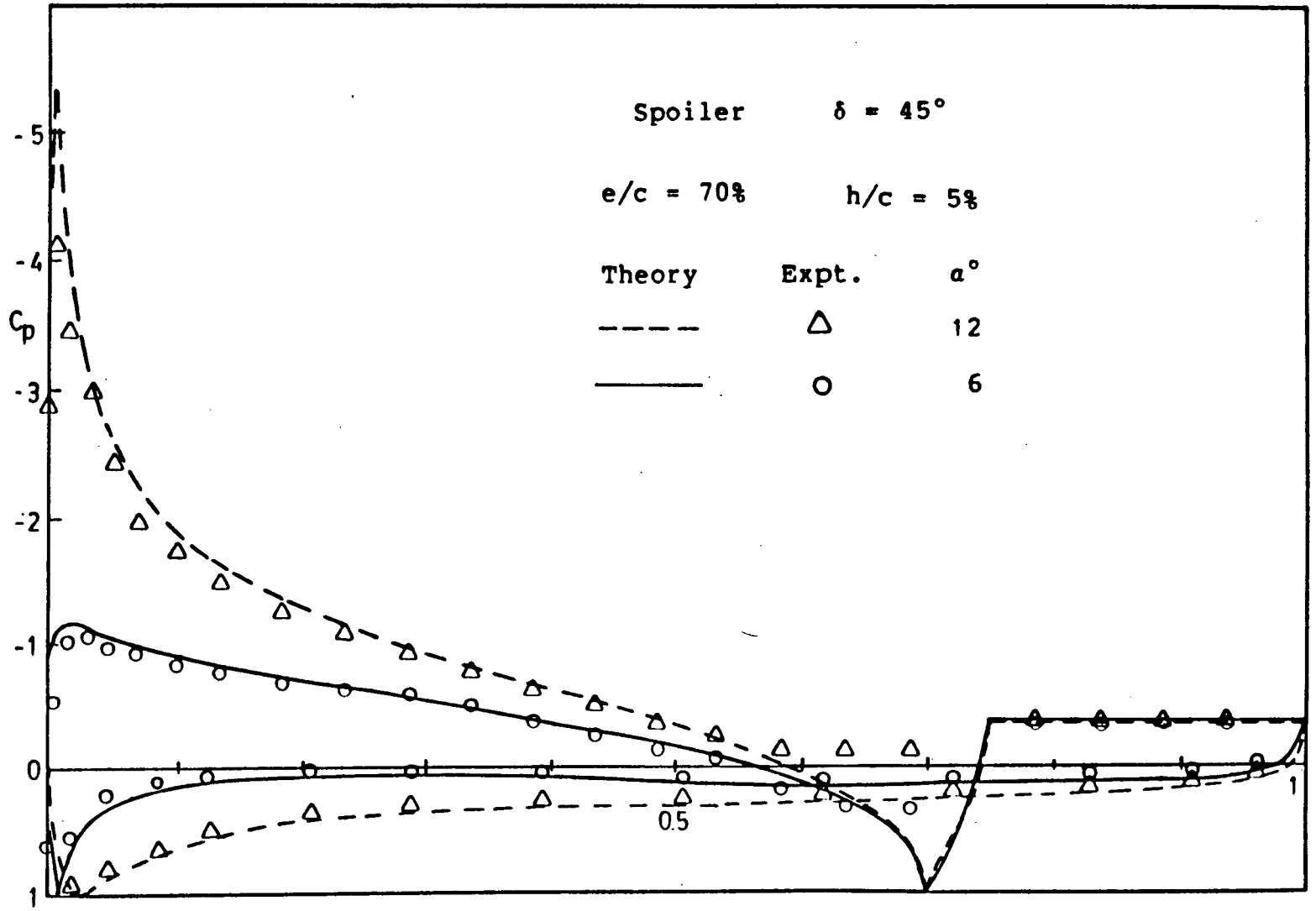

Fig. 19 C_p Distributions (spoiler, e/c = 70%, h/c = 5 %, δ = 45°)

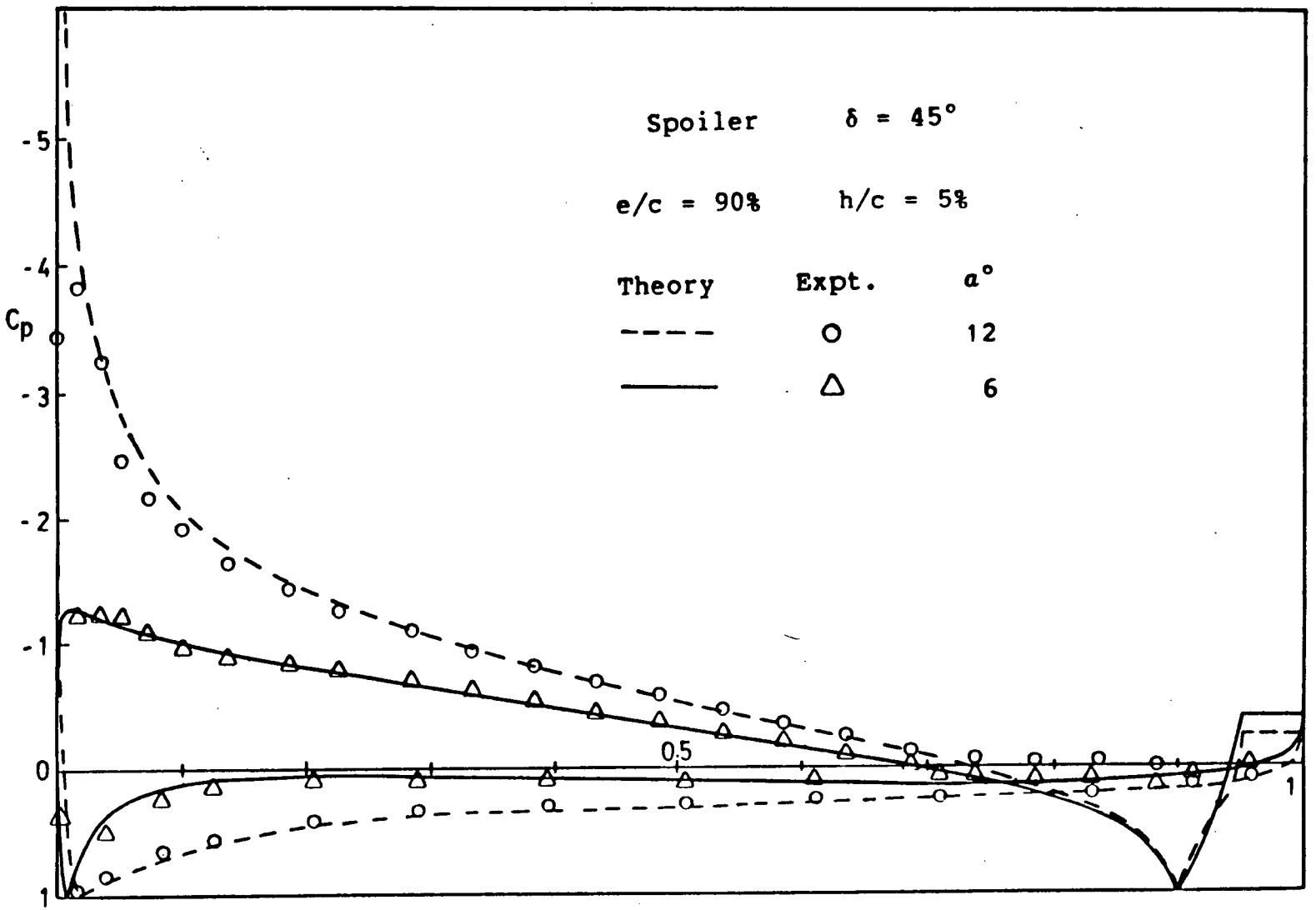

Fig. 20 C_p Distributions (spoiler, e/c = 90%, h/c = 5 %, δ = 45°)

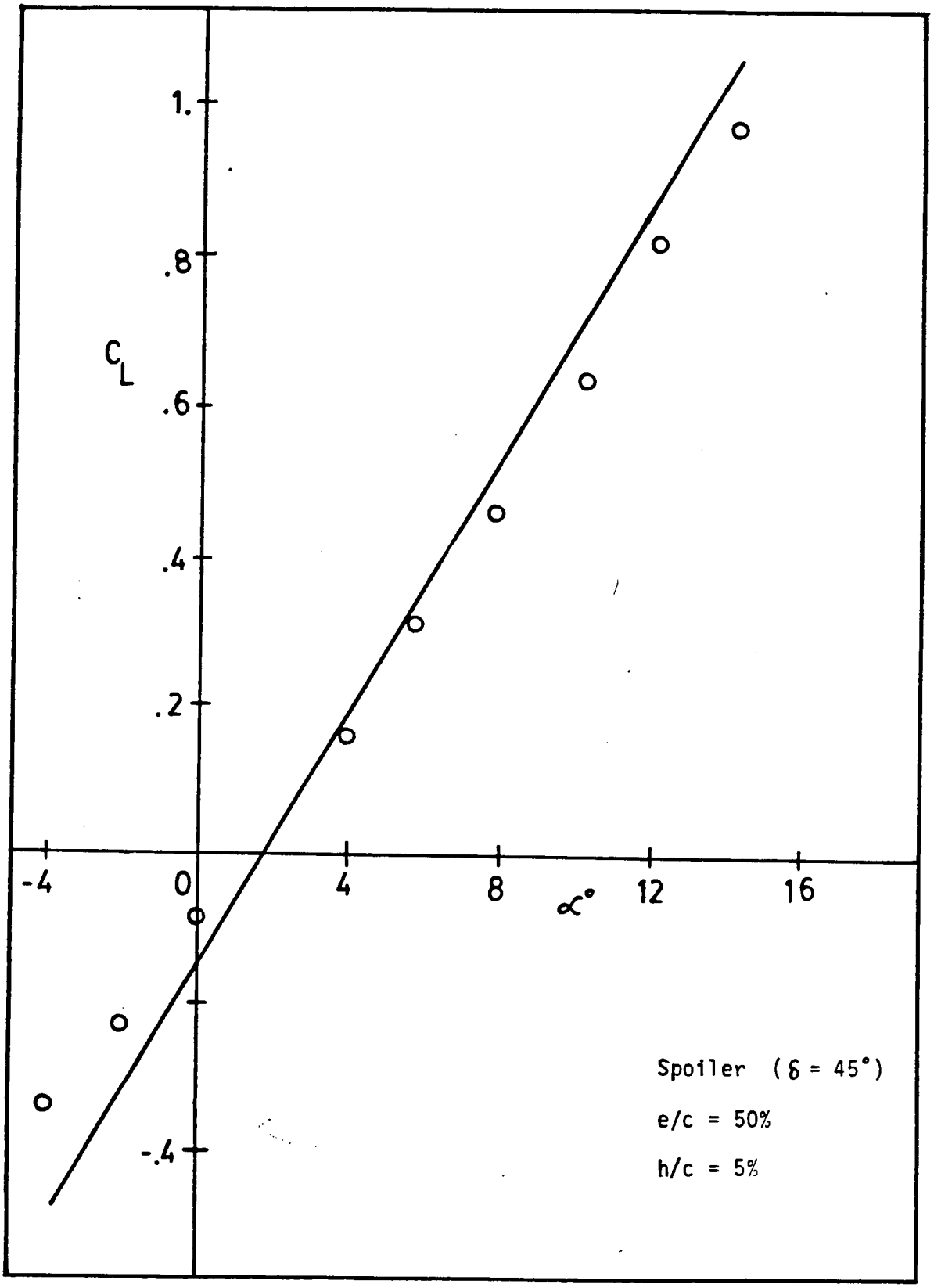

Fig. 21 C_L Variation over α

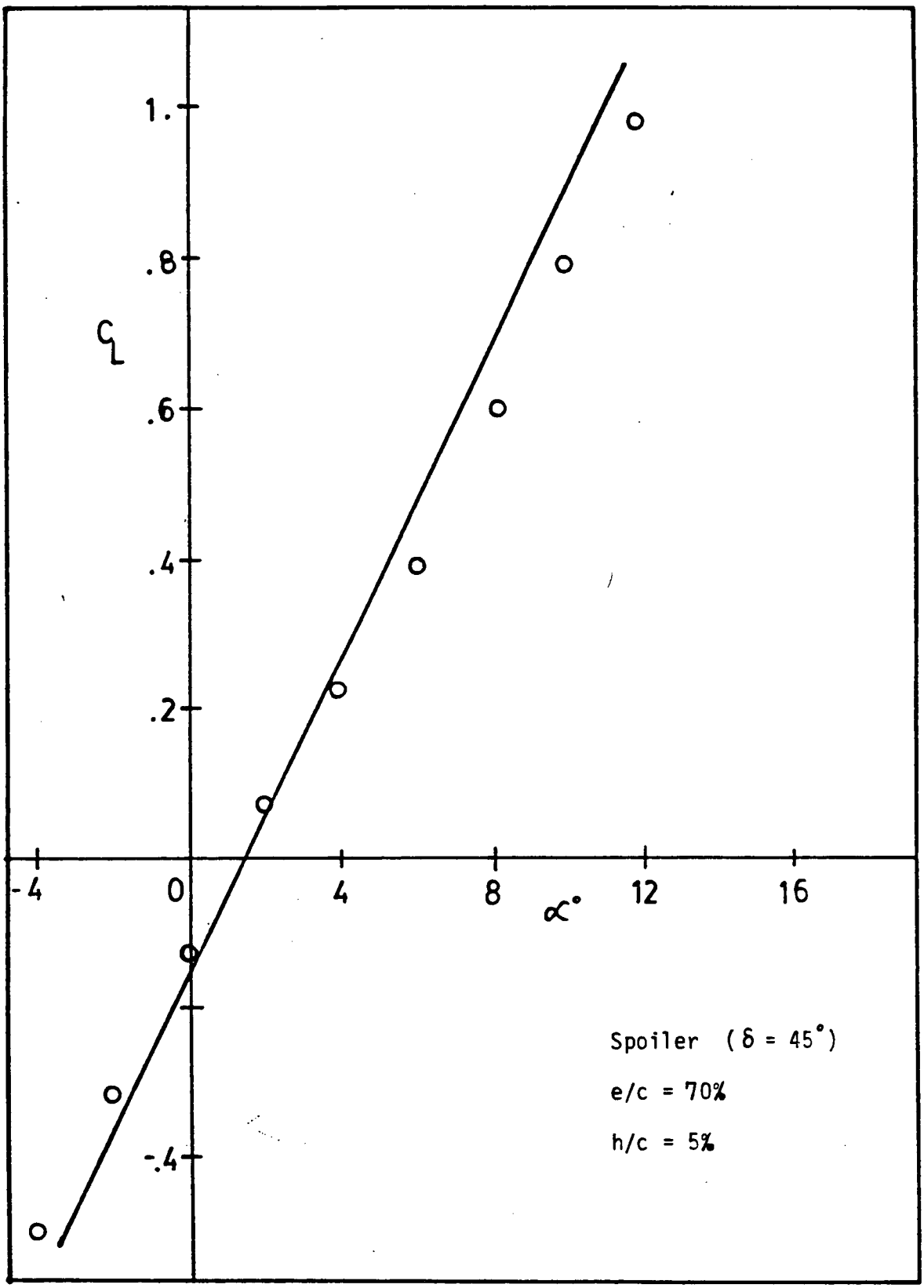

Fig. 22 C_L Variation over α

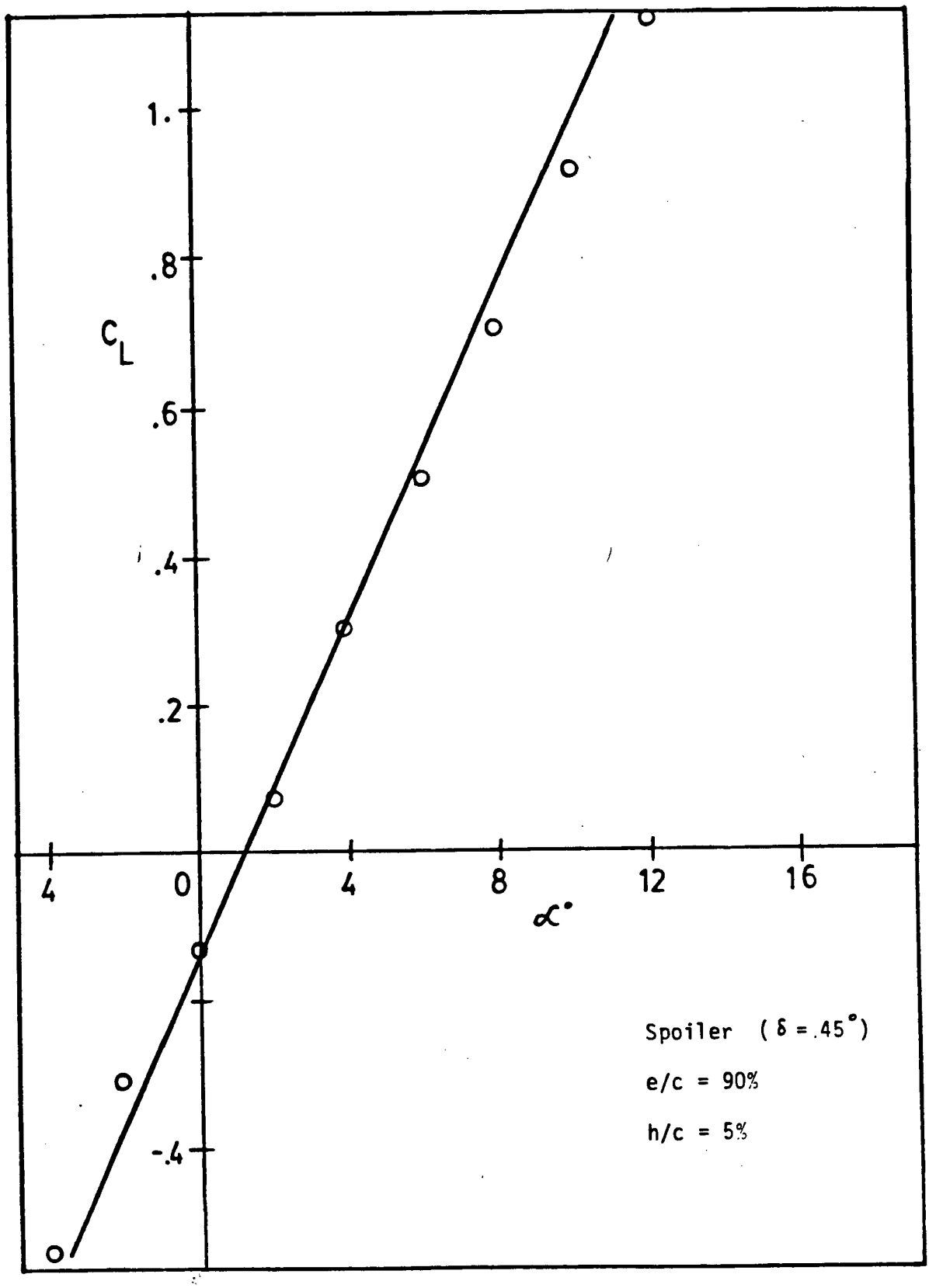

Fig. 23 C_L Variation over α

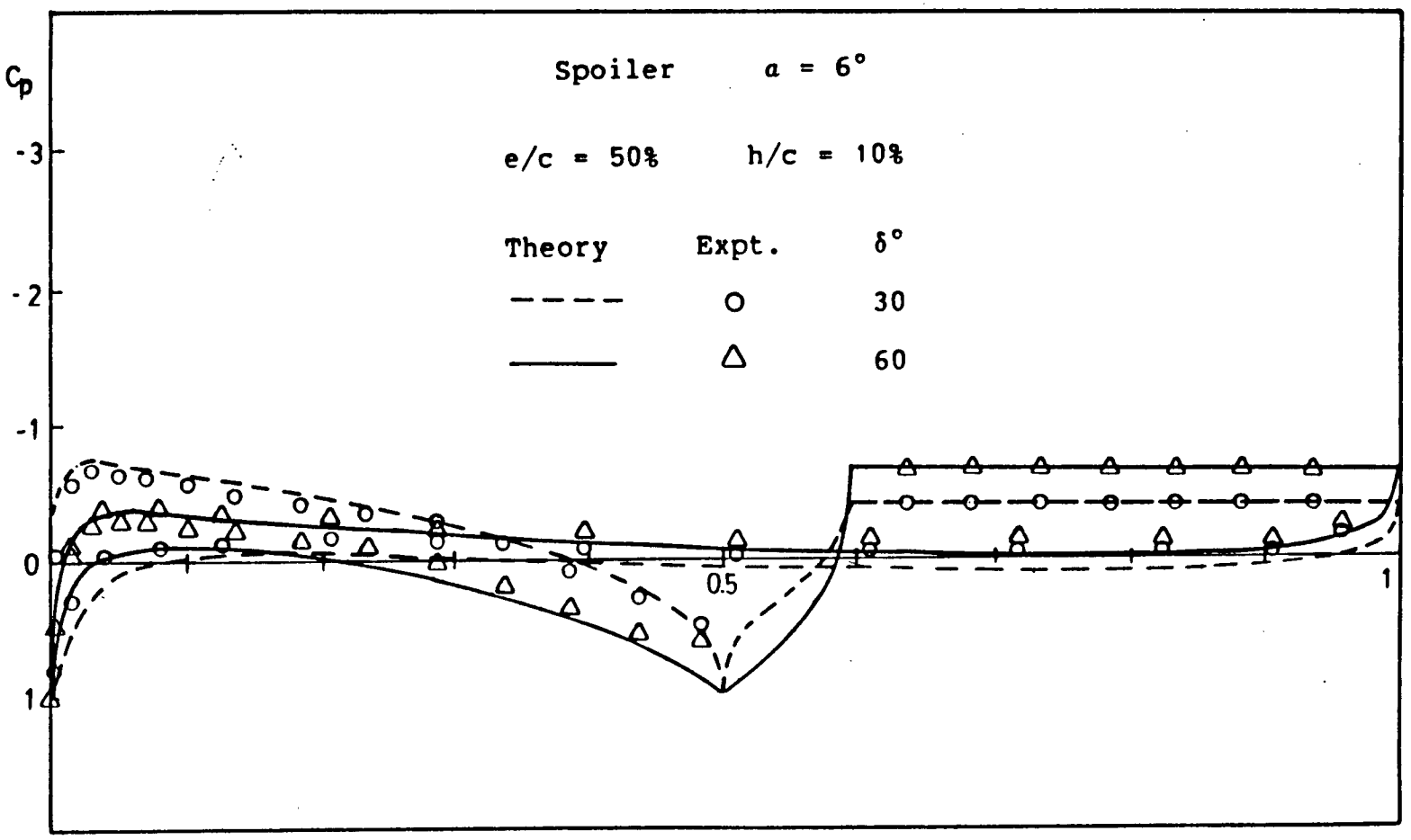

Fig. 24 C_p Distributions (spoiler, e/c = 50%, h/c = 10%, α = 6°)

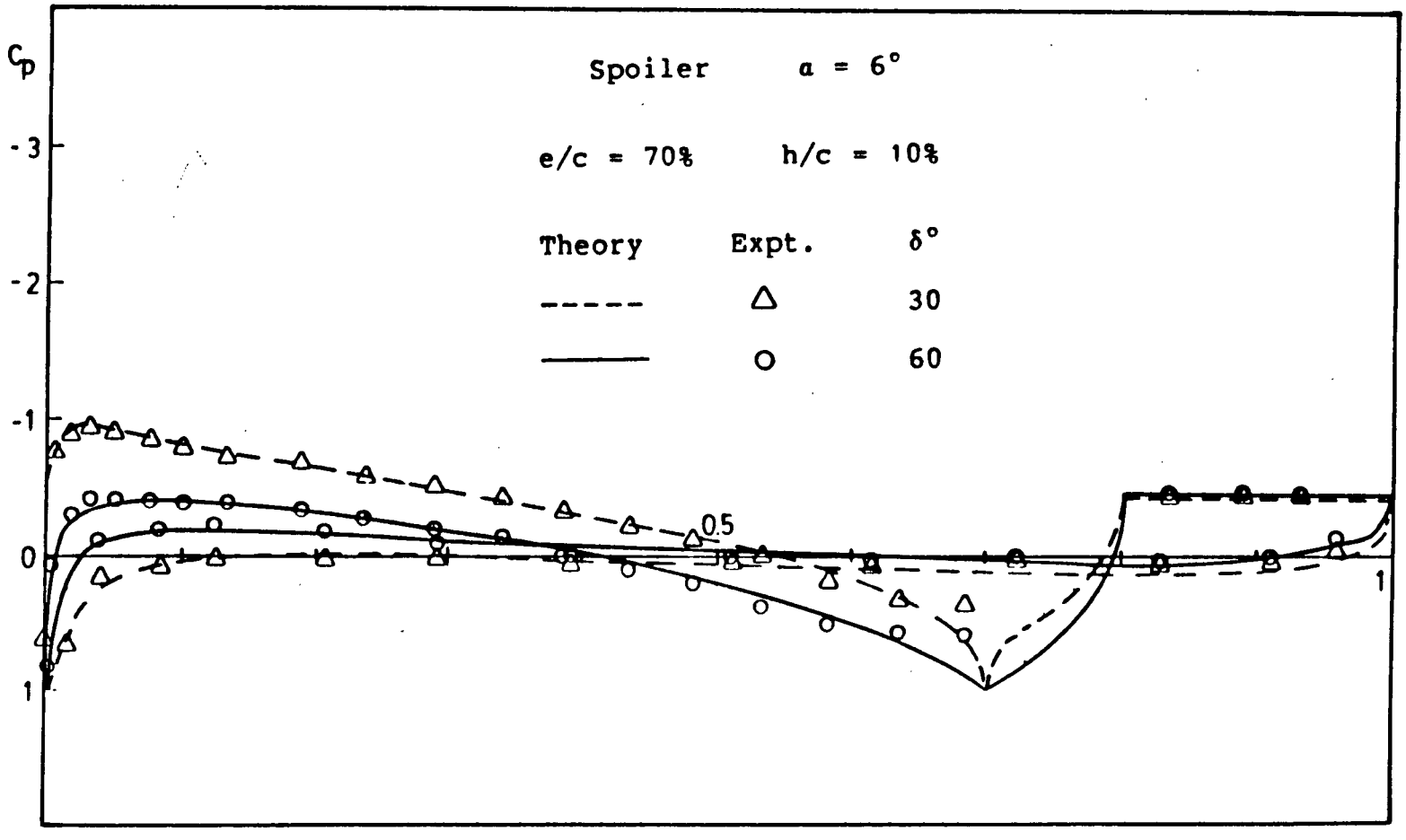

Fig. 25 C_p Distributions (spoiler, e/c = 70%, h/c = 10%, α = 6°)

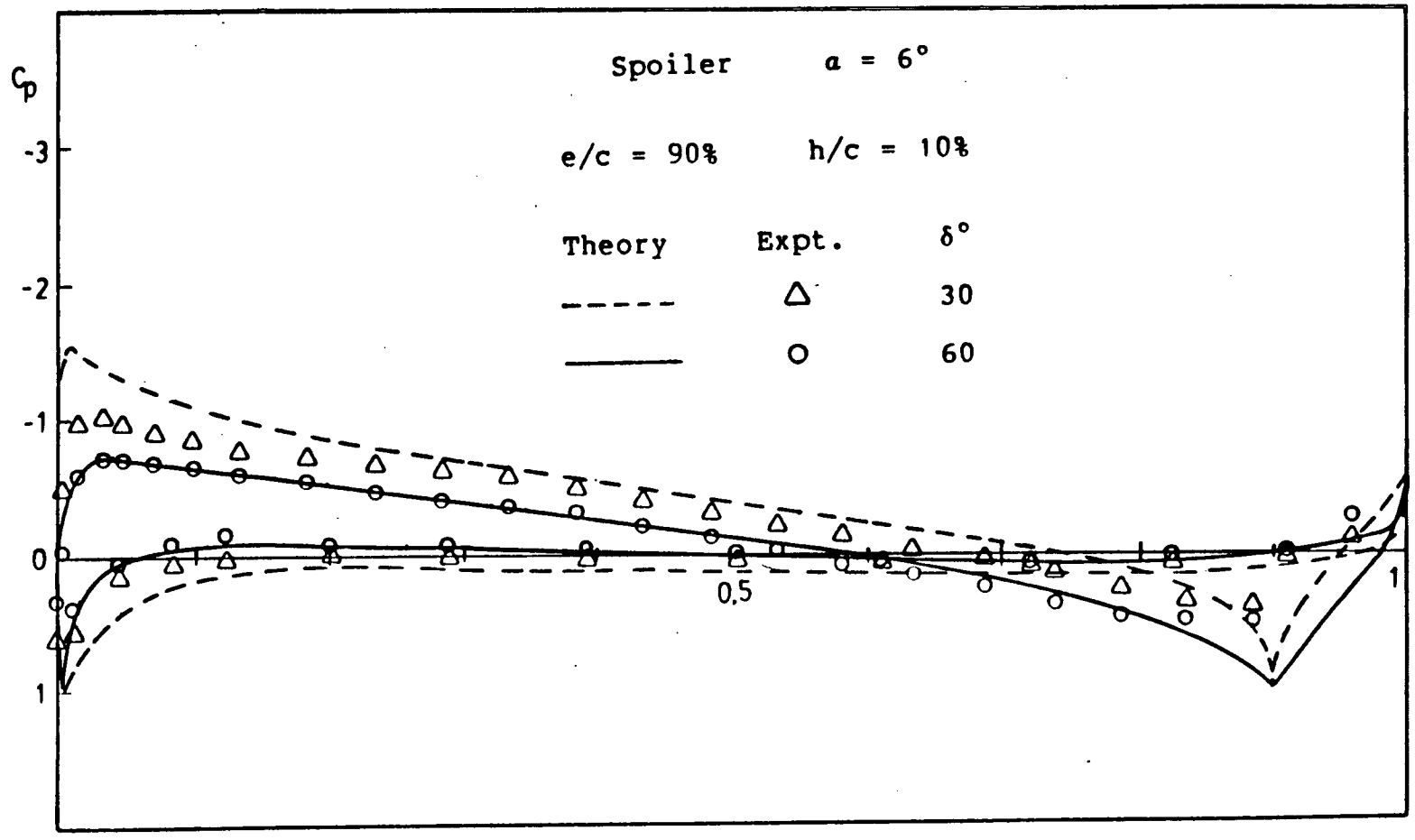

Fig. 26 C_p Distributions (spoiler, e/c = 90%, h/c = 10%, α = 6°)

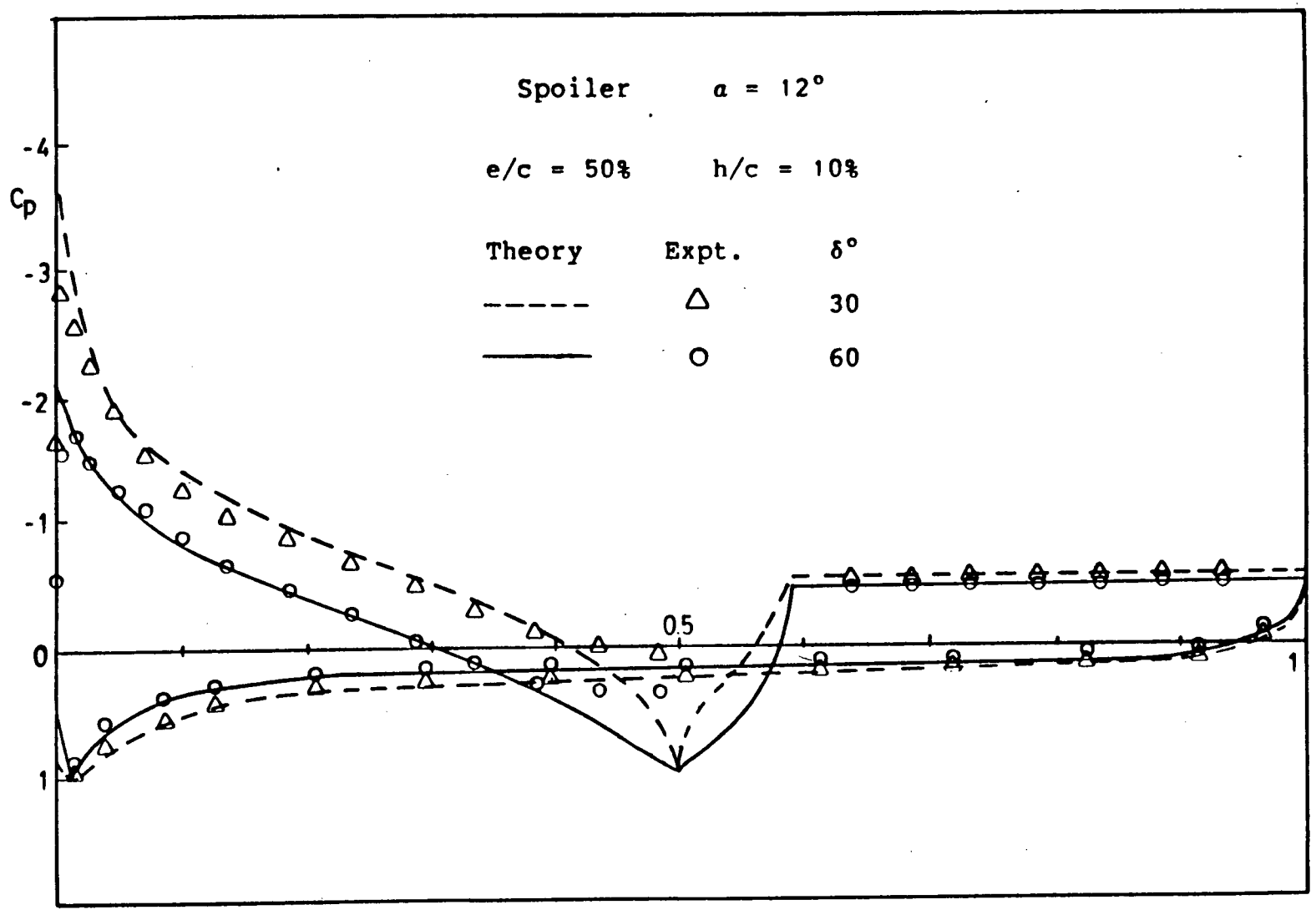

Fig. 27 C_p Distributions (spoiler, e/c = 50%, h/c = 10%, a = 12°)

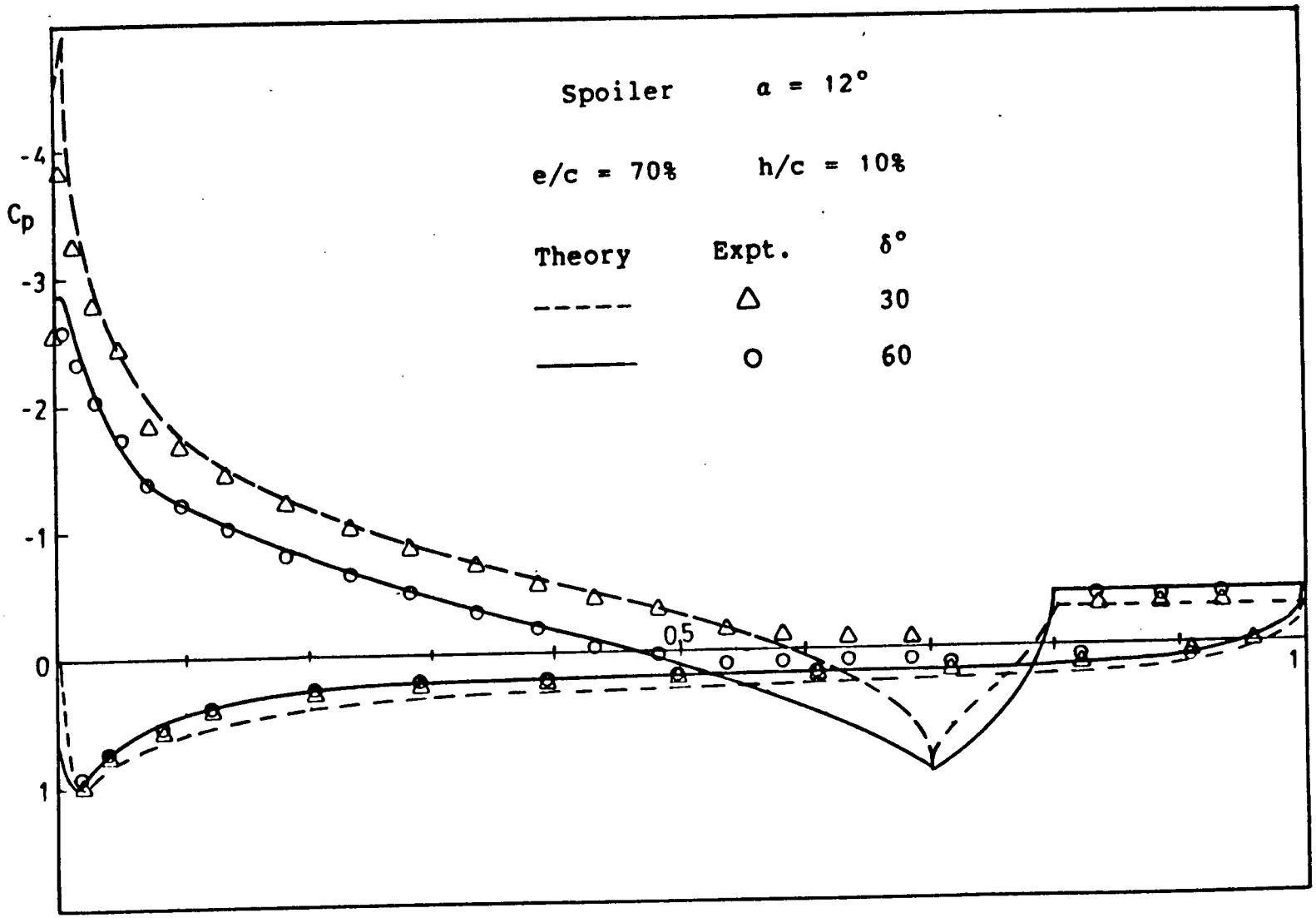

Fig. 28 C_p Distributions (spoiler, e/c = 70%, h/c = 10%, α = 12°)

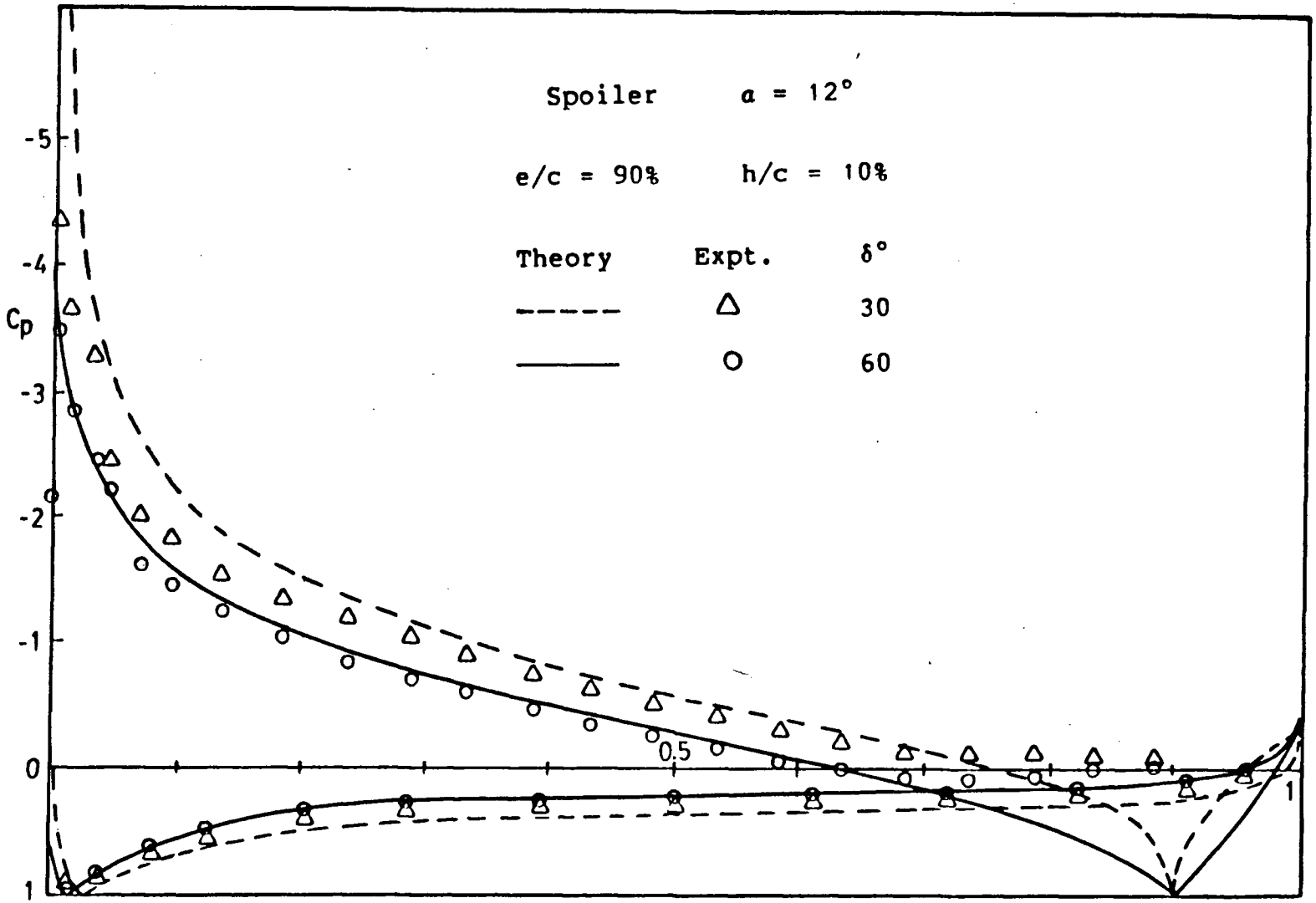

Fig. 29 C_p Distributions (spoiler, e/c = 90%, h/c = 10%, α = 12°)

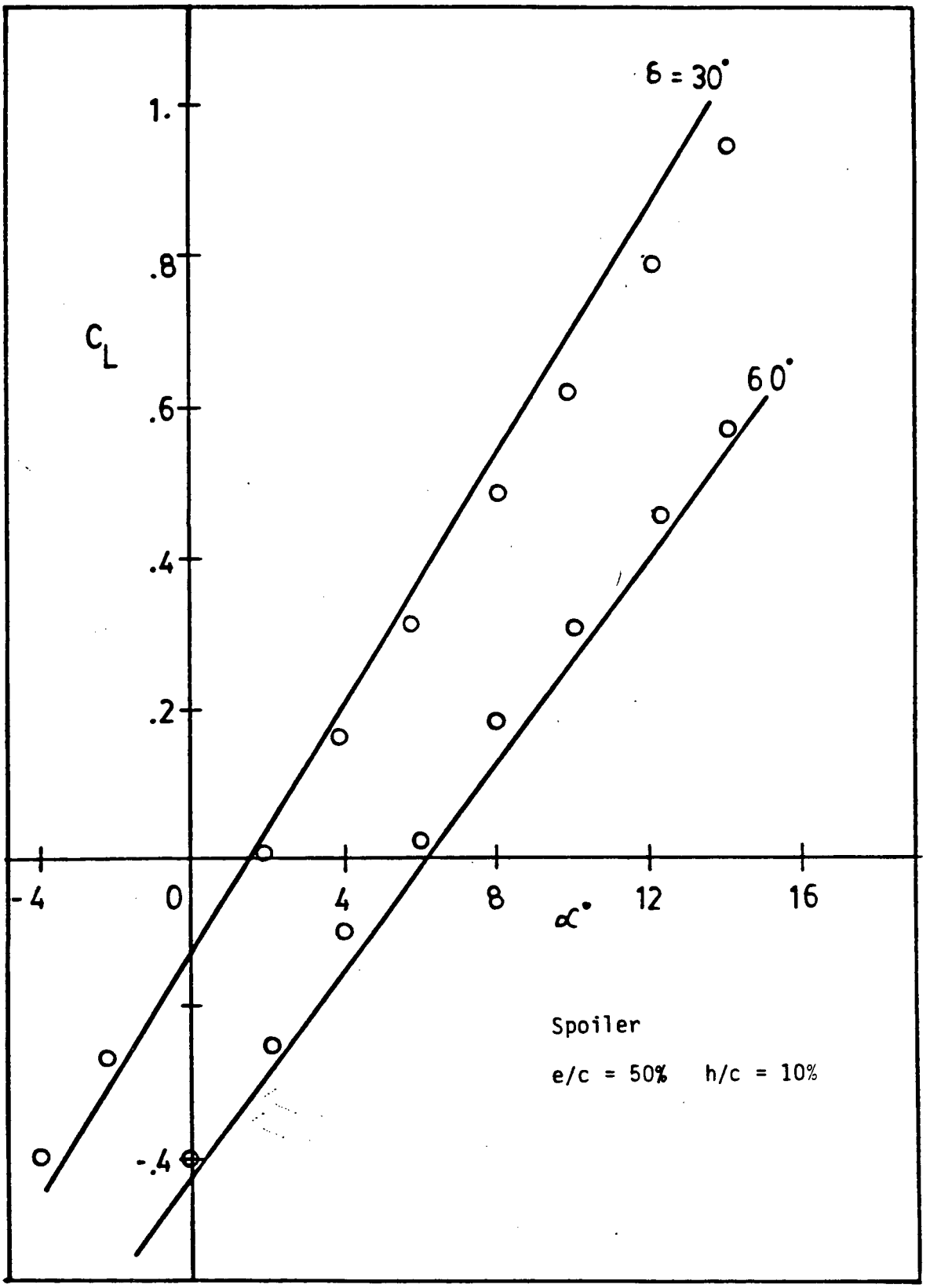

Fig. 30 C_L Variations over α

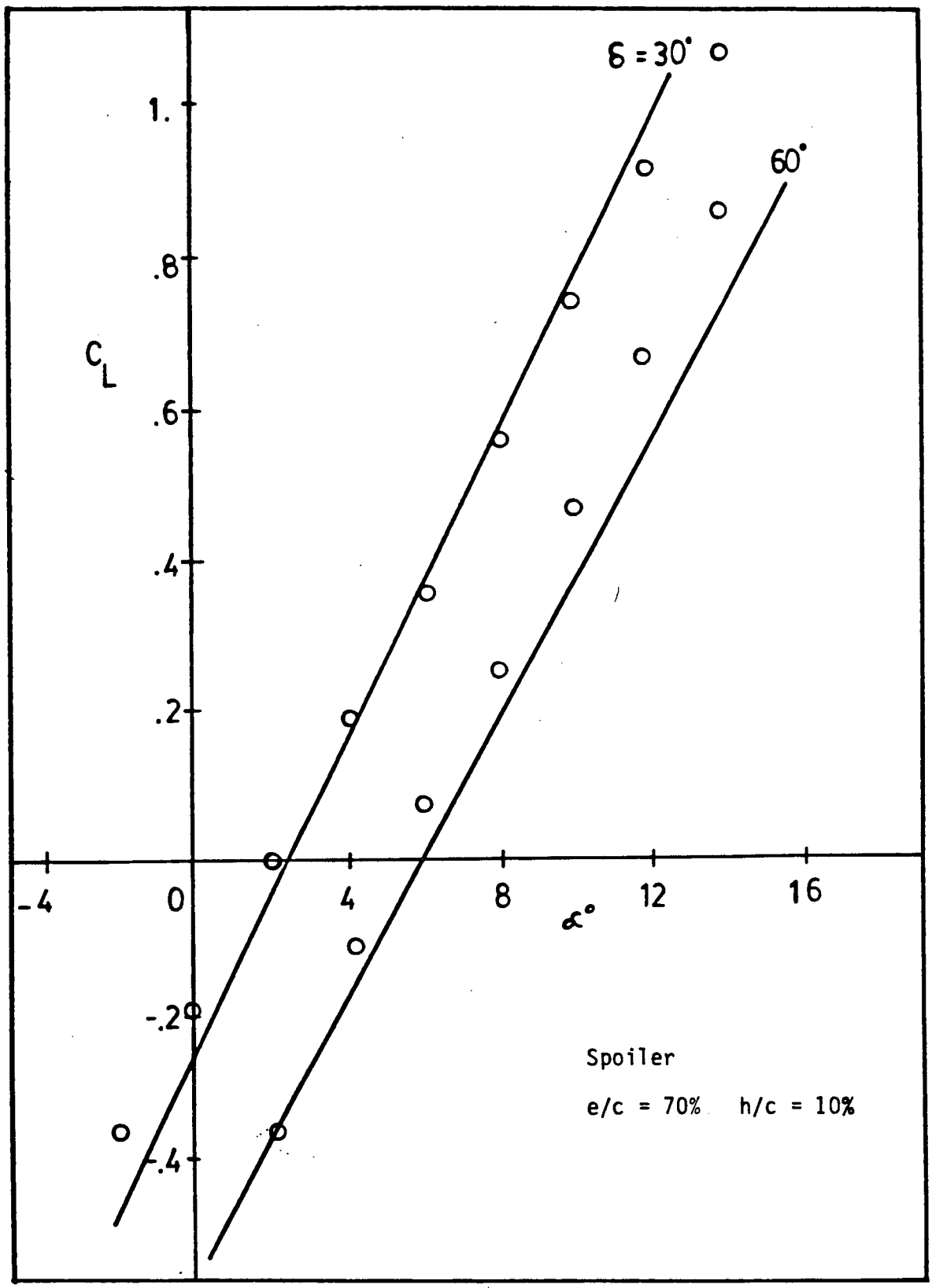

Fig. 31 C_L Variations over α

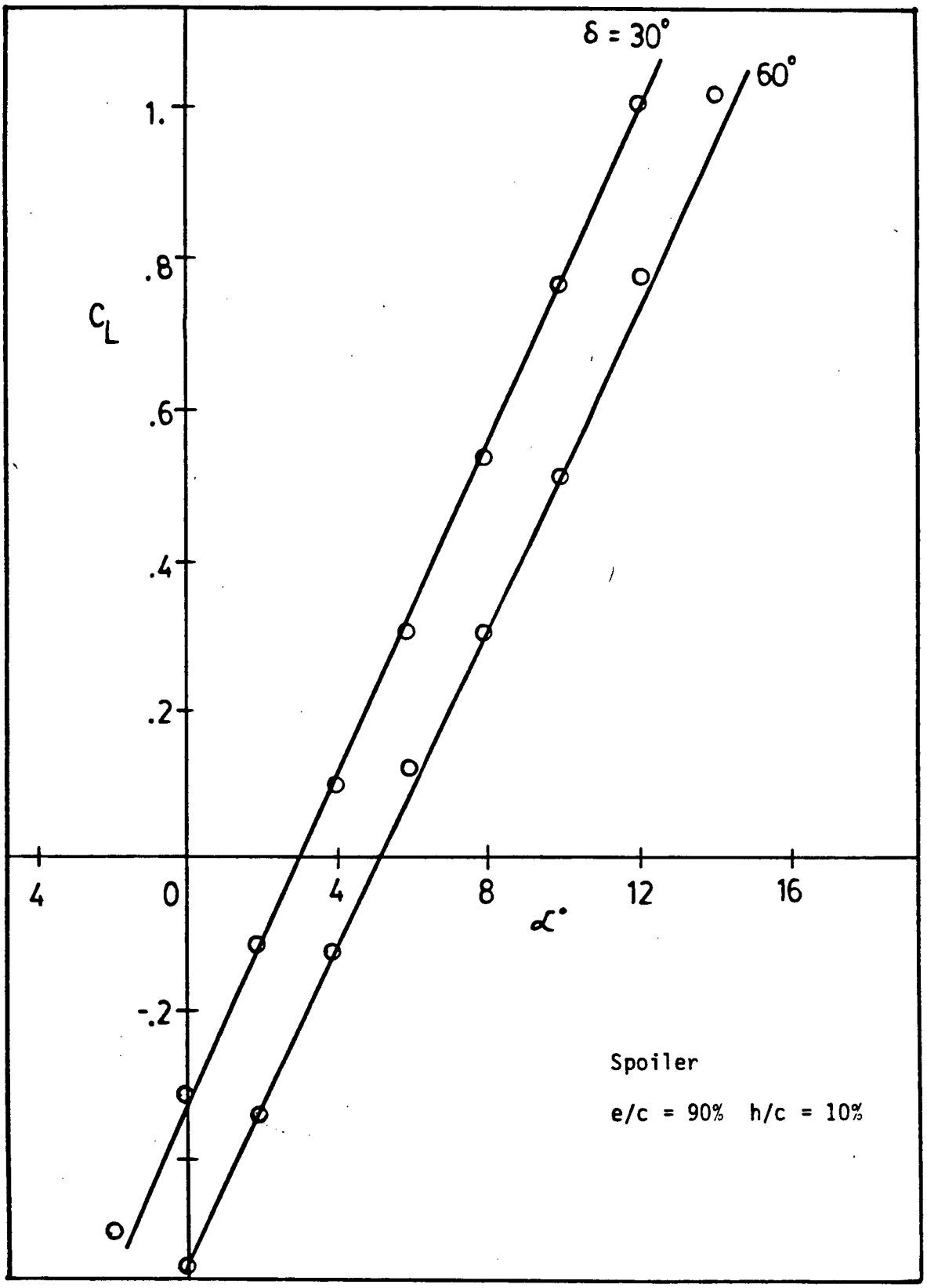

Fig. 32 C_L Variations over α

and experimental C_p values in this neighbourhood is inevitable.

Only within a small positive range of α do the experimental C_L curves behave linearly for split flaps, as shown in Figs. 15 and 17. This is probably due to the early flow separation taking place near the leading edge at higher angles of incidence. Therefore, the overall circulation generated is reduced and so is the lift force. On the other hand, the non-linearity of the C_L curves for spoilers is the consequence of the separation bubble explained above.

In general, the agreement between theory and experiments is the best for spoiler cases, fair for the clean airfoil and acceptable for split flaps. This may be due to the fact that the inviscid flow assumption overestimates the circulation around a clean airfoil. Erecting the spoiler, which helps reduce the overall circulation, therefore, produces better agreement. To the contrary, deflecting the split flap, which assists in enhancing the corresponding circulation, widens the already existed discrepancy in the clean airfoil case.

6. CONCLUSIONS AND RECOMMENDATIONS

A sequence of conformal transformations has been found useful for deforming the contour of an airfoil with an inclined spoiler or split flap onto the perimeter of the unit circle over which the flow problem is solved. The wake source model originally developed by Parkinson and Jandali was applied to deal with the current partially separated flow situation.

The 1-source models provide a first approximation of the C_p distribution in the sense that the experimental C_p distribution usually lies within the theoretical curves.

For the 2-source model, the criterion of the finite curvature of the separating streamlines or that of the finite pressure gradient at separation requires a modification of the experimental C_{pb} values. However, since the airfoil used in experiments has an artificially thickened trailing edge exposed to the outer flow for the case of split flaps, the modified section may have some influence on the measurements in the neighbourhood. Therefore, further work should be considered before the validity of the criterion can be pin-pointed.

The boundary condition, $\Gamma_{wake} = 0$, must be used with caution because the problem of accepting the C_{pb} comes up when

the angle of deflection δ increases. Investigations show that the range in which this criterion works well is $0 < \delta < 45°$ with the spoiler or split flap located no less than 80 % chord distance from the leading edge.

The modified version of $\Gamma_{wake} = 0$, equation (39), works well for most cases even though its physical significance is not obvious. This condition allows the use of the empirical C_{pb} with the two sources located within the simulated wake region. Although the pressure near the leading edge is often overestimated by the theory, the overall predicted C_p distribution is remarkably close to the experimental results.

Upstream of the spoiler where the separation bubble is located, the discrepancy of the C_p distributions from the theory and the experiments still prevails as obtained previously by Jandali [3]. This region in which viscous effects dominate can only be coped with if some mechanism of dissipation is introduced in the model. Further work should be interesting and challenging. To the contrary, the effect due to the bubble is not a pronounced one for the case of split flaps because the pressure gradient upstream of it is less prominent.

There is an interesting trend of the base pressure for split flaps when plotted against the angle of deflection, see (41) and Figs. 10a,b. This trend has not been discussed here for spoilers only because of the lack of data. However, it would be preferable to carry out more experiments to construct

a formula for C_{pb} for both inclined spoilers and split flaps.

Finally, the theory described above can be readily extended to deal with any arbitrary thick airfoil profile with the help of the Theodorsen transformation. By utilizing the Williams transformations [12], it would be interesting to apply the present work to multi-element airfoils.

References

1. McCormick, B.W.Jr. - Aerodynamics of V/STOL Flight, Academic Press, 1967.

2. Parkinson, G.V. and Jandali, T. - A Wake Source Model for Bluff Body Potential Flow, JFM, Vol. 40, No.3, pp577-594, Feb., 1970.

3. Jandali, T. - A Potential Flow Theory for Airfoil Spoilers, Ph.D Thesis, University of British Columbia, 1970.

4. Schlichting,H. and Truckenbrodt, E. - Aerodynamics of the Airplane, McGraw-Hill, 1979.

5. Whitehead, L.G., Cheers, F., and Mandl, P. - Flow about Airfoils with Split Flaps with Application to Circulation Control by Suction, NAE Laboratory Report LR-226, April, 1958.

6. Woods, L.C. - Theory of Subsonic Plane Flow, Cambridge University Press, 1961.

7. Parkinson, G.V. - Close Encounters with Separated Flows, The W. Rupert Turnbull Lecture at the CASI Annual General Meeting in Ottawa on May 2, 1979, CASJ, Vol. 25, No.3, Third Quarter, 1979.

8. Jandali, T. and Parkinson, G.V. - A Potential Flow Theory for Airfoil Spoilers, CASI Trans., Vol.3, No.1, pp1-7, March, 1970.

9. Chang, P.K. - Separation of Flow, Pergamon Press, 1970

10. Parkinson, G.V. and Yeung, W.W.H. - Improvements in Wake Singularity Potential Flow Models, Proceedings of the 10th CANCAM, London, Ontario, June, 1985.

11. Tam Doo, P. - A Prediction Method For Spoiler Performance, Ph.D. Thesis, University of British Columbia, 1977.

12. Williams, B.R. - An Exact Test Case for the Plane Potential Flow About Two Adjacent Lifting Aerofoils, ARC RM No. 3717, 1971.

13. Pope, A. and Harper, J.J. - Low-Speed Wind Tunnel testing, John Wiley and Sons, 1966.

Appendix A

Continuity of $|\frac{dz}{d\zeta}|$ at G

It is shown here that $|\frac{dz}{d\zeta}|$ is finite at the point G on the airfoil surface.

Using the trigonometric identity and equation (3), one gets

$$\csc^2(\frac{\omega}{2}) = 1 + \cot^2(\frac{\omega}{2})$$

$$= 1 + [\frac{s}{iR \sin \delta}]^2$$

$$= \frac{(R \sin \delta - s)(R \sin \delta + s)}{R^2 \sin^2 \delta}$$

Near point G, $s \longrightarrow -R \sin \delta$, and $\lambda, \bar{\lambda} \longrightarrow \pm\infty$ from Fig. 4d. Therefore, it is adequate to examine the product

$$|(s + R \sin \delta)\lambda| \qquad \ldots \quad (A1)$$

in the equation for $|\frac{dz}{d\zeta}|$, see (10).

Using (3) to rewrite $(s + R \sin \delta)$, one gets

$$(s + R \sin \delta) = R \sin \delta \, (1 + i \cot (\frac{\omega}{2}))$$

If $\omega = \omega_x + i \, \omega_y$, where ω_x and ω_y are real, it can be shown that

$$\cot (\frac{\omega}{2}) = \frac{\cos X \cosh Y - i \sin X \sinh Y}{\sin X \cosh Y + i \cos X \sinh Y} \qquad \ldots \quad (A2)$$

where $X = \omega_x/2, \qquad Y = \omega_y/2.$

With some manipulation,

$$|1 + i \cot (\frac{\omega}{2})| = \frac{\sinh Y + \cosh Y}{\sqrt{\sin^2 X + \sinh^2 Y}} \qquad \ldots \quad (A3)$$

In order to be precise, let us approach point G from point A in the ω-plane. Therefore, using (5),

$$\omega_x = -\frac{\pi}{2}(2-n),$$

$$\omega_y = h - \frac{1}{2}\{n \ln(\frac{\lambda}{n} + 1) + (2-n) \ln(\frac{\lambda}{2-n} - 1\}$$

$$\simeq h - \ln \lambda, \text{ since } \lambda \longrightarrow \infty$$

or, $e^{\omega_y} \simeq e^h/\lambda.$

The numerator of (A3) is just $e^{\omega_y/2}$, whereas its denominator approaches $\frac{1}{2}e^{-\omega_y/2}$ near point G since sinh $(\frac{\omega}{2}y)$ dominates. Therefore, (A1) can be written as

$$|(s + R \sin \delta)\lambda| \quad \propto \quad e^{\omega_y}\lambda = e^h, \text{ some finite value.}$$

Consequently, point G is not a singularity.

Q.E.D.

Appendix B

Continuity of $|\frac{dz}{d\zeta}|$ at ∞

The point at infinity, represented by $z = \infty$, $t = \infty$, $\bar{\lambda} = i$, or $\omega_\infty = 0$, is shown here to be a removable singularity of $\frac{dz}{d\zeta}$.

From equation (10), $\frac{dz}{d\zeta} \quad \csc^2(\frac{\omega}{2})(i - \bar{\lambda})^2$.

Since $\csc x \longrightarrow \frac{1}{x}$ as $x \longrightarrow 0$, it is easy to see that

$$\frac{dz}{d\zeta} \quad \propto \quad 4(\frac{i - \bar{\lambda}}{\omega})^2 \qquad \ldots \quad (B1)$$

Using equation (5), one can examine the nature of the point $z = \infty$ by writing

$$\omega - \omega_\infty = \frac{i}{2}[\{n \ln(\frac{\lambda_\infty}{n} + 1) + (2-n) \ln(\frac{\lambda_\infty}{2-n} - 1)\} -$$

$$\{n \ln(\frac{\lambda}{n} + 1) + (2-n) \ln(\frac{\lambda}{2-n} - 1)\}]$$

$$= -\frac{i}{2}[n \ln(\frac{\lambda + n}{\lambda_\infty + n}) + (2-n) \ln(\frac{\lambda - 2 + n}{\lambda_\infty - 2 + n})]$$

$$= -\frac{i}{2}[n \ln(1 + \frac{\lambda - \lambda_\infty}{\lambda_\infty + n}) + (2-n) \ln(1 + \frac{\lambda - \lambda_\infty}{\lambda_\infty - 2 + n})]$$

As $\omega \longrightarrow \omega_\infty \longrightarrow 0$, $\lambda \longrightarrow \lambda_\infty = \tilde{\xi} + \tilde{\eta}\, i$,

$$\omega \quad \longrightarrow -\frac{i}{2}[n \ (\frac{\lambda - \lambda_\infty}{\lambda_\infty + n}) + (2-n) \ (\frac{\lambda - \lambda_\infty}{\lambda_\infty - 2 + n})]$$

$$\text{or,} \quad (\frac{\omega}{\lambda - \lambda_\infty}) \longrightarrow \frac{-i\lambda_\infty}{(\lambda_\infty + n)(\lambda_\infty - 2 + n)} \qquad \ldots \quad (B2)$$

From (8), $\lambda - \lambda_\infty = \tilde{\eta}(\bar{\lambda} - i)$ $\qquad \ldots \quad (B3)$

Combining (10), (B1), (B2) and (B3), it can be shown that

$$\frac{dz}{d\zeta} = \frac{-(\lambda_\infty+n)(\lambda_\infty-2+n)R \sin \delta}{\tilde{\eta}\ \lambda_\infty} e^{i\psi} \qquad \ldots \quad (B4)$$

where $\psi = \frac{\pi}{2} + a_0 - \gamma$

It is easily seen that $\frac{dz}{d\zeta}$ is a complex number of finite magnitude. Therefore, the proof is completed.

A more simple proof suggested by Prof. Parkinson is to apply l'Hôpital rule to the right hand side of (B1). Since $\frac{d\tilde{\chi}}{d\omega}$ is finite at z_∞, $\frac{dz}{d\zeta}$ must also be so.

Q.E.D.

Appendix C

Locations of the Trailing Edge

The location of the point E in the t-plane can be expressed as

$$t = 1 \quad \text{or} \quad t = t_0 + R\, e^{-i\phi} \qquad \ldots \quad (C1)$$

where $\phi = \tan^{-1}(\frac{\mu}{1+\epsilon})$

and R is defined in (1a). Combining (C1),(2) and (2b), for the case of an inclined spoiler,

in the s-plane, $s_E = R \cos(\gamma-\phi) + iR\,[\sin(\gamma-\phi) - \cos\delta]$,

in the ω-plane, $\omega_E = -\frac{\pi}{2}(2-n) + i\omega_{E_y}$

where $\omega_{E_y} = -\frac{1}{2} \ln \{\frac{X^2 + Y^2}{Z^2 + Y^2}\}$ $\qquad \ldots \quad (C2)$

and $X = \cos(\gamma-\phi) - \sin\delta$

$Y = \sin(\gamma-\phi) - \cos\delta$

$Z = \cos(\gamma-\phi) + \sin\delta$

In the λ-plane, λ_E is given implicitly by

$$\omega_{E_y} = h - \frac{1}{2}\{ n \ln(\frac{\lambda_E}{n} + 1) + (2-n) \ln(\frac{\lambda_E}{2-n} - 1)\} \qquad \ldots \quad (C3)$$

Therefore, in the $\tilde{\lambda}$-plane, $\tilde{\lambda}_E = (\lambda_E - \tilde{\xi})/\tilde{\eta}$ $\qquad \ldots \quad (C4)$

For the case of a split flap, using (C1) and (17)

in the s-plane, $s_E = R \cos(\gamma+\phi) + iR\,[\cos\delta - \sin(\phi+\gamma)]$,

in the ω-plane, $\omega_E = \frac{\pi}{2}(2-n) + i\omega_{E_y}$

where $\omega_{E_y} = -\frac{1}{2} \ln \{\frac{X^2 + Y^2}{Z^2 + Y^2}\}$ ... (C5)

and $X = \cos(\gamma+\phi) - \sin \delta$

$Y = - \sin(\gamma+\phi) + \cos \delta$

$Z = \cos(\gamma+\phi) + \sin \delta$

In the λ-plane, λ_E is given implicitly by

$\omega_{E_y} = h - \frac{1}{2}\{ n \ln(\frac{\lambda_E}{n} - 1) + (2-n) \ln(\frac{\lambda_E}{2-n} + 1)\}$ ... (C6)

Therefore, in the $\tilde{\lambda}$-plane, $\tilde{\lambda}_E = (\lambda_E + \xi)/\tilde{\eta}$ ... (C7)

Appendix D

Derivation of Equations (4) & (5) from Jandali's Thesis

Jandali's equations (4) & (5) (from his thesis), will be re-derived in this appendix from the general expressions developed in this thesis for an inclined spoiler.

For a normal spoiler, $\delta = 90°$ and n=1, (6) and (7) provide

$$\xi = 0 \text{ and } \quad \tilde{\eta}^2 = e^{2h} - 1 \quad \ldots \quad (D1)$$

From (13a, b, c),

$$\theta_1 = \frac{\pi}{2}, \quad \theta_2 = \tan^{-1}(\tilde{\eta}), \quad \theta_3 = \tan^{-1}(\frac{\tilde{\eta}}{-1}) = \pi - \theta_2$$

Also from (2a), $\gamma = \frac{\pi}{2} - \theta_0 - \frac{\pi}{2} = - \theta_0$

Hence, (13) gives $a_0 = \frac{\pi}{2} + a - \theta_0 + \frac{\pi}{2} - \theta_2 - (\pi - \theta_2)$

$$= a - \theta_0$$

From equation (14), the location of point C on the unit circle is then

$$\theta_C = \pi - 2\,(\frac{\pi}{2}) - a_0$$

$$= \theta_0 - a$$

which is exactly the same as equation (4) in Jandali's thesis.

From (3b), one gets

$$e^h = 1 + \frac{2R}{\hbar}$$

Jandali [2] defines $\xi = \frac{R_2}{R_1}$, which is equivalent to $\xi = \frac{R+\hbar}{\hbar}$. Therefore,

$$e^h = \left(\frac{\xi+1}{\xi-1}\right)^2 \quad \ldots \quad (D2)$$

From appendix C, for normal spoiler, it is easily derived from (C1) that

$$\omega_{E_y} = -\frac{1}{2} \ln \left[\frac{1 - \cos(\theta_0+\phi)}{1 + \cos(\theta_0+\phi)}\right]$$

Or, $$1 - e^{-2\omega_y} = \frac{2\cos(\theta_0+\phi)}{1+\cos(\theta_0+\phi)} \quad \ldots \quad (D3a)$$

$$1 + e^{-2\omega_y} = \frac{2}{1+\cos(\theta_0+\phi)} \quad \ldots \quad (D3b)$$

It is also obvious from (C2) that

$$\lambda_E^2 = 1 + e^{2(\omega_y - h)} \quad \ldots \quad (D4)$$

and $$\tilde{\lambda}_E = \lambda_E/\tilde{\eta} \quad \ldots \quad (D5)$$

Using (D1), (D3a,b), (D4) and (D5), and after some manipulation, one gets

$$\frac{1 - \tilde{\lambda}_E^2}{1 + \tilde{\lambda}_E^2} = \frac{1 - e^{-2\omega_y} - 2e^{-2h}}{1+e^{-2\omega_y}}$$

$$= \cos(\theta_0+\phi) - [1+\cos(\theta_0+\phi)]\left(\frac{\xi-1}{\xi+1}\right)^2$$

$$= \cos(\theta_0+\phi)\left\{\frac{4\xi}{(\xi+1)^2}\right\} - \left(\frac{\xi-1}{\xi+1}\right)^2$$

$$= \frac{2\cos(\theta_0+\phi)+(1-k)}{(1+k)} \quad \ldots \quad (D6)$$

where $k = \frac{1}{2}\frac{\xi^2+1}{\xi}$

Substituting (D6) into (15) and replacing ϕ_0 by $\theta_0+\phi$,

Jandali's equation (5) is recovered.

Q.E.D.

Appendix E

Derivation of Equation (5)

Equation (5) will be derived by integrating (4).

Integrating (4),

$$\omega = \frac{k}{2} [\, n \ln (\lambda+n) + (2-n) \ln (\lambda-2+n)] + C \qquad \ldots \quad (E1)$$

where C is the integration constant. Note that both k and C can be complex so

$$k = k_1 + k_2 i \text{ and } \quad C = C_1 + C_2 i$$

where k_1, k_2, C_1, C_2 are real numbers.

When $\lambda = -n^-$ or $-n-\epsilon$ as $\epsilon \longrightarrow 0$, $\omega \longrightarrow n\pi/2 + \infty\, i$

Substituting into (E1)

$$n\pi/2+\infty i = (k_1+ k_2 i)[\, n \ln (-\epsilon) + (2-n) \ln (-2-\epsilon)\,]\, /2 + C_1 + C_2\, i$$

$$= (k_1+ k_2 i)[\, n \ln (\epsilon) + (2-n) \ln (2+\epsilon) + n\pi i/2 + (2-n)\pi i/2\,]\, /2 + C_1 + C_2\, i$$

Taking the real part of both sides

$$n\pi = k_1 [\, n \ln \epsilon + (2-n) \ln (2+\epsilon)\,] - k_2\pi + 2\, C_1$$

As $\epsilon \longrightarrow 0$, $\ln \epsilon \longrightarrow -\infty$. Therefore, k_1 must be 0.

$$n\pi = - k_2\pi + 2\, C_1 \qquad \ldots \quad (E2)$$

When $\lambda = -n^{+}$ or $-n+\epsilon$ as $\epsilon \dashrightarrow 0$, $\omega \dashrightarrow \infty i$

Substituting into (E1)

$$\infty i = (k_1 + k_2 i)[\, n \ln(\epsilon) + (2-n) \ln(-2+\epsilon) \,]/2 + C_1 + C_2 i$$

$$= (k_1 + k_2 i)[\, n \ln(\epsilon) + (2-n) \ln(2\epsilon) + (2-n)\pi i/2 \,]/2 + C_1 + C_2 i$$

Taking the real part of both sides

$$0 = 2 k_1 [\, n \ln \epsilon + (2-n) \ln(2-\epsilon) \,] - k_2(2-n)\pi/2 + 4 C_1$$

Since $k_1 = 0$,

$$4 C_1 = k_2(2-n)\pi \qquad \ldots \quad (E3)$$

Substituting (E3) into (E2),

$$k_2 = -2 \quad \text{and} \quad C_1 = -(2-n)\pi/2$$

When $\lambda = 0$ and $\omega = h\, i$, (E1) becomes, after equating the imaginary parts of both sides,

$$C_2 = h + n \ln n + (2-n) \ln(2-n)$$

Substituting k_1, k_2, C_1, C_2 into (E1), one obtains equation (5).

Appendix F

Derivation of Equation (35)

Equation (35) for finite pressure gradient at separation is derived here.

The pressure along the airfoil surface can be expressed most conveniently in terms of

$$C_p = 1 - \left|\frac{W(z)}{U}\right|^2$$

If s is measured from the forward stagnation point along the airfoil, see Fig. F1(a), then

$$\frac{dC_p}{ds}\Big|_E = -2\frac{k}{U}\frac{d}{ds}|W(z)|_E = -2\frac{k}{U}\frac{d}{d\theta}|W(z)|_E \quad \frac{d\theta}{ds}\Big|_E$$

where θ is the angular variable in the ζ-plane, Fig. F1(b), and $k = \sqrt{1 - C_{pb}}$, some non-zero number.

Since $dz = ds\, e^{i\epsilon}$ and $d\zeta = i\, e^{i\theta} d\theta$,

$$\left|\frac{dz}{d\zeta}\right| = -\frac{ds}{d\theta}$$

because s increases with decreasing θ. Also

$$|W(z)| = |W(\zeta)|/\left|\frac{dz}{d\zeta}\right| = f_1/f_2$$

Therefore,

$$\frac{dC_p}{ds}\Big|_E = 2\frac{k}{U}\frac{d}{d\theta}|W(z)|_E/\left|\frac{dz}{d\zeta}\right|_E = 2\frac{k}{U}\frac{d}{d\theta}\left(\frac{f_1}{f_2}\right)/f_2\Big|_E$$

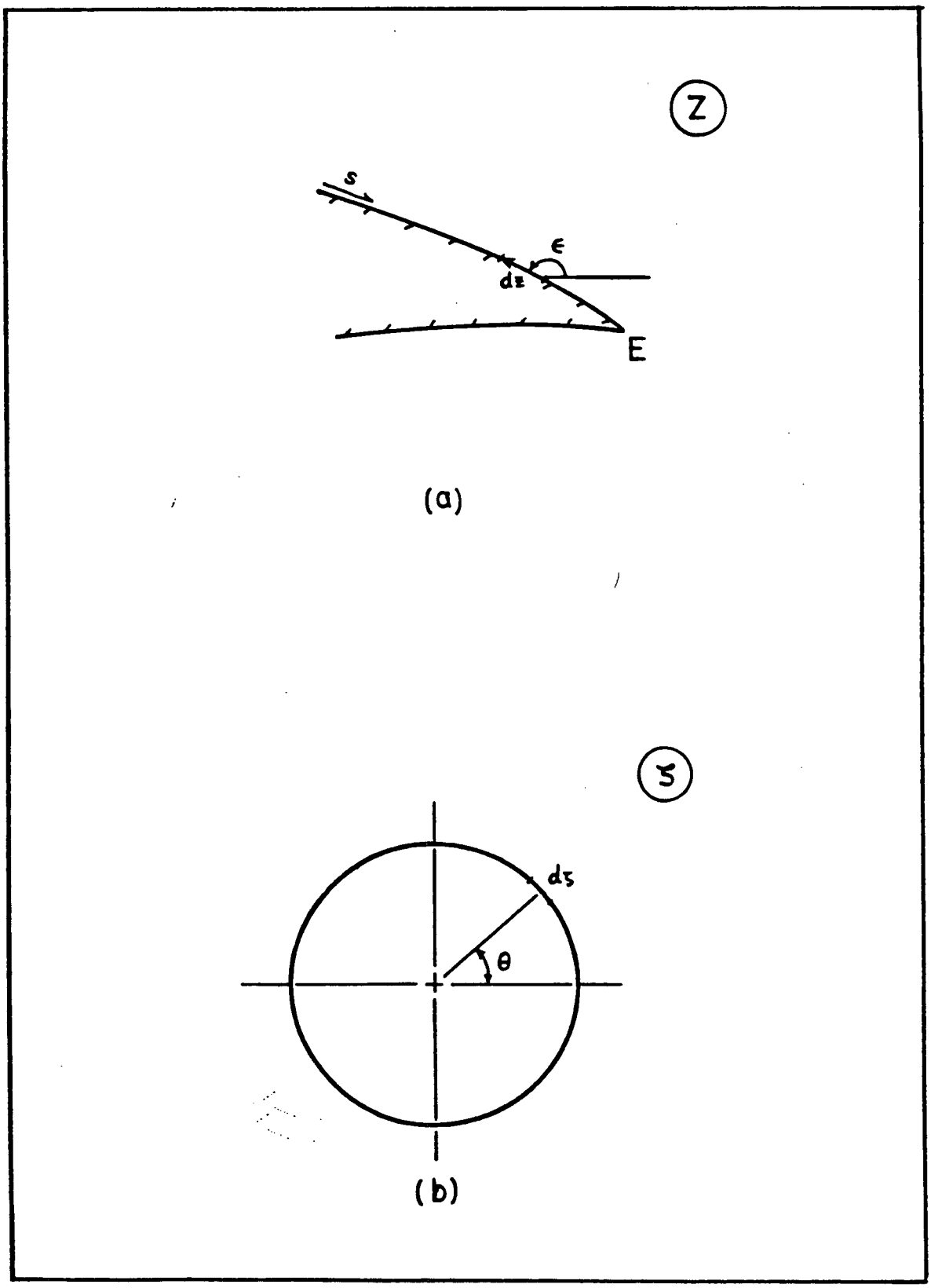

F1 Transform planes Z and ζ

Since $f_2|_E = 0$, $\frac{dC_p}{ds}|_E$ is finite only if

$$\frac{d}{d\theta}\left(\frac{f_1}{f_2}\right)|_E = g(\theta)|_E = 0$$

But $$g(\theta) = (f_2\, f_1' - f_1\, f_2')/f_2^2$$

Applying l'Hôpital's rule twice to $g(\theta)$ since both the numerator and denominator are zeros of order 2, then

$$f_2'\, f_1'' - f_1'\, f_2'' = 0 \qquad \text{at } \theta = \theta_E$$

Appendix G

Evaluations of f_1', f_1'', f_2' & f_2'' at Critical Points

Recall the following definitions:

$$f_1 = |W(\zeta)| \qquad \text{and} \qquad f_2 = |dz/d\zeta|$$

Since both f_1 and f_2 are made equal to zero at points E and C, equations (33) and (34) must be evaluated by L'Hôpital's rule. Therefore, at these critical points,

$$|W(z)| = \frac{f_1'}{f_2'} \quad , \text{ where } (\ )' = \frac{d}{d\theta}$$

This appendix is devoted to finding f_1', f_1'', f_2' and f_2'' at the critical points E and C for both spoilers and split flaps.

f_1 is a simple function of θ alone. It is rather straight forward to compute its 1^{st} and 2^{nd} derivatives.

$$f_1'(\theta) = -\frac{V}{2}[4 \cos \theta + \frac{q_1}{2} \csc^2(\frac{\theta - \delta_1}{2}) + \frac{q_2}{2} \csc^2(\frac{\theta - \delta_2}{2})]$$

$$f_1''(\theta) = \frac{V}{2}[4 \sin \theta + \frac{q_1}{2} \csc^2(\frac{\theta - \delta_1}{2}) \cot (\frac{\theta - \delta_1}{2}) + \frac{q_2}{2} \csc^2(\frac{\theta - \delta_2}{2}) \cot (\frac{\theta - \delta_2}{2})]$$

On the other hand, f_2 is a more complicated function involving more than one variable. Therefore, it is convenient to reduce it to a function of $\overline{\theta}$ and θ so that its derivatives can be obtained relatively easily. According to Figs. G1(a)

and G1(b),

$$t = t_0 + R\, e^{i\vartheta} \qquad \ldots \quad (G1)$$

and $$\zeta = e^{i\theta} \qquad \ldots \quad (G2)$$

It can be shown that, using Fig. G2,

$$\frac{|(t-1)(t+1)|}{|t|^2} = \sqrt{\frac{A\ B}{E}} \qquad \ldots \quad (G3)$$

where $A = 2 - 2\cos(\vartheta+\phi)$

$B = 1 + m^2 + 2m\cos(\vartheta-\Delta)$

$E = 1 + \eta^2 + 2\eta\cos(\vartheta-\nu)$

$\phi = \tan^{-1}\left(\frac{\mu}{1+\epsilon}\right) \qquad \Delta = \tan^{-1}\left(\frac{\mu}{1-\epsilon}\right) \qquad \nu = \pi - \tan^{-1}\left(\frac{\mu}{\epsilon}\right)$

$mR = \sqrt{\mu^2 + (1-\epsilon)^2}$

$\eta R = \sqrt{\epsilon^2 + \mu^2}$

and R is given by (1a).

Substituting (G1) to (17), the following expression results.

$$s = R\,[\cos(\vartheta-\gamma) + i\,\{\sin(\vartheta-\gamma) + \cos\delta\}] \qquad \ldots \quad (G4)$$

Using (G4) and appendix A, it can be shown that

$$\left|\csc^2\left(\frac{\omega}{2}\right)\right| = \frac{2}{\sin^2\delta}\sqrt{C(\vartheta)\ D(\vartheta)} \qquad \ldots \quad (G5)$$

where $C(\vartheta) = 1 + \sin(\vartheta-\gamma-\delta)$

$D(\vartheta) = 1 + \sin(\vartheta-\gamma+\delta)$

Substituting (G2) to (21) and making use of (20), it follows that

$$\chi = -\tan\left(\frac{\theta + a_0}{2}\right) \qquad \ldots \quad (G6)$$

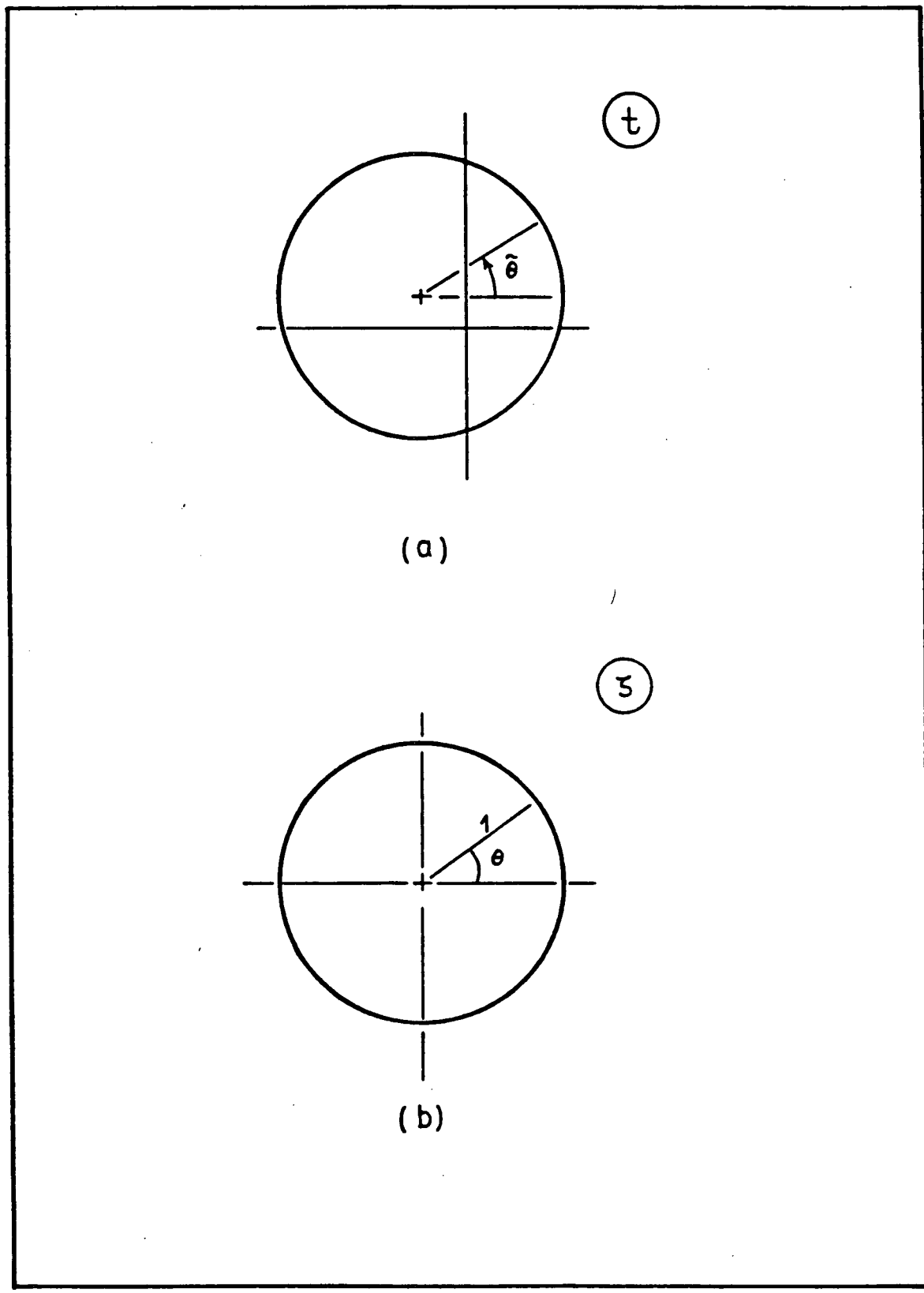

G1 Definitions of $\tilde{\theta}$ and θ

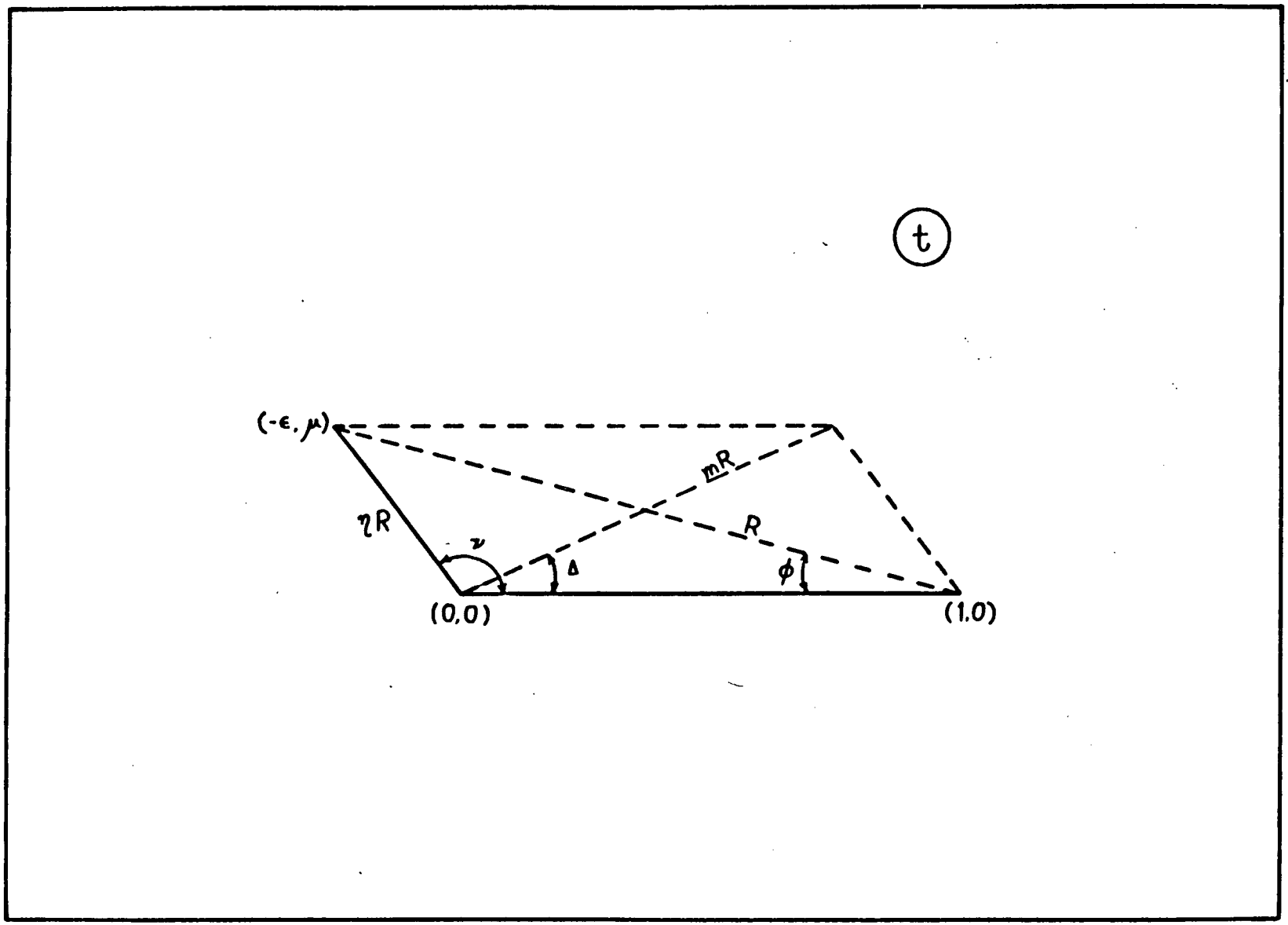

G2 Definitions of Δ, ν, ϕ, m, η and R

and $$\lambda = -\xi - \tilde{\eta} \tan\left(\frac{\theta + a_0}{2}\right) \quad \ldots \quad (G7)$$

As a result, for the split flaps,

$$f_2 = \kappa\, L(\vartheta)\, h(\theta) \quad \ldots \quad (G8)$$

where $\kappa = R\,\tilde{\eta}/(2 \sin \delta)$

$L(\vartheta) = \frac{|t^2-1|}{|t^2|}\sqrt{C(\vartheta)\, D(\vartheta)}$, as defined in (G3 and G5),

$h(\theta) = \frac{F(\theta)\, G(\theta)}{H(\theta) I(\theta)}$ $\quad F(\theta) = \sec^2\left(\frac{\theta + a_0}{2}\right)$, $\quad G(\theta) = -\lambda$

$H(\theta) = n - \lambda$ and $I(\theta) = n - 2 - \lambda$

An implicit relation between ϑ and θ can be found in the following way. Using (A2), equation (18) is simplified to

$$s = i\, R \sin \delta \left[\frac{1 - i \tan X \tanh Y}{\tan X + i \tanh Y}\right] \quad \ldots \quad (G9)$$

Equating the real parts of (G4) and (G9), when point E is approached,

$$\cos(\vartheta - \gamma) = \sin \delta \left[\frac{\sec^2 X \tanh Y}{\tan^2 X + \tanh^2 Y}\right] \quad \ldots \quad (G10)$$

where $2X = (2-n)\frac{\pi}{2}$

$$2Y = h - \{ n \ln\left(\frac{\lambda}{n} - 1\right) + (2-n) \ln\left(1 + \frac{\lambda}{2-n}\right)\}/2$$

Therefore, equations (G7) and (G10) can be used to calculate $\frac{d\vartheta}{d\theta}$ and $\frac{d^2\vartheta}{d\theta^2}$ in deriving f_2' and f_2'' since, from (G8),

$$f_2' = \kappa \left[L'(\vartheta)\, h(\theta) \frac{d\vartheta}{d\theta} + L(\vartheta)\, h'(\theta)\right]$$

$$f_2'' = \kappa \left[L''(\vartheta)h(\theta)\left(\frac{d\vartheta}{d\theta}\right)^2 + 2L'(\vartheta)h'(\theta)\frac{d\vartheta}{d\theta} + L'(\vartheta)h(\theta)\frac{d^2\vartheta}{d\theta^2} + \right.$$

$$L(\vartheta)h''(\theta)]$$

Note that the terms involving $L(\vartheta)$ can be ignored since at the point E, $\vartheta = -\phi$ and from (G3), $L(-\phi) = 0$.

Taking the derivative of (10) with respect to θ, after some manipulation,

$$\frac{d\vartheta}{d\theta} = \frac{k}{\sin(\vartheta-\gamma)} F(Y)\, h(\theta) \qquad \ldots \quad (G11)$$

where $F(Y) = \dfrac{(\tan^2 X - \tanh^2 Y)\operatorname{sech}^2 Y}{(\tan^2 X + \tanh^2 Y)^2}$

and $k = \dfrac{\sin\delta \sec^2 X\, \tilde{\eta}}{4}$

Taking the derivative of (G11) again, it can be shown that

$$\frac{d^2\vartheta}{d\theta^2} = \frac{1}{\sin(\vartheta-\gamma)}\{k[F(Y)h'(\theta) - \frac{F'(Y)h^2(\theta)\tilde{\eta}}{4}] - \cos(\vartheta-\gamma)(\frac{d\vartheta}{d\theta})^2\}$$

where $F'(Y) = \dfrac{-2\tanh Y \operatorname{sech}^2 Y}{(\tan^2 X + \tanh^2 Y)^3}[\{\operatorname{sech}^2 Y + (\tan^2 X - \tanh^2 Y)\}$
$(\tan^2 X + \tanh^2 Y) + 2\operatorname{sech}^2 Y(\tan^2 X - \tanh^2 Y)]$

Making use of (G3), (G5), it can be shown that

$$L'(\vartheta) = \frac{\sqrt{B(\vartheta)\, C(\vartheta)\, D(\vartheta)}}{E(\vartheta)}$$

and at $\vartheta = -\phi$

$$L''(\vartheta) = \sqrt{BCD}\ \{\frac{B'}{BE} + \frac{C'}{CE} + \frac{D'}{DE} - \frac{2E'}{E^2}\}$$

where $B' = -2\, m \sin(\vartheta-\Delta)$

$C' = \cos(\vartheta-\gamma-\delta)$

$D' = \cos(\vartheta-\gamma+\delta)$

$E' = -2\,\eta \sin(\vartheta-\nu)$

and

$$h'(\theta)\Big|_{\theta_E} = (F' G + F G')(H I)^{-1} - F G G' (H^{-2}I^{-1} + H^{-1}I^{-2})$$

where $F' = - F \tilde{\lambda}$

$G' = \tilde{\eta} F/2$

$H' = G'$

$I' = G'$

Therefore, f_2' and f_2'' at $\theta = \theta_E$ can be calculated.

Near point E, for spoilers, f_2 takes the form similar to that of (G8) with

$$\lambda = \tilde{\xi} - \tilde{\eta} \tan(\frac{\theta + a_0}{2})$$

except $C = 1 - \sin (\tilde{\theta}+\gamma+\delta)$

$D = 1 - \sin (\tilde{\theta}+\gamma-\delta)$

The relation between $\tilde{\theta}$ and θ is

$$\cos (\tilde{\theta} + \gamma) = \sin \theta \left[\frac{\sec^2 X \tanh Y}{\tan^2 X + \tanh^2 Y} \right]$$

with $2X = -(2-n) \frac{\pi}{2}$

$$2Y = h - \{ n \ln(\frac{\lambda}{n} + 1) + (2-n) \ln(\frac{\lambda}{2-n} - 1\}/2$$

Therefore, $$\frac{d\tilde{\theta}}{d\theta} = \frac{k}{\sin (\tilde{\theta}+\gamma)} F(Y) h(\theta)$$

and

$$f_2'|_{\theta_E} = \kappa L'(\theta)h(\theta) \frac{d\tilde{\theta}}{d\theta}|_{\theta_E}$$

where k, $F(Y)$, $h(\theta)$, κ, $L'(\theta)$ are the same as those defined in above. f_2'' can be calculated by using the similar procedure

outlined above.

By examining equations (10) and (22), it is clear that f_2 is zero at point C because $\lambda \longrightarrow 0$ there. $f_2'|_C$ can easily be calculated and is equal to

$$f_2'|_C = \frac{|t_c^2 - 1|}{|t_c^2|} \frac{R \sin \delta}{4n(2-n)} [\tilde{\xi}^2 + \tilde{\eta}^2] \sec^2\left(\frac{\theta + a_0}{2}\right) [\sinh^2\left(\frac{h}{2}\right)]^{-1}$$

since $\omega_C = ih$. So $|\sin^2\left(\frac{\omega C}{2}\right)| = \sinh^2\left(\frac{h}{2}\right)$

For spoilers, $t_C = t_0 + R\, e^{-i\theta_0} + \hbar\, e^{+i\gamma}$,

but $t_C = t_0 + R\, e^{+i\theta_0} + \hbar\, e^{-i\gamma}$ for split flaps.